The Theory of Photon-Impact Bound-Free Pair Production and Applications to Relativistic Heavy-Ion Collisions

Carsten Kallesø Agger

March 11, 1996

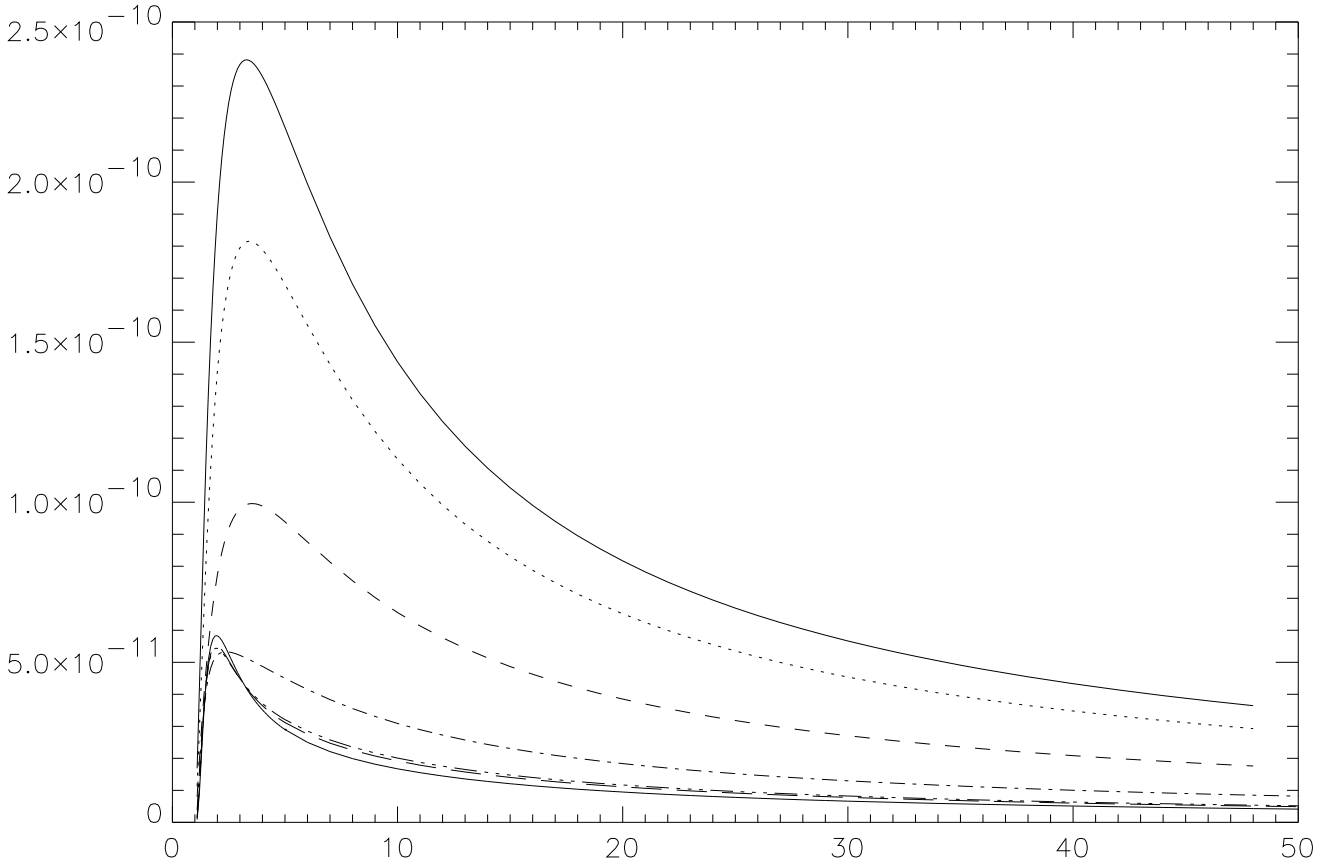

Comments, criticism and questions will be appreciated and may be directed to the author by email to *agger@modspil.dk*

Contents

1 Preface

1.1 Prehistory

This thesis is intended to fulfil the requirements for obtaining the *cand. scient.* degree at the Institute of Physics and Astronomy (IFA) at the University of Aarhus. It is mainly concerned with electron-positron pair production by photon impact with capture into an atomic shell,[1] and attempts to use the results thus obtained for the calculation of cross sections for pair production with capture in relativistic heavy-ion collisions (RHIC).

This subject was chosen since after taking graduate courses on atomic physics and quantum field theory I wanted to keep on working with atomic physics - at the same time I had found the course on quantum field theory both fascinating and confusing, since there had been no time for discussing the applications of the quite involved formalism. Thus, I found it natural looking for a subject under the general heading of "applications of quantum electrodynamics in atomic physics".

This led me to talking with Allan Hvidkjær Sørensen who is mainly concerned with relativistic atomic physics, and who had just completed a project concerning bound-free pair production in RHIC. He suggested I examine the somewhat simpler process of pair production with capture by *photon* impact.

This process is less easily observed experimentally than, for instance, free-free pair production or the photoelectric effect, since it requires the presence of fully (or almost fully) stripped ions and as opposed to free pair production has no relevance to γ-ray absorption. The reason is that this process will not be observed by directing a beam of photons upon a solid, since the cross sections are very strongly suppressed for the higher atomic shells, and the lower atomic shells are always occupied in a solid; of course, the atoms in a solid are actually normally neutral, so that bound-free pair production would be to negative ion states. But this could hardly be a significant effect, since the strong electron correlation usually found in the ground state of negative ions would demand a higher-order process.

The results, however, may be used in the so-called virtual photon or Weizsäcker-Williams(WW) method for calculating cross sections for bound-free pair production in RHIC: previous WW-calculations had used approximate wave functions only valid for high energies and small target charges.

Moreover, photon-impact bound-free pair production is of interest in its own right as an electrodynamic process which can be calculated exactly. The exact numerical calculation of cross sections of these processes is the main result of this work, and the main part of the effort has gone into the preparation of reliable

[1] This process will also be referred to as *bound-free pair production*, since one free and one bound particle is produced. In the literature, one may frequently find the terminology "pair production with *subsequent* capture". This is, however, entirely misleading since it implies that a free particle is created and then captured.

and reasonably efficient computer programs to do the calculations.
Having thus decided that this would be an interesting project of a reasonable size, I went ahead, the result of which is the present thesis.

1.2 An Overall View

This treatise is naturally divided into three parts; in part I, we introduce the theory of the process of bound-free pair and sketch the theoretical and conceptual framework upon which we build; in part II, we present the results of calculations based on the formulae obtained in part I, while in part III we discuss the possibility of using the results of part two in RHIC.
As we will see in section 2, our subject matter is both very simple and very complicated.

It is simple, because it is concerned with one of the very simplest electrodynamical processes we know, the creation of an electron-positron pair; the bound-free variety is conceptually and computationally exactly equivalent (though of course not identical) to the well-known photoelectric effect. It is further simple, because we are working with the extremely well-described and eminently solvable Coulomb problem.

And it is complicated, because reliable predictions of the cross sections of this process cannot be attained in perturbation theory - for heavy elements, both the first and second Born approximations are totally wrong (this is also discussed in part II, as well as by Pratt *et al* in their review article). If we want our results to have any predictive value, we must account *exactly* for the Coulomb field of the nucleus within the framework of relativistic quantum mechanics. This turns out to be a both mathematically and computationally nontrivial task.

1.2.1 Summary of Part I

The presentation of theory and results is intended to be as self-contained as possible, and for this reason I have included a quite extensive presentation of the theoretical background.
Most of this theory is treated quite well by a number of authors - the books by Greiner and Rose are good introductions to relativistic quantum theory, and contain detailed derivations of the exact relativistic Coulomb waves which we merely quote. An overview of elementary electrodynamical processes may be found in the books by Heitler and Akhiezer & Berestetskii, as well as in H. Olsen's review article from 1968.

After stating and delineating the problem and the model to be used, we proceed to present the basic formalism and wave functions. A discussion of the derivation of the first-order transition amplitudes and cross sections and the general description of pair production in quantum mechanics and quantum field theory is also included.

After this presentation, we derive and present expressions for the total and differential cross sections for bound-free pair production in terms of partial wave matrix elements, and in section 5 we obtain analytical expressions for these matrix elements.

At this point, we give a brief account of the work done by other researchers in the case of related processes, namely, the atomic photoelectric effect and single-photon pair annihilation, and sketch a few of the various approximations which have been applied.

1.2.2 Summary of Part II

The results of a numerical calculation based on the analytical cross sections obtained in part I are presented and compared to previous work; this concludes the main part of the thesis, the one concerned with photon-induced pair production. We also include a description of the programs we have used to implement the formulae, as well as a discussion of some of the dangers and possible errors connected with numerical calculations.

1.2.3 Summary of Part III

The process of bound-free pair production in RHIC has been the target of intense investigation in recent years, for a number of reasons. First of all, it is highly nonperturbative: if a highly charged projectile collides with a highly charged target, it is *not* enough to take exact account of the target ion and treat the electromagnetic field of the particle as a perturbation. Secondly, the cross section for this process increases as the collision energy increases, and at high energies, it may limit the lifetimes of ion beams (since they cannot be controlled in an accelerator, if their charge state is changed).
In part III, we attempt to use the total cross sections obtained in parts I and II for estimating the cross sections of this process in the virtual photon approximation mentioned above.
This approximation is perturbative and indeed our main conclusion is, that for high collision energies it seems to reproduce the results previously obtained in first order perturbation theory (Becker *et al*). Bound-free pair production in RHIC has been observed experimentally by Belkacem *et al*, but at rather low collision energies, so that the results obtained in the present thesis cannot be expected to give accurate results.

Before proceeding to the treatment of the virtual photon approach, we introduce the theory of atomic processes in RHIC and review three of the approximation methods which have been attempted (the Born approximation, coupled-channel calculations with a finite basis set, and the so-called *sudden collision* or first Magnus approximation.)

1.2.4 Comparison to Previous Work

What results do we arrive at, and what is their relation to the results obtained by previous investigators? We give a brief overview:

The total cross sections of the process of K- and L-shell bound-free pair production have been calculated for seven values of the target charge (four for the L-shell) for impact photon energies up to about 25 MeV (enough to deduce the high-energy behaviour), and differential cross sections for the $1s$, $2s$ and $2p_{\frac{1}{2}}$ subshells, also for a number of energies.
Programs have been developed, which calculate the total or differential cross sections for any target charge or angle in an energy range from threshold to the high-energy limit.

The cross sections for bound-free pair production with capture to the K shell have previously been calculated by Aste *et al* for energies up to about 15 MeV, and they obtained the same results as in the present thesis - it should be mentioned, that when their article was published, the present work was already in progress.
The differential cross sections for single-photon pair annihilation, the inverse of bound-free pair production, were calculated by Johnson in 1967 for a few, low energies. Johnson *et al* had already calculated the *total* cross sections for this process for positron energies up to 3.5 mc^2 (about 1.8 MeV). The cross sections for bound-free pair production with emission of a positron in this energy range may be deduced directly from their results.
L-shell calculations for the atomic photoelectric effect, assuming a pure Coulomb potential, were performed by Alling & Johnson. These calculations are equivalent to the ones performed in the present thesis, but they were done at so low energies, that they cannot be compared directly to our results.

On the other hand, the cross sections for bound-free pair production and those for the photoelectric effect do become equal in the high-energy limit, and the exact high-energy limit for the total photoelectric effect cross sections was obtained by Pratt ($1960^{a,b}$).

So, which *new* results do we obtain in the present work?
First of all, the calculation of the L-shell total cross sections from threshold to the high energy limit, that is, in the region where the approximation methods fail because of the nonperturbative character of the process at high target charges.
Secondly, we calculate the differential cross sections for the K- and two L-subshells both near threshold, at intermediate and high energies.
The results we obtain in part III are equivalent to those already published by Aste *et al*; but we argue that one must choose the minimum impact parameter larger than commonly used in the literature; moreover, we find that the results of the Weizsäcker-Williams approximation nearly exactly reproduce those of the first Born approximation of time-dependent perturbation theory.

1.3 Note on Units and Terminology

The Planck constant, the mass of the electron and the velocity of light will be taken to unity throughout ($\hbar = m = c = 1$). In a few equations, they are retained for the sake of clarity. Electromagnetic units are fixed by the relation $e^2 = 4\pi\alpha$, where e is the elementary charge and α the fine structure constant.

Units may conveniently be introduced in terms of the electron mass m or the Compton wave length $\lambda_C = \frac{\hbar}{mc}$. If the result of some calculations is a cross section, as will indeed be the case, it may be given the proper dimensions by using

$$\lambda_C = 386.159 \cdot 10^{-15} m$$

or (in the case of cross sections perhaps more convenient to use directly)

$$\lambda_C^2 = 1491.188 b$$

In the present work, we are only concerned with bound-free pair production on fully stripped ions. This means that we will refer to the various nuclei either by specifying their nuclear charge (Z=1, 8,8 2, 92 etc.), their name (hydrogen, oxygen, lead, uranium), or their chemical symbol (H, O, Pb, U). Thus, by U we will mean U^{92+}, and so on.

References are given by mentioning the name of the author(s), and the year of publication if necessary. The sources may then be localised by referring to the alphabetical list in section 18.

A number of special functions are used: hypergeometric functions, Bessel functions etc. These are all described in the handbook by Abramowitz & Stegun.

1.4 Four-vectors

As is natural in a relativistic treatment, four-vector notation appears in a few of the formulae. A couple of observations:

- the metric is defined by the usual device of an imaginary fourth component - the position vector is thus

  $$x = (\mathbf{x}, ix_0),$$

  and so forth ($x_0 = t$, of course). There is then no distinction between lower and upper indices.

- The convention of implicit summation over repeated indices is used - thus, $p_\mu p_\mu$ is a compact notation for

  $$p_x^2 + p_y^2 + p_z^2 - E^2$$

  and xp is a compact notation for

  $$xp_x + yp_y + zp_z - Et$$

Figure 1: The basic Feynman diagram of quantum electrodynamics

Part I
Photon-Impact Pair Production: Theory

2 Introduction

The process we wish to investigate in the present work is depicted on figure 1, which may be regarded either as a Feynman diagram or as a graphical representation of the process: a photon coming in from the left creates an electron-positron-pair - or: an electron is moving upward, emits a photon and is deflected; - or: a positron and an electron move left, collide and annihilate, thus emitting a photon - or: ...

The many possible interpretations of this Feynman diagram is quite well-known, of course, as is the following fact: The probability of actually observing the process described on figure 1 is identically zero, since it cannot conserve both energy and momentum. In order to get nonzero probabilities we must introduce an external field capable of absorbing the exchanged momentum, a very relevant example being the field of an atomic nucleus. Thus, a pictorial representation of the process would be like figure 2. In the present work we shall always be concerned with the case where particle 1 is in a bound state, while particle 2 belongs to the (positive or negative) continuum. If we assume that this is indeed the case, four different processes are described by figure 1:

1. electron-positron pair production with capture
2. its inverse, single-photon annihilation by a positron on an electron bound in an atomic field.

Figure 2: The lowest-order Feynman diagram of pair production and related processes

3. radiative capture of a free electron ("decay from the continuum")

4. its inverse, the atomic photoelectric effect.

The matrix elements determining the cross sections for these processes are related, and it may be shown (Erber 1959) that in the high energy limit their total cross sections become identical:

$$\sigma_1 = \sigma_2 = \sigma_3 = \sigma_4 \tag{1}$$

If the contribution from this diagram is calculated according to the usual Feynman rules (as described e.g. by Nielsen or Akhiezer and Berestetskii) the cross section is obtained to first order in both the photon and external fields. Alternatively, one may *exactly* account for the external field by using the Feynman rules for the diagram on figure 1, but representing the fermions by solutions to the Dirac equation of this field[2]. And this is the approach which will be taken in the present thesis.

These processes are thus characterised by the matrix element

$$M = \int d^3\mathbf{r}\psi_1^\dagger(\mathbf{r})\boldsymbol{\alpha}\cdot\mathbf{e}_\lambda e^{i\mathbf{k_0}\cdot\mathbf{r}}\psi_2(\mathbf{r}). \tag{2}$$

A very great part of the work done this far on the processes described by figure 1 has gone into the evaluation of this matrix element with wave functions corresponding to various approximations: nonrelativistic calculations have been performed for the atomic photoelectric effect and pair production; relativistic calculations have been performed using Sommerfeld-Maue wave functions (which

[2]This will be explained in more detail in section 3 below

are valid for large energies and low target charges), Coulomb-Dirac wave functions, and different approximations have also been applied in order to account for screening.

In the present work we are concerned with bound-free pair production on a fully stripped ion, and we shall always assume we are dealing with a pure Coulomb field and use the appropriate relativistic wave functions.
The process will be treated to first order in the radiation field, and we shall thus ignore the all radiative corrections including the Lamb shift.
We shall also neglect all recoil effects - in Appendix C, the justification of this is discussed on the basis of some simple kinematical observations.

The perturbation result may obviously only be expected to give adequate results when the perturbing field is indeed weak; if we are concerned with heavy ions like U^{92+} this is hardly the case, and perturbation theory yields, it turns out, too large cross sections for high energies and large Z. In the last section of Part I, the results of the present calculations are compared with previous work, both the various attempts at perturbation calculations and exact calculations.

3 Wave Functions and Notation

3.1 Dirac Equation

In the framework of relativistic quantum mechanics, the electron is described by the Dirac equation, usually given in the covariant form

$$\left(\gamma_\mu \frac{\partial}{\partial x_\mu} + m\right)\psi(x) = ie\gamma_\mu A_\mu(x)\psi(x). \tag{3}$$

Here, e denotes the elementary charge, and $A_\mu(x)$ the four-vector electromagnetic potential. The γ matrices may (in the so-called *Pauli representation*) be written

$$\boldsymbol{\gamma} = \begin{pmatrix} \mathbf{0} & -i\boldsymbol{\sigma} \\ i\boldsymbol{\sigma} & \mathbf{0} \end{pmatrix}, \qquad \gamma_4 = \begin{pmatrix} 1 & 0 \\ 0 & -1 \end{pmatrix}, \tag{4}$$

where σ as usual denotes the *Pauli matrices*

$$\sigma_x = \begin{pmatrix} 0 & 1 \\ 1 & 0 \end{pmatrix}, \qquad \sigma_y = \begin{pmatrix} 0 & i \\ -i & 0 \end{pmatrix}, \qquad \sigma_z = \begin{pmatrix} 1 & 0 \\ 0 & -1 \end{pmatrix} \tag{5}$$

Alternatively, the Dirac equation may be written in the *Hamiltonian form*

$$i\frac{\partial\psi(\mathbf{r},t)}{\partial t} = H_D\psi(\mathbf{r},t), \qquad H_D = \boldsymbol{\alpha}\cdot(\mathbf{p} - e\mathbf{A}) + e\phi + \beta m \tag{6}$$

where the electromagnetic potential is given by its scalar and vector components and

$$\boldsymbol{\alpha} = \begin{pmatrix} \mathbf{0} & \boldsymbol{\sigma} \\ \boldsymbol{\sigma} & \mathbf{0} \end{pmatrix}, \qquad \beta = \gamma_4. \tag{7}$$

Which representation to use is mainly a question of convenience: the 4-spinor form (3) is appropriate in order to obtain relativistically invariant Green's functions or to give a general description of spin-$\frac{1}{2}$ fermions, while (6) is easier to deal with in many applications of relativistic quantum mechanics.

3.2 Free Solutions

The stationary solutions to the Dirac equation corresponding to free spin $\frac{1}{2}$-particles ($A_\mu(x) = 0$) may be written in the following form:

$$\psi^0(\mathbf{p},\sigma,\mathbf{r}) = u(\mathbf{p},\sigma)e^{i(\mathbf{p}\cdot\mathbf{r}-Et)} = \sqrt{\frac{E+m}{2E}}\begin{pmatrix} 1 \\ \frac{\boldsymbol{\sigma}\cdot\boldsymbol{p}}{E+m} \end{pmatrix}\chi_\sigma(\hat{\mathbf{p}})e^{i(\mathbf{p}\cdot\mathbf{r}-Et)} \tag{8}$$

where σ denotes the helicity of the particle in question, so that $\chi_\sigma(\hat{\mathbf{p}})$ is defined by the requirement

$$(\boldsymbol{\sigma}\cdot\boldsymbol{p})\chi_\sigma(\hat{\mathbf{p}}) = \sigma\chi_\sigma(\hat{\mathbf{p}}) \tag{9}$$

An explicit solution to (9) is

$$\chi_{\sigma=1}(\hat{\mathbf{p}}) = \begin{pmatrix} \cos\frac{\vartheta}{2} \\ \sin\frac{\vartheta}{2}e^{i\phi} \end{pmatrix}, \qquad \chi_{\sigma=-\mathbf{1}}(\hat{\mathbf{p}}) = \begin{pmatrix} \sin\frac{\vartheta}{2} \\ -\cos\frac{\vartheta}{2}e^{i\phi} \end{pmatrix}, \tag{10}$$

where ϑ and ϕ denote the polar and azimuthal angle of the direction $\hat{\mathbf{p}}$.

One might, of course, choose to consider polarisation in an arbitrary direction and not just the helicity - such a description is given by Olsen. This will not be pursued further here, since the description in terms of the helicity seems quite adequate for our purpose.

The solutions (8) applies for both positive and negative energies - if we set $\varepsilon = |E|$, the wave functions may be written so that the difference of the two kind of solutions is appreciated:

$$\psi^0(\mathbf{p},\sigma,\mathbf{r}) = \sqrt{\frac{\varepsilon \pm m}{2\varepsilon}} \begin{pmatrix} 1 \\ \frac{\pm\boldsymbol{\sigma}\cdot\boldsymbol{p}}{\varepsilon\pm m} \end{pmatrix} \chi_\sigma(\hat{\mathbf{p}}) e^{i(\mathbf{p}\cdot\mathbf{r}\mp\varepsilon t)}, \qquad \varepsilon = \pm E \tag{11}$$

The negative energy solutions may be used to represent positrons in the *Dirac hole picture*, which will be discussed in section (3.5) below.
Here, we mention that the rules for charge conjugation imply that the solutions corresponding to an electron with energy $-E$, momentum $\mathbf{p}$ and helicity σ may be interpreted as the wave function of a *positron* with energy E, momentum $-\mathbf{p}$ and helicity $-\sigma$.

A consequence of this interpretation is that in matrix elements involving free positrons, these may be described by substituting

$$E \to -E, \qquad \mathbf{p} \to -\mathbf{p}, \qquad \sigma \to -\sigma \tag{12}$$

in the free electron states.

3.3 Continuum Coulomb States

The continuum solutions of the Dirac equation corresponding to scattering states cannot be given in closed form - the Dirac equation for the Coulomb potential does not separate in parabolic coordinates. Thus it is necessary to expand the scattering states in angular momentum eigenstates, *id est* partial waves and separate in spherical polar coordinates.

The wave function of a state with energy E characterised by the quantum numbers J, L and M is given by (setting $m = 1$ in this section as well as the following)

$$\psi_{JLM}(\mathbf{r}) = \begin{pmatrix} g_\kappa(r)\Omega_{JLM}(\vartheta,\phi) \\ if_\kappa(r)\Omega_{JL'M}(\vartheta,\phi) \end{pmatrix}, \tag{13}$$

$$\Omega_{JLM} = \sum_{m_s=\pm\frac{1}{2}} < L\tfrac{1}{2}M - m_s, m_s | L\tfrac{1}{2}JM > Y_{L,M-m_s}(\vartheta,\phi)\chi_{m_s},$$

$$\kappa = \mp(J + \tfrac{1}{2}), \qquad L' = L \pm 1 \text{ for } J = L \pm \tfrac{1}{2}$$

where $< \ldots | \ldots >$ is a Clebsch-Gordan coefficient, Y_{LM} a spherical harmonic and χ denotes a Pauli spinor. For actual calculations, the explicit expressions for the Ω's, which are given by Greiner, are very convenient:

$$\Omega_{JLM} = \begin{cases} \begin{pmatrix} \sqrt{\frac{J+M}{2J}} Y_{L,M-\frac{1}{2}} \\ \sqrt{\frac{J-M}{2J}} Y_{L,M+\frac{1}{2}} \end{pmatrix}, & J = L + \frac{1}{2} \\ \begin{pmatrix} -\sqrt{\frac{J-M+1}{2J+2}} Y_{L,M-\frac{1}{2}} \\ \sqrt{\frac{J+M+1}{2J+2}} Y_{L,M+\frac{1}{2}} \end{pmatrix}, & J = L - \frac{1}{2} \end{cases} \tag{14}$$

The radial solutions are given by

$$g(r) = N_g (2pr)^{s-1} \mathrm{Re}\{e^{i\delta}(s + i\eta) e^{-ipr} F(s + 1 + i\eta, 2s + 1, 2ipr)\} \tag{15}$$

and

$$f(r) = N_f (2pr)^{s-1} \mathrm{Im}\{e^{i\delta}(s + i\eta) e^{-ipr} F(s + 1 + i\eta, 2s + 1, 2ipr)\} \tag{16}$$

where $F(\ldots, \ldots, \ldots) = {}_1F_1(\ldots, \ldots; \ldots)$ as usual denotes the confluent hypergeometric function and the various parameters and normalisation constants are given below:

$$N_g = 2\sqrt{\frac{pS_E(E+1)}{\pi}} e^{\frac{1}{2}\pi\eta} \frac{|\Gamma(s + i\eta)|}{\Gamma(2s + 1)} \tag{17}$$

$$N_f = -N_g S_E \sqrt{\frac{E-1}{E+1}}$$

$$p = \sqrt{E^2 - 1}, \qquad \eta = \frac{\alpha Z E}{p}, \qquad e^{2i\delta} = \frac{-\kappa + i\frac{\eta}{E}}{s + i\eta} \tag{18}$$

$$s = \sqrt{\kappa^2 - \alpha^2 Z^2}, \qquad S_E = \frac{E}{|E|}.$$

In these equations, $\alpha \sim \frac{1}{137}$ is the fine structure constant, while Z denotes the charge in units of e. αZ is thus a measure of the strength of the Coulomb potential, and it may be noted that the wave functions given in this and the next section give no real sense unless $\alpha Z \leq 1$; it is unphysical to assume the existence of a *point* charge with $Z > 137$.

When doing calculations on scattering processes it is often necessary to represent the wave functions of the scattered particles not by partial waves but by scattering states $\Psi^{\pm}$, corresponding to incoming (outgoing) plane waves plus outgoing (incoming) spherical waves: in the asymptotic limit $r \to \infty$,

$$\Psi^{+}_{\mathbf{p}} \sim u(\mathbf{p}, \sigma) + \sum_{\sigma'} f_{\sigma\sigma'}(\mathbf{p}, \mathbf{p}') u(\mathbf{p}', \sigma') \frac{e^{ipr}}{r} \text{ for } r \to \infty \tag{19}$$

In potential scattering, the coefficients $f_{\sigma\sigma\prime}$ are related to the differential cross section of the scattering process by

$$\frac{d\sigma}{d\Omega} = |f_{\sigma\sigma\prime}|^2 \tag{20}$$

In the case of the Coulomb potential it turns out to be impossible to fulfil such boundary conditions and the asymptotic behaviour will be modified by a position-dependent phase.

In the nonrelativistic case, such states are obtained in closed form by separating the Schrödinger equation for the Coulomb potential in parabolic coordinates (see, for instance, Merzbacher chapter 11).
Relativistic Coulomb scattering states are only available in a partial wave expansion. This is given by Rose and may be written

$$\Psi^{\pm} = 4\pi\sqrt{\frac{\pi}{2Ep}}\sum_{JLM} i^L e^{\pm i\delta_\kappa} < L\tfrac{1}{2}(M-\tfrac{1}{2}\sigma)\tfrac{1}{2}\sigma|L\tfrac{1}{2}JM > Y^*_{L,M-\sigma}(\hat{\mathbf{p}})\psi_{JLM} \tag{21}$$

where ψ_{JLM} are the partial waves and δ_κ is the Coulomb phase shift, given by

$$\delta_\kappa = \delta + (L+1-s)\frac{\pi}{2} - \arg\{\Gamma(s+i\eta)\} \tag{22}$$

3.4 Bound Coulomb States

These wave functions may be written in the form (13); in this case, the radial functions turn out to be

$$g_\kappa(r) = N_b r^{s-1} e^{-p_0 r}\left\{\left(\frac{(n'+s)}{E}-\kappa\right)F(-n',2s+1,2p_0r) - n'F(1-n',2s+1,2p_0r)\right\} \tag{23}$$

$$f_\kappa(r) = -\sqrt{\frac{1-E}{1+E}}N_b r^{s-1}e^{-p_0 r}\cdot$$
$$\left\{\left(\frac{(n'+s)}{E}-\kappa\right)F(-n',2s+1,2p_0r) + n'F(1-n',2s+1,2p_0r)\right\}$$

where

$$N_b = \frac{(2p_0)^{s+\frac{1}{2}}}{\Gamma(2s+1)}\sqrt{\frac{(1+E)\Gamma(2s+n'+1)}{4^{\frac{(n'+s)}{E}}(\frac{(n'+s)}{E}-\kappa)n'!}}, \tag{24}$$
$$p_0 = \sqrt{1-E^2}, \qquad n' = n - |\kappa|$$

while s and κ are as defined in the previous section and n denotes the main quantum number. These expressions are very much simpler for the lowest shells (for small n' and κ). For the ground state wave function we may thus write

$$g(r) = N_0 r^{s_{1s}-1}e^{-\alpha Z r}, f(r) = -\sqrt{\frac{1-s_{1s}}{1+s_{1s}}}g(r), \tag{25}$$

where N_0 turns out to be

$$N_0 = (2\alpha Z)^{s_{1s}+\frac{1}{2}}\sqrt{\frac{1+s_{1s}}{2\Gamma(2s_1 s+1)}}. \tag{26}$$

Similarly, the radial functions for the L shell (the only other shell with which we are concerned in this thesis) may be written out explicitly:

- $2s$:

$$g(r) = N_{2s} r^{s-1} e^{-p_0 r}\left\{2E - \frac{2p_0 r}{2E-1}\right\}, \tag{27}$$

$$f(r) = -\sqrt{\frac{1-E}{1+E}} N_{2s} r^{s-1} e^{-p_0 r}\left\{(2E+2) - \frac{2p_0 r}{2E-1}\right\},$$

$$N_{2s} = \frac{(2p_0)^{s+\frac{1}{2}}}{2}\sqrt{\frac{(1+E)(2E-1)}{2E\Gamma(2s+1)}}, \qquad E = \sqrt{\frac{1+s}{2}}$$

- $2p_{\frac{1}{2}}$:

$$g(r) = N_{2p_{\frac{1}{2}}} r^{s-1} e^{-p_0 r}\left\{(2E-2) - \frac{2p_0 r}{2E+1}\right\}, \tag{28}$$

$$f(r) = -\sqrt{\frac{1-E}{1+E}} N_{2p_{\frac{1}{2}}} r^{s-1} e^{-p_0 r}\left\{2E - \frac{2p_0 r}{2E+1}\right\}$$

$$N_{2p_{\frac{1}{2}}} = \frac{(2p_0)^{s+\frac{1}{2}}}{2}\sqrt{\frac{(1+E)(2E+1)}{2E\Gamma(2s+1)}}, \qquad E = \sqrt{\frac{1+s}{2}}$$

- $2p_{\frac{3}{2}}$:

$$g(r) = N_{2p_{\frac{3}{2}}} r^{s-1} e^{-\frac{\alpha Z}{2} r}, \qquad N_{2p_{\frac{3}{2}}} = (\alpha Z)^{s+\frac{1}{2}}\sqrt{\frac{1+E}{2\Gamma(2s+1)}} \tag{29}$$

$$f(r) = -\sqrt{\frac{1-E}{1+E}} g(r), \qquad E_{2p_{\frac{3}{2}}} = \frac{\sqrt{4-(\alpha Z)^2}}{2} = \tfrac{1}{2}s$$

3.5 Formal Descriptions of Pair Production in Atomic Fields

The process of pair production in an atomic field may be described in two equivalent ways, namely in the *Dirac hole picture* as the excitation of a negative-energy electron to a positive-energy state: The electron emerges with positive energy, and the hole in the negative-electron sea behaves like a particle of equal mass, but positive charge (figure 3).

Though mathematically unambiguous, the hole theory has often been considered unsatisfactory from a conceptual point of view; in most presentations

Figure 3: Pair production viewed as the excitation of a negative energy electron (from Greiner *et al*).

of quantum electrodynamics electrons and positrons are described in terms of the electron absorption (and positron emission) operator ψ and the positron absorption (and electron emission) operator $\bar{\psi}$. The descriptions of particle and antiparticle thus become completely symmetric. On the other hand, the hole picture certainly does have its advantages. In this section we will first give a brief discussion of the advantages and disadvantages of the two different ways of describing pair production.
After that, we will turn to the question of how it is possible to include the interaction with the atomic field exactly by taking the initial and final states to be solutions of the Dirac equation in this field.

3.5.1 Comparison of the Hole Picture and QED

In the Dirac hole picture, solutions to the Dirac equation with energy $E < -mc^2$ are viewed as corresponding to states of negative energy which the electrons may occupy. But does that not mean that all electrons would immediately decay into negative energy states, leaving us with a lot of radiation and ionised matter and no electrons at all? It does indeed, were it not so that these negative energy states are postulated to be already occupied - so the electrons do not decay to these levels because they cannot, according to the Pauli principle.

So these filled energy levels act like a constant "background" charge density, which of course does not cause any observable electric field. We may imagine having a number of positive-energy electrons and a vast, completely filled, sea of

Figure 4: Bound-free pair production - excitation from the negative energy continuum to the 1s-state (from Bertulani & Baur)

negative-energy electrons.
But if this is so, then a sufficiently strong interaction should be able lift one of these electrons from the negative-energy sea to a state of positive energy. Then we would see an electron, appearing out of nowhere, and, additionally, there would be a hole in the negative energy sea; this hole would act exactly as if it were a particle with the same rest mass as an electron, but oppositely charged - a positron.

This is, of course, Dirac's famous prediction of the existence of the positron, and it offers a very practical view of the pair creation process, as depicted on figure 3: pair production (which otherwise should be regarded as a process where particle number is not conserved, and therefore, strictly speaking, outside the scope of ordinary quantum mechanics) is simply the transition of a negative energy electron to a positive energy state, wherefore we can calculate the correct transition probabilities in complete analogy with bremsstrahlung and the photoelectric effect.
But the hole picture must only be regarded as a convenient way of motivating the expressions for the transition amplitudes, since there exist, as has been stated, a number of reasons to regard it as unsatisfactory. First of all, the complete equivalence of the physical properties of electrons and positrons (differing only in their charge) would lead one to want a theory in which the two particles are treated symmetrically. Not so in the hole theory: the electrons are effectively regarded as the "real" particles, while the positrons are "holes", *absences* in a fundamentally unobservable sea of infinitely many negative energy electrons.

"Why not?" might one ask. After all, the electrons are the "normal" variety, since they are so very much more abundant under normal circumstances, so why not have a physical description that gives them some (albeit unnecessary) precedence?

Well, because this asymmetry, of course, represents a *choice*. As discussed by Greiner *et al*, one might instead start with the charge conjugate Dirac equation and describe the *positron* as the positive energy particle and treat the electrons as holes in a filled sea of negative energy *positrons*. This possible choice between two asymmetrical models rather accentuates than ameliorates the conceptual inadequacy of the (w)hole picture.

Secondly, this picture applies only to *fermions*: The Pauli principle would not be able to save the charged bosons contained by some theories from decaying into the negative energy continuum, and a theory containing emission and annihilation operators (as discussed in the previous section) must be constructed. And thus, in order to secure a proper connection in the particle physical theories of bosons and fermions, the Dirac hole picture becomes one of the first victims of the transition from relativistic quantum mechanics to quantum field theory.

3.5.2 Including the Atomic Field

Normally, one derives the Feynman rules used in perturbation theory by introducing free-particle field operators - these must obey the Dirac equation for free electrons and positrons, corresponding to $A_\mu(x) = 0$ in (3).
Instead, we introduce field operators which obey the Dirac equation for the *atomic field*, which is of the type

$$\left(\gamma_\mu \frac{\partial}{\partial x_\mu} + m + V\right)\psi(x) = 0 \tag{30}$$

These field operators must satisfy the anti-commutation relations

$$\left\{\psi(x), \bar{\psi}(y)\right\} = -iS(x-y) \tag{31}$$

$$\{\psi(x), \psi(y)\} = \left\{\bar{\psi}(x), \bar{\psi}(y)\right\} = 0, \qquad \bar{\psi}(x) = \psi^\dagger(x)\gamma_4 \tag{32}$$

Here, the function $S(x)$ is the Green's function satisfying the Dirac equation (30) with the additional condition

$$S(x)|_{x_0=0} = i\gamma_4\delta(\mathbf{x}) \tag{33}$$

The atomic field is represented by the potential energy term V, which is not, in spite of appearances, necessarily to be interpreted as a scalar field; rather, it will represent any kind of atomic field without specifying its detailed properties. In the case of a Coulomb potential, it is of course to be regarded as a four-vector whose space-like components are zero in the rest frame of its source.

With these definitions, we wish to arrive at the following interpretation. If Ψ is any state vector, the wave function

$$\Psi(x) =< 0|\psi(x)|\Psi > \tag{34}$$

is its one-electron component in the presence of the atomic field V. In the same way,

$$\Phi(x) =< 0|\bar{\psi}(x)|\Psi >$$

is its one-positron component in the presence of the atomic field V.
In the free-particle theory, the state vector is usually given in terms of the momentum-space basis vectors $|\mathbf{p}, \sigma >$.

When we include the atomic field, the state vector Ψ is most conveniently given in a basis of stationary atomic states - in this notation, the ground state vector of a Coulomb field is written $|1s >$, while the corresponding wave function in configuration space is given by

$$< \mathbf{r}|1s >= \psi_{1s}(\mathbf{r}) \tag{35}$$

In free-particle perturbation theory, we find that, on accounting for the interaction of the electron and positron field with the *photon* field (introduced by minimal coupling), the probability amplitude of a first-order process is given by

$$S_{fi} = -e \int dx < f|\psi^0(x)\gamma_\mu A^0_\mu(x)\bar{\psi}^0(x)|i > \tag{36}$$

where A^0_μ is the free-photon field operator and ψ^0 and $\bar{\psi}^0$ are the corresponding free-particle lepton operators. If we go from the free-particle formalism to the atomic-field formalism, we only have to replace these with the atomic field operators. The role of the photon field remains unchanged, of course, and the photon contribution to the matrix element (36) is obtained from the relation

$$< 0|A^0_\mu(x)|k_0, \lambda >= \frac{e_{\mu\lambda}(k_0)}{\sqrt{2k_0}} e^{ik_0 x} \tag{37}$$

where k_0 is the photon energy-momentum four-vector and $e_{\mu\lambda}(k_0)$ is the polarisation tensor.

In the case of pair production with K-shell capture, this becomes

$$S_{fi} = -e \int dx < E; 1s|\psi(x)\gamma_\mu A_\mu(x)\bar{\psi}(x)|k_0, \lambda > \tag{38}$$

Introducing the definition of $A^0_\mu(x)$, we find

$$\gamma_\mu A^0_\mu(x)\bar{\psi}(x)|k_0, \lambda >= \gamma_\mu \frac{e_{\mu\lambda}(k_0)}{\sqrt{2k_0}} e^{ik_0 x}\gamma_4\psi^\dagger(x) \tag{39}$$

$$= \boldsymbol{\alpha} \cdot \boldsymbol{e_\lambda} e^{ik_0 x}\psi^\dagger(x)$$

and the S-matrix element[3] is

$$S_{fi} = -\frac{e}{\sqrt{2k_0}} \int dx \psi_{1s}^{\dagger}(\mathbf{r}) \boldsymbol{\alpha} \cdot \boldsymbol{e_\lambda} \psi_E(\mathbf{r}) e^{i(k_0 - E_{1s} - E)t} = -\frac{2\pi e}{\sqrt{2k_0}} M \delta(k_0 - E_{1s} - E) \tag{40}$$

where M is the matrix element (2).

It is interesting to note, that while the time integral in the free-particle case leads to conservation of energy *and momentum* in the vertices, with the inclusion of the atomic field only *energy* is conserved, and the process in figure 1 may indeed be observed.

The probability of the transition is obtained by squaring (40), and so the cross section is obtained by multiplying with the density of final states and dividing by the flux of incoming particles. Or is it, now?

Actually, the δ-function which is so helpful in securing the conservation of energy makes things a little more complicated, since the "probability" obtained by merely squaring it does not seem very meaningful. It has to do with the fact that when "representing the photon" by a plane wave of finite amplitude at all times and in all space and treating the positron as a stationary state, that is, with a constant flux of outgoing positron at all times, we do not really have to do with a single process (which should be described by normalised waves) with a finite probability, but rather with rates, with probabilities per unit time. This can be remedied by assuming a normalised initial state photon described by some superposition of different wave numbers,

$$|\varphi_{\mathbf{k_0}}(\mathbf{k}) >= \int d^3\mathbf{k} \varphi(\mathbf{k}) A_\mu^0(\mathbf{k}) |0>, < \varphi|\varphi >= 1, \qquad \varphi_{\mathbf{k_0}}(\mathbf{k}) \sim 0 \text{ for } \mathbf{k} \neq \mathbf{k_0}$$

Alternatively, it may be assumed that the process is actually only observed during a finite time span. The result is, in all cases, that of spiriting away one of the δ functions, so that we end up with the transition rate

$$\Gamma = \frac{4\pi^2 \alpha}{k_0} |M|^2 \delta(k_0 - E_{1s} - E) \tag{41}$$

The cross section may now be obtained by dividing with the flux of incoming particles (which in our case is $c = 1$), multiplying with the density of final states and taking the integral. Assuming the final states to be given as scattering states, we obtain

$$\sigma = \frac{\alpha}{2\pi k_0} \int d^3\mathbf{p} |M|^2 \delta(k_0 - E_{1s} - E) \tag{42}$$

It should be noted that in connection with higher order processes, the procedure outlined here is not necessarily very practical, first of all because the various propagators and other Green's functions are very difficult to obtain, so that there can be no question of merely introducing a set of simple Feynman

[3]The definition of the S-matrix is also discussed in section 11.1.

rules for the scattering amplitudes as in the free-particle case. Moreover, some of the expressions for the higher-order scattering amplitudes will diverge, and a renormalisation is needed - this is to be performed in exact analogy with the procedure in the free-particle case.

4 Cross Sections

4.1 Total Cross Sections

The total cross section for bound-free pair production may be obtained by summing the partial cross sections for ending up in a particular state from some complete set; usually, this set is taken to be scattering states, so that

$$\sigma = \tfrac{1}{2} \sum_{\sigma,\lambda,m} \int d\Omega \frac{d\sigma(\vartheta,\phi)}{d\Omega} \tag{43}$$

Alternatively, the complete set may be taken to be angular momentum eigenstates (partial waves) so that

$$\sigma = \tfrac{1}{2} \sum_{\lambda} \sum_{JLMm} \sigma_{JLM} \tag{44}$$

In these equations, λ, σ and m represent the helicities of the incoming photon and outgoing positron, respectively, m the magnetic quantum number of the bound electron and finally J,L and M are the angular momentum quantum numbers of the partial wave. Obviously, σ is absent from equation (44) and J,L,and M from equation (43). Since the Coulomb-Dirac wave functions may only be obtained as a partial wave expansion, the second approach has been taken in the present work; thus, the task to be performed has been to calculate the cross section for ending in a particular angular momentum state and sum these contributions.

The angular momentum eigenstates may be treated in analogy with bound states, and the partial cross section is obtained by taking the density of final states to be unity and doing the energy integral in (41). Since the process of pair production with capture may be viewed as the excitation of an electron from the negative energy continuum to a bound state, this cross section is equal to the usual photoabsorption cross section given, for instance, by Bethe and Salpeter and by Merzbacher; introducing the Compton length, it becomes

$$\sigma_{JLM} = \frac{4\pi^2\alpha}{k_0} |M|^2 \lambda_c^2 \tag{45}$$

where as in section 3.5.2 k_0 denotes the energy of the incoming photon - the positron will be emitted with the energy $k_0 - E_b$. M is, of course, to be understood as a partial wave version of equation (2), that is,

$$M = M_{\lambda JLM} = \int d^3\mathbf{r} \psi_b^\dagger(\mathbf{r}) \boldsymbol{\alpha} \cdot \mathbf{e}_\lambda e^{i\mathbf{k_0}\cdot\mathbf{r}} \psi_{JLM}(\mathbf{r}), \tag{46}$$

where ψ_{JLM} is the appropriate negative continuum wave function as described in section 3.3. It should be noted that the expression (45) for the partial wave cross sections may also be derived from the expression for the differential cross section; we shall actually do that in the next section.

4.2 Differential Cross Sections

In this case, the cross section must be calculated utilising the scattering states (21), where as remarked in section 3.1 we must perform the substitutions (12) and the minus sign should be chosen in (21).

The scattering state to be used is thus

$$\Psi^-_{\mathbf{p}} = 4\pi\sqrt{\frac{\pi}{2Ep}}\sum_{JLM} i^L e^{-i\delta_\kappa} < L\tfrac{1}{2}(M+\tfrac{1}{2}\sigma)\tfrac{1}{2}\sigma|L\tfrac{1}{2}JM > Y^*_{L,M+\frac{1}{2}\sigma}(-\hat{\mathbf{p}}) \qquad (47)$$

The differential cross section is now obtained by use of the formula (42) which we derived in section 3.5.2, that is,

$$\sigma = \frac{\alpha}{2\pi k_0}\int d^3\mathbf{p}\delta(k_0 - E - E_b)|\tilde{M}|^2$$

where E denotes the energy of the emitted positron, E_b the bound state energy and the $\tilde{M}$ has got a tilde in order to distinguish it from the partial wave matrix elements mentioned above.

$\tilde{M}$ is thus the matrix element of the bound state and the scattering state, explicitly

$$\tilde{M} = \int d^3\mathbf{r}\psi^\dagger_b(\mathbf{r})\boldsymbol{\alpha}\cdot\mathbf{e}_\lambda e^{i\mathbf{k_0}\cdot\mathbf{r}}\Psi^-_{\mathbf{p}}$$

$$= 4\pi\sqrt{\frac{\pi}{2Ep}}\sum_{JLM} i^L e^{-i\delta_\kappa} < L\tfrac{1}{2}(M+\tfrac{1}{2}\sigma)\tfrac{1}{2}\sigma|L\tfrac{1}{2}JM > Y^*_{L,M+\frac{1}{2}\sigma}(-\hat{\mathbf{p}})M_{\lambda JLM}. \quad (48)$$

Once more, $M_{\lambda JLM}$ are the partial wave matrix elements already mentioned. The next section will be dedicated to the exact calculations of these matrix elements.

We may check the consistency between the approaches for obtaining the partial wave and differential cross sections by deriving (45) directly from (42). Squaring and inserting in expression (42) above yields

$$\frac{d\sigma}{d\Omega} = \frac{\alpha pE}{2\pi k_0}|\tilde{M}|^2 \qquad (49)$$

$$= \frac{\alpha pE}{2\pi k_0}\left[\frac{16\pi^3}{2Ep}|\sum_{JLM} i^L e^{-i\delta_\kappa} < L\tfrac{1}{2}(M+\tfrac{1}{2}\sigma)\tfrac{1}{2}\sigma|L\tfrac{1}{2}JM > Y^*_{L,M+\frac{1}{2}\sigma}(-\mathbf{p})M_{\lambda JLM}|^2\right].$$

$$= \frac{4\pi^2\alpha}{k_0}|\sum_{JLM} i^L e^{-i\delta_\kappa} < L\tfrac{1}{2}(M+\tfrac{1}{2}\sigma)\tfrac{1}{2}\sigma|L\tfrac{1}{2}JM > Y^*_{L,M+\frac{1}{2}\sigma}(-\mathbf{p})M_{\lambda JLM}|^2$$

In order to obtain the cross section for scattering into a particular angle it is necessary to average over the photon helicities λ and sum over the positron helicities σ. As mentioned above, we may obtain the total cross section given by (45) and (44). To show this, we will combine equations (49) and (43) to obtain

$$\sigma = \tfrac{1}{2}\sum_{\lambda,\sigma}\frac{4\pi^2\alpha}{k_0}\int d\Omega\sum_{JLM}\sum_{J'L'M'} i^{L-L'}e^{i(\delta_{\kappa'}-\delta_\kappa)} < L\tfrac{1}{2}(M+\tfrac{1}{2}\sigma)\tfrac{1}{2}\sigma|L\tfrac{1}{2}JM > \times \quad (50)$$

$$\times < L'\tfrac{1}{2}J'M'|1\tfrac{1}{2}(M'+\tfrac{1}{2}\sigma)\tfrac{1}{2}\sigma > Y^*_{L,M+\frac{1}{2}\sigma}(-\hat{\mathbf{p}})Y_{L',M'+\frac{1}{2}\sigma}(-\hat{\mathbf{p}})M_{\lambda JLM}M^*_{\lambda J'L'M'}.$$

Since the total cross section cannot depend on the photon helicity, this average is easily done (multiply by two to get the two possibilities, then divide by two to do the average ...). The integration over all angles is equivalent to computing the scalar product of two spherical harmonics and yields $\delta_{LL'}\delta_{MM'}$. Then, as a result of the completeness relation for the Clebsch-Gordan coefficients the sum over σ may be carried out by replacing these coefficients by $\delta_{JJ'}$. The primed summation thus becomes trivial, and all in all we have

$$\sigma = \frac{4\pi^2\alpha}{k_0}\sum_{JLM}|M_{JLM}|^2,$$

which (as it should be) is exactly the result (45) we derived in the previous subsection.

So having obtained the expressions for the total and differential cross sections in terms of the partial wave matrix elements (46), the only thing we need in order to start getting some actual results is a prescription for actually computing these matrix elements. To this, the next section will be devoted.

5 Exact Calculation of Matrix Elements

In this section, we wish to calculate the matrix elements between bound states and spherical waves, the photon being represented by a plane wave, as discussed in section 3.5.2. As we recall, this matrix element was given by (46)

$$M = \int d^3\mathbf{r}\psi_b^\dagger(\mathbf{r})\boldsymbol{\alpha}\cdot\mathbf{e}_\lambda e^{i\mathbf{k_0}\cdot\mathbf{r}}\psi_E(\mathbf{r}).$$

where the bound state is characterised by the quantum numbers j,l and m, while the positron is represented by a negative energy solution to the Dirac equation for the Coulomb potential as given in section 3.3, characterised by the energy E and the quantum number J,L and M. These matrix elements are needed for the calculation of cross sections in the next section.

It should be noted that it is not necessary to read this section in great detail in order to read the following sections; the calculations are given in elaborate and perhaps even overwhelming detail. It has been found natural, however, to include in the present thesis a detailed account of the steps that lead to the results as well as the results themselves.

In the following calculation, let us choose the polarisation vector $\mathbf{e}_\lambda$ to correspond to a photon of positive helicity, that is, $\lambda = +$. Inserting equation (13) in the expression for the matrix element then yields ($\kappa' = \mp(j+\frac{1}{2})$)

$$M = i\int d^3\mathbf{r}e^{i\mathbf{k_0}\cdot\mathbf{r}}[g_{\kappa'}(r)f_\kappa(r)\Omega^\dagger_{jlm}\sigma_+\Omega_{JL'M} - f_{\kappa'}(r)g_\kappa(r)\Omega^\dagger_{jl'm}\sigma_+\Omega_{JLM}], \quad (51)$$

where

$$\sigma_+ = \begin{pmatrix} 0 & \sqrt{2} \\ 0 & 0 \end{pmatrix} \quad (52)$$

In order to do the integral $\mathbf{k_0}$ is assumed to be in the direction of the z-axis, allowing us to write $\mathbf{k_0} = k_0\mathbf{e_z}$ and use the expansion

$$e^{ik_0z} = \sum_{k=0}^{\infty} i^k\sqrt{4\pi(2k+1)}j_k(k_0r)Y_{k0}(\vartheta,\phi), \quad (53)$$

where j_k as usual denotes a spherical Bessel function. Inserting this and exchanging the order in which we $\int$ and $\sum$ enables us to express the matrix element as a sum of integrals:

$$M = \sum_{k=0}^{\infty} i^{k+1}[I_1^{(k)} - I_2^{(k)}] \quad (54)$$

where

$$I_1^{(k)} = \sqrt{4\pi(2k+1)}\int_0^\infty drr^2 j_k(k_0r)g_{jl}(r)f_{JL'}(r)\int d\Omega\Omega^\dagger_{jlm}\sigma_+\Omega_{JL'M}Y_{k0} \quad (55)$$

while of course

$$I_2^{(k)} = \sqrt{4\pi(2k+1)}\int_0^\infty drr^2 j_k(k_0r)f_{jl'}(r)g_{JL}(r)\int d\Omega\Omega^\dagger_{jl'm}\sigma_+\Omega_{JLM}Y_{k0}. \quad (56)$$

Only a finite amount of the terms in (54) do in fact contribute to the sum: the rest vanish due to the angular selection rules: as an example, the contributions from I_1 are only nonzero if

$$|l - L'| \leq k \leq l + L'.$$

We may now separate the radial and angular integrals by defining

$$I_i^{(k)} = I_{i,\vartheta}^k I_{i,r}^{(k)}, \qquad i = 1, 2 \tag{57}$$

The sum over k may be performed as soon as the angular integration is done. Having done this we are left with a (finite) number of radial integrals, the calculation of which we shall subsequently address.

5.1 Angular Integrals

According to the definition in (57) above the angular integrals to be performed are

$$I_{1,\vartheta}^{(k)} = \sqrt{4\pi(2k+1)} \int d\Omega \Omega_{jlm}^\dagger \sigma_+ \Omega_{JL'M} Y_{k0}, \tag{58}$$

$$I_{2,\vartheta}^{(k)} = \sqrt{4\pi(2k+1)} \int d\Omega \Omega_{jl'm}^\dagger \sigma_+ \Omega_{JLM} Y_{k0}$$

The quantity $\Omega_{jlm}^\dagger \sigma_+ \Omega_{JL'M}$ depends on whether $j = l \pm \frac{1}{2}$, and whether $J = L \pm \frac{1}{2}$. If we recall that σ_+ is given by (52), insertion of the explicit expressions (14) for the Ω's yields

$$\Omega_{jlm}^\dagger \sigma_+ \Omega_{JL'M} = \frac{C_{jlm}^{JLM}}{\sqrt{(2l+1)(2L+1)}} Y_{l,m-\frac{1}{2}}^* Y_{L',M+\frac{1}{2}} \tag{59}$$

where the C's arise in connection with products of Clebsch-Gordan coefficients and are conveniently defined by

$$C_{jlm}^{JLM} = \begin{cases} \sqrt{2(j+m)(J-M)} & j = l + \frac{1}{2}, J = L + \frac{1}{2} \\ \sqrt{2(j+m)(J+M+1)} & j = l + \frac{1}{2}, J = L - \frac{1}{2} \\ -\sqrt{2(j-m+1)(J-M)} & j = l - \frac{1}{2}, J = L + \frac{1}{2} \\ -\sqrt{2(j-m+1)(J+M+1)} & j = l - \frac{1}{2}, J = L - \frac{1}{2} \end{cases} \tag{60}$$

With these relations in place we may write

$$I_{1,\vartheta}^{(k)} = \sqrt{\frac{4\pi(2k+1)}{(2l+1)(2L+1)}} C_{jlm}^{JLM} \int d\Omega Y_{l,m-\frac{1}{2}}^* Y_{L',M+\frac{1}{2}} Y_{k0} \tag{61}$$

Now we use the formula for integrals of products of three spherical harmonics (of this, and $3j$-symbols in general, see Weissbluth, chapter 1 or Sobel'man, who gives more special formulas for $3j$-symbols)

$$\int d\Omega Y^*_{lm} Y_{LM} Y_{k\mu} = (-1)^m \sqrt{\frac{(2l+1)(2L+1)(2k+1)}{4\pi}} \begin{pmatrix} l & L & k \\ -m & M & \mu \end{pmatrix} \begin{pmatrix} l & L & k \\ 0 & 0 & 0 \end{pmatrix} \tag{62}$$

Consequently, we may obtain the result by writing (the result for I_2 may be obtained merely by letting $l \to l'$,$L' \to L$)

$$I^{(k)}_{1,\vartheta} = (-1)^{m-\frac{1}{2}} (2k+1) C^{JL'M}_{jlm} \begin{pmatrix} l & L' & k \\ -m+\frac{1}{2} & M+\frac{1}{2} & 0 \end{pmatrix} \begin{pmatrix} l & L' & k \\ 0 & 0 & 0 \end{pmatrix} \tag{63}$$

From the selection rules for the Clebsch-Gordan coefficients one may note that this matrix element vanishes identically unless

- $M = m - 1$
- $|l - L'| \leq k \leq l + L'$ or $|l' - L| \leq k \leq l' + L$
- $l + L' + k$ or $l' + L + k$ is an even number

In the present work we are only concerned with processes in which the bound state is an s- or p-state.

In the actual calculation, it is practical to write out explicitly the $3j$-symbols rather than calculating them (on a computer) by a more general procedure. As an example, the matrix element for s- (and $p_{\frac{1}{2}}$-) states will be written down explicitly in terms of the radial integrals of (57), while for $p_{\frac{3}{2}}$-states expressions for the necessary $3j$-symbols will be given.

5.1.1 s- and $p_{\frac{1}{2}}$-states

We begin by noting that the case of $s_{\frac{1}{2}}$- and $p_{\frac{1}{2}}$-states are completely equivalent, since according to equation (13) the matrix elements will be completely equivalent: The $p_{\frac{1}{2}}$-state has $l = 1$ and $l' = 0$ as opposed to the $l = 0$ and $l' = 1$ of the s-state - comparing with equations (54)-(57), wee see that the result for the $p_{\frac{1}{2}}$-states may be obtained by merely substituting I_1 for I_2, L for L' and *vice versa*.

To return to the s-states, the relevant $3j$-symbols for I_1 turn out to be

$$\begin{pmatrix} 0 & L' & k \\ -m+\frac{1}{2} & m-\frac{1}{2} & 0 \end{pmatrix}, \qquad \begin{pmatrix} 0 & L' & k \\ 0 & 0 & 0 \end{pmatrix} \tag{64}$$

and, similarly, for I_2

$$\begin{pmatrix} 1 & L & k \\ -m+\frac{1}{2} & m-\frac{1}{2} & 0 \end{pmatrix}, \qquad \begin{pmatrix} 1 & L & k \\ 0 & 0 & 0 \end{pmatrix} \tag{65}$$

where we have used, that $M = m - 1$. m may of course only assume the values $\pm\frac{1}{2}$, which means that M is -$\frac{1}{2}$ or -$\frac{3}{2}$. Thus, we need the formulae

$$\begin{pmatrix} j_1 & j_2 & 0 \\ -m_1 & m_2 & 0 \end{pmatrix} = (-1)^{j_1-m_2}\frac{\delta_{j_1 j_2}\delta_{m_1 m_2}}{\sqrt{2j_1+1}}, \tag{66}$$

$$\begin{pmatrix} j+1 & j & 1 \\ m & -m-1 & 1 \end{pmatrix} = (-1)^{j-m-1}\sqrt{\frac{(j-m)(j-m+1)}{(2j+3)(2j+2)(2j+1)}}$$

$$\begin{pmatrix} j+1 & j & 1 \\ m & -m & 0 \end{pmatrix} = (-1)^{j-m-1}\sqrt{\frac{(j+m+1)(j-m+1)}{(2j+3)(j+1)(2j+1)}}$$

Insertion of these in the expression (63) gives us

$$I^{(k)}_{1,\vartheta}(m=\tfrac{1}{2}) = (-1)^{m-\frac{1}{2}}C^{JL'M}_{\frac{1}{2}0\frac{1}{2}}\delta_{kL'} = \sqrt{2J+1}\delta_{kL'}, \qquad I^{(k)}_{1,\vartheta}(m=-\tfrac{1}{2}) = 0 \tag{67}$$

$$I^{(k)}_{2,\vartheta}(m=\tfrac{1}{2}) = -\sqrt{2J+1}\frac{L+1}{2L+1}\delta_{k,L+1} - \sqrt{2J+1}\frac{L}{2L+1}\delta_{k,L-1}, \qquad J = L \pm \tfrac{1}{2} \tag{68}$$

$$I^{(k)}_{2,\vartheta}(m=-\tfrac{1}{2}) = -\frac{\sqrt{(2J+3)L(L+1)}}{2L+1}[\delta_{k,L+1} - \delta_{k,L-1}], \qquad J = L + \tfrac{1}{2} \tag{69}$$

$$= -\frac{\sqrt{(2J-1)L(L+1)}}{2L+1}[\delta_{k,L+1} - \delta_{k,L-1}], \qquad J = L - \tfrac{1}{2}$$

The summation over k may now be performed to yield (finally) the result for the matrix elements for s-states ($J = \pm\frac{1}{2}$)

$$M = i^{L'+1}\sqrt{2J+1}\left[I^{L'}_{1,r} \mp \frac{L-1}{2L+1}I^{(L-1)}_{2,r} \pm \frac{L}{2L+1}I^{(L+1)}_{2,r}\right], \qquad m = +\tfrac{1}{2} \tag{70}$$

$$= i^{L}\sqrt{2J+1\pm 2}\frac{\sqrt{L(L+1)}}{2L+1}\left[I^{(L+1)}_{2,r} + I^{(L-1)}_{2,r}\right], \qquad m = -\tfrac{1}{2}$$

As remarked above, the result for the $p_{\frac{1}{2}}$-states follow from interchanging L and L', I_1 and I_2 and, needless to say, using the appropriate radial integrals.

5.1.2 $p_{\frac{3}{2}}$-states

For these states we will not write down the results that explicitly, but limit ourselves to giving the most important information needed in order to do the actual calculation.
For $p_{\frac{3}{2}}$ the angular integral is found by insertion in the formula (63) above:

$$I^{(k)}_{1,\vartheta} = (-1)^{m-\frac{1}{2}}(2k+1)C^{JL'm-1}_{\frac{3}{2}1m}\begin{pmatrix} 1 & L' & k \\ -m+\frac{1}{2} & m-\frac{1}{2} & 0 \end{pmatrix}\begin{pmatrix} 1 & L' & k \\ 0 & 0 & 0 \end{pmatrix} \quad (71)$$

$$I^{(k)}_{2,\vartheta} = (-1)^{m-\frac{1}{2}}(2k+1)C^{JLm-1}_{\frac{3}{2}2m}\begin{pmatrix} 2 & L & k \\ -m+\frac{1}{2} & m-\frac{1}{2} & 0 \end{pmatrix}\begin{pmatrix} 2 & L & k \\ 0 & 0 & 0 \end{pmatrix} \quad (72)$$

This may be computed by use of the relations

$$\begin{pmatrix} j+2 & j & 2 \\ m & -m & 0 \end{pmatrix} = (-1)^{j-m}\left[\frac{6(j+m+2)(j+m+1)(j-m+2)(j-m+1)}{(2j+5)(2j+4)(2j+3)(2j+2)(2j+1)}\right]^{\frac{1}{2}} \quad (73)$$

$$\begin{pmatrix} j+2 & j & 2 \\ m & -m-1 & 1 \end{pmatrix} = 2(-1)^{j-m}\left[\frac{(j+m+2)(j-m+2)(j-m+1)(j-m)}{(2j+5)(2j+4)(2j+3)(2j+2)(2j+1)}\right]^{\frac{1}{2}} \quad (74)$$

$$\begin{pmatrix} j+2 & j & 2 \\ m & -m-2 & 2 \end{pmatrix} = (-1)^{j-m}\left[\frac{(j-m-1)(j-m)(j-m+1)(j-m+2)}{(2j+5)(2j+4)(2j+3)(2j+2)(2j+1)}\right]^{\frac{1}{2}} \quad (75)$$

together with the symmetry properties of the $3j$-symbols, described in Weissbluth, chapter 1. The actual calculation would of course be the same as for the s-state, only now we have four possible values of the quantum number m and some slightly more complicated $3j$-symbols.

5.2 Radial Integrals: Initial Remarks

Let us start by considering the radial integrals from (57) for any given bound state and thus characterise the bound state quantum numbers by b. Our radial integrals then become

$$I^{(k)}_{1,r} = \int_0^\infty dr r^2 j_k(k_0 r) g_b(r) f_\kappa(r) \quad (76)$$

$$I^{(k)}_{2,r} = \int_0^\infty dr r^2 j_k(k_0 r) f_b(r) g_\kappa(r) \quad (77)$$

Let us examine these closer. The radial continuum waves are as in section 3 given by

$$g(r) = N_g(2pr)^{s-1}\mathrm{Re}\{e^{i\delta}(s+i\eta)e^{-ipr}F(s+1+i\eta, 2s+1, 2ipr)\} \quad (78)$$

$$f(r) = N_f(2pr)^{s-1}\mathrm{Im}\{e^{i\delta}(s+i\eta)e^{-ipr}F(s+1+i\eta,2s+1,2ipr)\} \tag{79}$$

Now, if (78) is inserted in (56) and (5.2) in (55) and constant factors are taken outside the integral, this may be written

$$I_{1,r}^{(k)} = N_f(2p)^{s-1}\mathrm{Im}\left\{e^{i\delta}(s+i\eta)\int_0^\infty drr^{s+1}e^{-ipr}j_k(k_0r)g_b(r)F(s+1+i\eta,2s+1,2ipr)\right\} \tag{80}$$

$$I_{2,r}^{(k)} = N_g(2p)^{s-1}\mathrm{Re}\left\{e^{i\delta}(s+i\eta)\int_0^\infty drr^{s+1}e^{-ipr}j_k(k_0r)f_b(r)F(s+1+i\eta,2s+1,2ipr)\right\}$$

With this result and the expression (63) for the angular integrals the matrix elements corresponding to all bound states may be calculated. Since we are only concerned with the cases corresponding to a bound state in the K- or L-shell, these will be the only ones considered here; it would, as a matter of fact, be possible to express the degenerate hypergeometric function of the bound state wave functions by its expansion or in terms of Laguerre polynomials and thus with the aid of the techniques presented below arrive at an analytical expression for the matrix element of *any* bound state. Such an expression would, however, be so complicated that it has been deemed unnecessary for the present purpose.

Actually, it turns out that the integrals (80) always involve sums of integrals of the same type, since the bound state wave functions are of the type

(a polynomium) times r^{s-1} times (an exponential).

And therefore we will start focusing on the ground state integrals, since this will demonstrate all nontrivial aspects of the calculations; when this is done, it will be a relatively easy matter to write down the equivalent expressions for the L-shell.

5.3 Radial Integrals for the Ground State

As mentioned, this is the simplest case. Inserting the ground state wave function (25) in (80) above, we obtain

$$I_{1,r}^{(k)} = N_f N_0(2p)^{s-1}\mathrm{Im}\left\{e^{i\delta}(s+i\eta)\int_0^\infty drr^{s+s_{1s}}e^{-(\alpha Z+ip)r}j_k(k_0r)F(s+1+i\eta,2s+1,2ipr)\right\}, \tag{81}$$

$$= N_f N_0(2p)^s\mathrm{Im}\{e^{i\delta}(s+i\eta)K(s,s_{1s},k,\alpha Z,p,k_0)\}$$

and, similarly, for I_2,

$$I_{2,r}^{(k)} = -N_g N_0\sqrt{\frac{1-s_{1s}}{1+s_{1s}}}(2p)^{s-1}\mathrm{Re}\left\{e^{i\delta}(s+i\eta)K(s,s_{1s},k,\alpha Z,p,k_0)\right\}. \tag{82}$$

It is thus clear that calculating the radial integral for all k is equivalent to calculating the integral

$$K(s,s_b,k,p_0,p,k_0) = \int_0^\infty drr^{s+s_b}e^{-(p_0+ip)r}j_k(k_0r)F(s+1+i\eta,2s+1,2ipr) \tag{83}$$

As a matter of fact, various approaches may be taken (and have been taken) in order to evaluate this integral. The approach to be taken here is similar to the method of Øverbø *et al* and was also used by Alling & Johnson as well as by Johnson *et al.* It consists of expressing the spherical Bessel function of the integrand as a finite sum of exponentials, that is,

$$j_k(z) = \sum_{\iota=0}^{k} \frac{(k+\iota)!}{\iota!(k-\iota)!} i^{k+1-\iota}(2z)^{-\iota-1}[(-1)^{k+1-\iota}e^{iz} + e^{-iz}] \tag{84}$$

Inserting this expression in our K above (and taking constant factors outside the integral), (83) reduces to

$$K(s, s_b, k, p_0, p, k_0) = \sum_{\iota=0}^{k} \frac{(k+\iota)!}{\iota!(k-\iota)!} i^{k+1-\iota}(2k_0)^{(-\iota-1)}[(-1)^{k+1-\iota}\tilde{I}^- + \tilde{I}^+] \tag{85}$$

where we have defined

$$\tilde{I}^{\pm} = \int_0^\infty dr r^{s+s_b-1-\iota} e^{-(p_0+i(p\pm k_0))r} F(s+1+i\eta, 2s+1, 2ipr)$$

We will first examine $\tilde{I}^+$, since it turns out to be simplest. First of all, we introduce the integral representation of the confluent hypergeometric function and write

$$F(a,b,z) = \frac{\Gamma(b)}{\Gamma(a)\Gamma(b-a)} \int_0^1 du u^{a-1}(1-u)^{b-a-1}e^{zu} \tag{86}$$

But this yields

$$\tilde{I}^+ = \frac{\Gamma(2s+1)}{\Gamma(s+1+i\eta)\Gamma(s-i\eta)} \int_0^1 du u^{s+i\eta}(1-u)^{s-i\eta-1} \int_0^\infty dr r^{s+s_b-1-\iota} e^{-(p_0+i[p(1-2u)+k_0]r)} \tag{87}$$

Upon elementary substitutions the r integral will just yield a Γ function[4]

$$\tilde{I}^+ = \frac{\Gamma(s+s_b-\iota)\Gamma(2s+1)}{\Gamma(s+1+i\eta)\Gamma(s-i\eta)} \int_0^1 du u^{s+i\eta}(1-u)^{s-i\eta-1} \left[p_0 + i\left[p(1-2u)+k_0\right]\right]^{\iota-s-s_b}. \tag{88}$$

If we now rewrite the factor in the integrand involving p,p_0 and k_0, making use of the simple algebraic fact

$$p_0 + i\left[p(1-2u)+k_0\right] = (p_0 + i(p+k_0))(1 - \frac{2pu}{p+k_0-ip_0}), \tag{89}$$

[4]But one might look one more time on the integral in (87) and note that this integral is only convergent if $s + s_b - \iota < 0$. If not, it is divergent. As a matter of fact, this condition is not fulfilled for all the integrals appearing in the sum (85). The divergence is artificial and is introduced by the expansion (84). This is also discussed by Øverbø and by Alling and Johnson. The solution is to multiply the integrand by a factor r^m, m being a real number chosen large enough for the integral to exist: after that, m is set equal to zero.

the remaining integral over u may conveniently be expressed in terms of the integral representation of the (non-degenerate) hypergeometric function

$$F(a,b;c;z) = {}_2F_1(a,b;c;z) = \frac{\Gamma(c)}{\Gamma(a)\Gamma(c-a)} \int_0^1 du u^{a-1}(1-u)^{c-a-1}(1-zu)^{-b}. \tag{90}$$

Upon comparison, we obviously have

$$\tilde{I}^+ = \frac{\Gamma(s+s_b-\iota)}{[p_0+i(p+k_0)]^{s+s_b-\iota}} F(s+1+i\eta, s+s_b-\iota; 2s+1; \frac{2p}{p+k_0-ip_0}) \tag{91}$$

As for $\tilde{I}^-$, we will first apply the Kummer transformation $F(a,b,z) = e^z F(b-a,b,-z)$, as a consequence of which we may write

$$\tilde{I}^- = \frac{\Gamma(s+s_b-\iota)}{[p_0-i(p+k_0)]^{s+s_b-\iota}} F(s-i\eta, s+s_b-\iota; 2s+1; \frac{2p}{p+k_0+ip_0}) \tag{92}$$

But now we may sum up the result of our present effort, a result which is of considerable use in evaluating the radial integrals for *all* bound states:

$$\begin{aligned} K(s,s_b,k,p_0,p,k_0) &= \int_0^\infty dr r^{s+s_b} e^{-(p_0+ip)r} j_k(k_0 r) F(s+1+i\eta, 2s+1, 2ipr) \\ &= \sum_{\iota=0}^{k} \frac{(k+\iota)!}{\iota!(k-\iota)!} i^{k+1-\iota} (2k_0)^{(-\iota-1)} \left[(-1)^{k+1-\iota}\tilde{I}^- + \tilde{I}^+\right] \end{aligned} \tag{93}$$

where

$$\tilde{I}^+ = \frac{\Gamma(s+s_b-\iota)}{[p_0+i(p+k_0)]^{s+s_b-\iota}} F(s+1+i\eta, s+s_b-\iota; 2s+1; \frac{2p}{p+k_0-ip_0})$$

while

$$\tilde{I}^- = \frac{\Gamma(s+s_b-\iota)}{[p_0-i(p+k_0)]^{s+s_b-\iota}} F(s-i\eta, s+s_b-\iota; 2s+1; \frac{2p}{p+k_0+ip_0}).$$

And now the radial integrals for the ground state are simply given by (81) and (82), where K is known from equation (93).
As in Sørensen and Belkacem we might arrive at the very same result by using, not the integral representation for the confluent hypergeometric function but the series expansion. This would lead to the same result, with the hypergeometric function expressed by the Gauss series. The present approach is more general, however, since it is immediately valid in the case $|\frac{2p}{p+k_0+ip_0}| > 1$, where the Gauss series fails to converge.

This makes no difference at all for the calculations considered in the present thesis, but for calculations involving the photoelectric effect the Gauss series would be inapplicable. Indeed, the only reason for introducing the Kummer transformation in (92) was that this step gives the expressions a form that enables us to use the Gauss series.

5.4 Radial Integrals for the L shell

Here we must insert the wave functions of section 3.4 in equation (80). We get, for the $2p_{\frac{3}{2}}$ state:

$$I_{1,r}^{(k)} = N_f(2p)^{s-1}\mathrm{Im}\left\{e^{i\delta}(s+i\eta)\int_0^\infty drr^{s+1}e^{-ipr}j_k(k_0r)g_{2p_{\frac{3}{2}}}(r)F(s+1+i\eta,2s+1,2ipr)\right\} \tag{94}$$

$$= N_fN_{2p_{\frac{3}{2}}}(2p)^{s-1}\mathrm{Im}\left\{e^{i\delta}(s+i\eta)K(s,s_{p_{\frac{3}{2}}},k,\tfrac{1}{2}\alpha Z,p,k_0)\right\},$$

$$I_{2,r}^{(k)} = -\sqrt{\frac{1-E_{2p_{\frac{3}{2}}}}{E_{2p_{\frac{3}{2}}}+1}}N_gN_{2p_{\frac{3}{2}}}(2p)^{s-1}\mathrm{Re}\left\{e^{i\delta}(s+i\eta)K(s,s_{p_{\frac{3}{2}}},k,\tfrac{1}{2}\alpha Z,p,k_0)\right\}$$

The integrals corresponding to the $2s$ and $2p_{\frac{1}{2}}$ states are more complicated but very similar, as might be expected. They have the same energy, so we may write

$$E_2 = E_{2s} = E_{2p_{\frac{1}{2}}} = \sqrt{\frac{1+s_1}{2}}, \qquad p_0 = \sqrt{\frac{1-s_1}{2}}, \qquad s_1 = \sqrt{1-\alpha^2Z^2}, \tag{95}$$

$$K_1 = K(s,s_1,k,p_0,p,k_0), K_2 = K(s,s_1+1,k,p_0,p,k_0)$$

As with the $2p_{\frac{3}{2}}$ case we merely insert in the formulae from the preceding sections, and get for the $2s$-state:

$$I_{1,r}^{(k)} = N_fN_{2s}(2p)^{s-1}\mathrm{Im}\left\{e^{i\delta}(s+i\eta)\left[2E_2K_1 - \frac{2p_0}{2E_2-1}K_2\right]\right\} \tag{96}$$

$$I_{2,r}^{(k)} = -\sqrt{\frac{1-E_2}{E_2+1}}N_gN_{2s}(2p)^{s-1}\mathrm{Re}\left\{e^{i\delta}(s+i\eta)\left[(2E_2+2)K_1 - \frac{2p_0}{2E_2-1}K_2\right]\right\}$$

And, very similarly for $2p_{\frac{1}{2}}$:

$$I_{1,r}^{(k)} = N_fN_{2p_{\frac{1}{2}}}(2p)^{s-1}\mathrm{Im}\left\{e^{i\delta}(s+i\eta)\left[(2E_2-2)K_1 - \frac{2p_0}{2E_2+1}K_2\right]\right\} \tag{97}$$

$$I_{2,r}^{(k)} = -\sqrt{\frac{1-E_2}{E_2+1}}N_gN_{2p_{\frac{1}{2}}}(2p)^{s-1}\mathrm{Re}\left\{e^{i\delta}(s+i\eta)\left[2E_2K_1 - \frac{2p_0}{2E_2+1}K_2\right]\right\}$$

6 Previous Work on Bound-Free Transitions: A Brief History

The aim of the present section is to give a brief account of previous research on the subject, while at the same time reviewing the simplifications that arise in the case of high energies and low target charges.
Regarding the former, we will give a history of the research done on the four processes mentioned in section 2 - apart from the work of Aste *et al*, the most interesting work was done on the photoelectric effect and single-photon annihilation.

In order to limit the extent of the treatment, we will only discuss the photoelectric effect in the relativistic regime, just as we shall only be concerned with work using the Coulomb field for the target ion, since this is especially relevant for the subject matter of the present thesis - in the case of photoelectric effect or single-quantum annihilation, screening effects are important, but not for bound-free pair production.

As for the latter aim, it is well worth noting that the exact, analytical expressions for cross sections and matrix elements we obtained in the preceding sections are not convenient for the calculation of high-energy cross sections, since more and more terms of the partial wave expansion contribute, and each of these terms become increasingly labourious to calculate as the angular momentum quantum numbers increase.
On the other hand, in the limiting cases of low target charge (Z) and high photon energy a number of approximations become valid, yielding expressions which may be computed with considerably less effort. We will focus on four such possibilities.
Extensive calculations will, on the other hand, not be attempted - rather, we shall give an outline of how they *might* have been done.

6.1 The Born Approximation: Plane Waves

The quantum theoretical study of the processes described in section 2 and characterised by the electromagnetic matrix element (2) may be said to have started in 1905, where Einstein published his paper on the photoelectric effect, introducing the quantisation or corpuscular nature of light.

After the advent of quantum mechanics proper, the processes of excitation and photoelectric effect were investigated by a number of authors. The first fully relativistic treatment of the photoelectric effect was given by Sauter, who obtained the K-shell cross section in the Born approximation.

Sauter was, it may be added, probably the first author to refer to the process treated in the present thesis, since he notes that

> Die Durchführung der Störungsrechnung nach den üblichen Methoden

ergibt zwei Resonanznenner an den beiden Stellen

$$E = E_1 + h\nu \text{ und } E = E_1 - h\nu$$

(..) Während für den hier ausschließlich behandelten Fall

$$h\nu > E_0 - E_1$$

(E_0 = Ruheenergie) die erste Resonanzstelle in das Gebiet des positiv kontinuierlichen Energiespektrums fällt und den für den Photoeffekt maßgebenden Beitrag zur gestörten Funktion liefert, entspricht der zweiten Resonanzstelle entweder überhaupt kein reeller Energiewert oder, für den Fall

$$h\nu > E_0 + E_1$$

ein solcher des negativ kontinuierlichen Energiespektrums.

The existence of the positron was not experimentally confirmed at the time, and Dirac's theoretical prediction apparently not universally accepted [5], so he reached the unfortunate conclusion that

> Diese zweite mögliche Resonanzstelle führt zu physikalisch absurden Resultaten und soll daher unberücksichtigt bleiben. (p. 456-57)

Sauter, as it happens, obtained his result by some quite complicated calculations, departing from the exact partial wave expansion which he then simplified, so that he first set $\sqrt{\kappa^2 - (\alpha Z)^2} = L + 1$ or L for $L = J \pm 1$, respectively, in the terms of the partial wave expansion. Afterwards, he expanded in powers of the Sommerfeld parameter $\eta = \frac{\alpha Z E}{p}$ and was able to perform the sum over angular momentum quantum numbers analytically.
His result, however, may be obtained by the simplest possible approach, that is, representing the final state positron by a plane wave using the spinor (8) with the substitutions (12)[6].

For bound-free pair production this method was applied by Munger *et al*, who used it for the calculation of cross sections for the production of anti-hydrogen in proton-antiproton collisions in the storage ring at Fermi-lab.
This method cannot be expected to give good results if the energy is too low or the target charge too high, since it does not include the characteristic r-dependent phase shift characteristic for Coulomb waves.

[5] It must be admitted, that Dirac's prediction of the existence of the positron was accompanied by an attempt to identify the proton with the positron and to find reasons that the holes would appear to be 1836 times as massive as the electrons, which made his theory less convincing. Indeed, Oppenheimer calculated that if this were true, all matter would annihilate with a lifetime of $10^{-10}s$. Years later, Gell-Mann reportedly asked Dirac why he did not predict the positron right away, and received the answer: "Pure cowardice."

[6] This was, I believe, first shown by Fano *et al* in 1959.

Let us outline how such a calculation might be done (similar calculations are given by a number of authors, for instance Olsen and Akhiezer & Berestetskii). For this purpose, it is convenient to write the ground state wave function as

$$\psi_{1s}(\mathbf{r}) = \frac{g(r)}{\sqrt{4\pi}} \begin{pmatrix} 1 \\ i\sqrt{\frac{1-s_{1s}}{1+s_{1s}}}\boldsymbol{\sigma}\cdot\hat{\mathbf{r}} \end{pmatrix} \chi_m, \tag{98}$$

where, not surprisingly,

$$\chi_m = \begin{cases} \begin{pmatrix} 1 \\ 0 \end{pmatrix} & m = \frac{1}{2} \\ \begin{pmatrix} 0 \\ 1 \end{pmatrix} & m = -\frac{1}{2} \end{cases} \tag{99}$$

The cross section is readily found from formula (49) given in section 4.2. Since the matrix element to be calculated as mentioned above is obtained from (2),

$$M = \int d^3\mathbf{r}\psi_{1s}^{\dagger}(\mathbf{r})\boldsymbol{\alpha}\cdot e_\lambda e^{i\mathbf{k_0}\cdot\mathbf{r}}\psi_E(\mathbf{r}),$$

we may insert the wave functions and rewrite:

$$M = \chi_m^{\dagger}\left[\mathbf{I}^{+}\cdot\mathbf{e}_\lambda - i\boldsymbol{\sigma}\cdot\mathbf{I}^{-}\times\mathbf{e}_\lambda\right]\chi_\sigma(-\hat{\mathbf{p}}), \tag{100}$$

where the relation

$$(\boldsymbol{\sigma}\cdot\boldsymbol{A})(\boldsymbol{\sigma}\cdot\boldsymbol{B}) = \mathbf{A}\cdot\mathbf{B} + \mathbf{i}\boldsymbol{\sigma}\cdot\boldsymbol{A}\times\boldsymbol{B} \tag{101}$$

has been used. The calculation of the matrix element is now reduced to that of computing the integrals $\mathbf{I}^{\pm}$ of (100). These are defined by

$$\mathbf{I}^{\pm} = N_0\sqrt{\frac{E-m}{2E}}\left\{\frac{\mathbf{p}}{E-m}\int d^3\mathbf{r}r^{s_{1s}-1}e^{-\alpha Zr}e^{i\mathbf{q}\cdot\mathbf{r}} \pm \sqrt{\frac{1-s_1 s}{1+s_1 s}}\int d^3\mathbf{r}r^{s_{1s}-1}e^{-\alpha Zr}\hat{\mathbf{r}}e^{i\mathbf{q}\cdot\mathbf{r}}\right\}, \tag{102}$$

$$\hat{\mathbf{r}} = \begin{pmatrix} \sin\vartheta cos\phi \\ \sin\vartheta\sin\phi \\ \cos\vartheta \end{pmatrix}$$

where we have inserted the ground state wave function (25) and

$$\mathbf{q} = \mathbf{k_0} - \mathbf{p} \tag{103}$$

is the momentum transfer. The angular and radial parts of these integrals are easily separated, and the resulting radial integrals are not difficult to evaluate in the low-Z limit (and for high Z the plane wave approach is invalid).

The total Born approximation cross section for pair production with capture to the K-shell may be obtained by performing the appropriate substitutions in

Sauter's result for the photoelectric effect, as discussed in section 3.2.
It reads

$$\sigma_B = 4\pi\lambda_C^2\alpha(\alpha Z)^5\frac{p^3}{k_0^5}\left(\frac{4}{3}+\frac{E(E-2)}{E+1}\left[1-\frac{\ln\frac{E+p}{E-p}}{2EP}\right]\right) \tag{104}$$

In the extreme high-energy limit, this result reduces to the so-called *Sauter cross section*

$$\sigma_0 = \frac{4\pi\alpha(\alpha Z)^5}{k_0}\lambda_C^2, \qquad \alpha Z \ll 1 \wedge k_0 \gg 1 \tag{105}$$

The *differential cross section* for the K-shell photoelectric effect was also obtained by Sauter, and for bound-free pair production by unpolarised photons the result is:

$$\frac{d\sigma}{d\Omega} = \alpha(\alpha Z)^5\lambda_C^2\frac{\beta^3}{k_0^4}\frac{\sin^2\vartheta}{(1-\beta\cos\vartheta)^3}\left[E+2-\frac{2}{Ek_0(1-\beta\cos\vartheta)}\right], \tag{106}$$

where $\beta = \frac{p}{E}$ is the "velocity" of the emitted positron.

In 1959, Gavrila computed the second order Born approximation for the photoelectric effect. Although the result gives a somewhat better picture of the energy dependence, it fails to reproduce the correct high energy limit for high Z (Pratt *et al*).
Born approximation calculations for the L-shell photoelectric effect were also performed by Gavrila (1961).

6.2 Simplifying the Exact Result

As mentioned, Sauter started out with the exact wave functions and subsequently introduced some simplifications ($\sqrt{\kappa^2-(\alpha Z)^2} \to L+1$ or L and expansion in the Sommerfeld parameter) in order to evaluate the integrals and perform the sum over partial waves.

It might be feasible to make further attempts on getting a closed-form result from the exact expressions. Especially, it should be possible to obtain the correct high energy limit by making simplifications based not on the supposition that the interaction is weak, but that the energy is high. This path was taken by Hall, who assumed that the sum over partial waves might be replaced with an integral, since the angular momentum quantum numbers may "almost" be treated as a continuous variable at high energies. He reduced the photo-electric effect cross section to a double integral which, however, could not be evaluated exactly.

Instead, he made some additional approximations and arrived at the result, that the high-energy limit for our cross-section would be given by

$$\sigma = \sigma_0(\alpha Z)^{2\xi}e^{-2\alpha Z\cos^{-1}\alpha Z}, \tag{107}$$

where

$$\xi = \sqrt{1-\alpha^2Z^2}-1$$

is the negative binding energy of the 1s-electron.
This formula is quoted by some authors and said to yield good agreement with exact calculations (for instance by Heitler), so a warning may be appropriate here: Hall's formula (107) is *not* a good approximation for high Z: actually, the approximations which led to the result were wrong, as discussed by Erber and by Pratt (1960[a]).
In order to be consistent, Hall's formula should be modified by a factor of $1-\frac{4\pi\alpha Z}{15}$, so that the correct version of (107) reads

$$\sigma = \sigma_0(\alpha Z)^{2\xi} e^{-2\alpha Z \cos^{-1}\alpha Z}(1 - \frac{4\pi\alpha Z}{15}) \tag{108}$$

A similar approach was taken by Erber. These attempts to derive a useful analytical high-energy limit have largely failed, because the angular momentum integrals simply become too complicated to evaluate analytically. The problem is, of course, that on taking the limit in equation (44),

$$\sum_{JLM} \sigma_{JLM} \to \int dL \sigma_L, \qquad \sigma_L = \sum_{JM} \sigma_{JLM} \tag{109}$$

the L integral involves integrating over the arguments of Γ functions and the parameters of hypergeometric functions. Erber succeeded in making a derivation that justified the use of the Sommerfeld-Maue wave functions (to be described below) for high-energy calculations, but his results were no better than what can be obtained from (108) (Pratt 1960[a]).

6.3 Modified Plane Waves

Instead of discarding altogether the plane waves from the Born approximation calculation, one might try to include the phase modulation characteristic of the Coulomb field, thus obtaining *modified plane waves*, so that in the spinor representing the positron we let

$$e^{-i\mathbf{p}\cdot\mathbf{r}} \to e^{-i\mathbf{p}\cdot\mathbf{r} - i\alpha Z \ln(pr - \mathbf{p}\cdot\mathbf{r})} \tag{110}$$

These waves may be obtained from the Dirac equation, written in the form (6), without the vector potential. For stationary solutions it may thus be written

$$(E + i\boldsymbol{\alpha}\cdot\boldsymbol{\nabla} - V(r) - \beta m)\,\psi = 0 \tag{111}$$

where V(r) is the potential energy, $V = \pm e\phi$ for a positively (negatively) charged fermion. If we now multiply (111) by the operator

$$E - V + \beta m - i\boldsymbol{\alpha}\cdot\boldsymbol{\nabla}$$

we can utilise the anti-commutation relations for the γ matrices and finally obtain the second order equation ($p^2 = E^2 - m^2$)

$$\left(\nabla^2 + p^2 - 2EV + V^2 + i\boldsymbol{\alpha}\cdot\boldsymbol{\nabla}V\right)\psi = 0 \tag{112}$$

Since ψ is expected to behave asymptotically as a plane wave, we can make the Ansatz

$$\psi = e^{i\mathbf{p}\cdot\mathbf{r}}Fu \tag{113}$$

where u is the free-particle spinor occuring in (8). F, on the other hand, must then satisfy the differential equation

$$\left(2i\mathbf{p}\cdot\boldsymbol{\nabla} + \nabla^2 - 2EV + V^2 + i\boldsymbol{\alpha}\cdot\boldsymbol{\nabla}V\right)F = 0 \tag{114}$$

For extremely large energies we may neglect the terms containing $\boldsymbol{\alpha}\cdot\boldsymbol{\nabla}V$, V^2 and ∇^2, and the equation for F is then

$$\left(i\mathbf{p}\cdot\boldsymbol{\nabla} - EV\right)F = 0 \tag{115}$$

The solutions of this equation for incoming (outgoing) plane waves may be written for *positrons*

$$F = e^{i\eta_\pm}, \qquad \eta_\pm = \pm\alpha Z\ln(pr \mp \mathbf{p}\cdot\mathbf{r}) \tag{116}$$

For electrons, the sign of the charge must of course be reversed. This is the approach of Pratt ($1960^{a,b}$) who used it to obtain the high energy limit for the photoelectric effect cross section. The results of Pratt will be seen to be in quite good (if not exact) agreement with the numerical results based upon the exact formulae obtained in the present thesis.

And the interesting point is that since the modified plane wave represents the exact high energy limit of the Sommerfeld-Maue wave function *which* in turn is the exact high energy limit of the Coulomb-Dirac scattering states (21), it should yield the exact Z-dependence in the high energy limit; the drawback is that while the "pure" plane waves lead to matrix elements which are simple Fourier transforms, the modified plane waves give rise to some quite complicated integrals.

Pratt was thus only able to *assume* that his calculations would give the Sauter result in the low-Z limit since he was not able to perform his calculations for αZ lower than 0.1.

The results of Pratt, originally intended to estimate the high-energy limit of the atomic photoelectric effect, were also used for the process of bound-free pair production by Milstein and Strakhovenko, who used them in their estimate of the *total* (that is, including all bound states) cross section for this process in the high-energy limit.

6.4 More Elaborate Waves

A third possibility is to use a more detailed approximate wave function, such as the Sommerfeld-Maue wave function. This method was used by Bethe & Maximon for calculating pair production and bremsstrahlung cross sections, and in their book, Akhiezer & Berestetskii demonstrate how they may be used for deriving Sauter's Born approximation (as discussed in section 6.1) for the photoelectric effect.[7]

Although we will not use such wave functions in the present work, they are very much used in the literature, so a short discussion of them will be included. The point of departure is once again the stationary Dirac equation in the form (112). Using once more the Ansatz (113), for high energies we may again neglect the terms occurring in equation (114) containing V^2 and $\boldsymbol{\nabla} V$, which leaves us with the equation (see also the discussion in Pratt *et al* or Bethe and Maximon)

$$\left[2i\boldsymbol{p}\cdot\boldsymbol{\nabla}+\nabla^2-2EV\right]F=0 \tag{117}$$

The solutions to this equation corresponding to incoming (outgoing) plane waves read

$$\Psi^{\pm}_{SM}(\mathbf{r})=\Gamma(1\pm i\eta)e^{\frac{1}{2}\pi\eta}e^{i\mathbf{p}\cdot\mathbf{r}}\left[1-\frac{i}{2E}\boldsymbol{\alpha}\cdot\boldsymbol{\nabla}\right]F(\mp i\eta,1;-i(\mathbf{p}\cdot\mathbf{r}\mp pr))u \tag{118}$$

The advantage of using such wave functions lies in tractability, in the fact that it is not necessary to perform the partial wave expansion.

Under which conditions are these wave functions valid? The answer lies in the fact, that they may also be obtained from the partial wave expansion in (21) by putting $s=|\kappa|$ and performing the sum, that is, one assumes that

$$\frac{\alpha^2Z^2}{|\kappa|}\ll 1 \tag{119}$$

in the partial waves that contribute to the scattering state (Pratt *et al*, Olsen). This means that the approximation should be used with caution in the case of high target charge even at moderate to high energies (Olsen). In order to obtain the high energy limit for arbitrary charges these wave functions, therefore, seem to have no specific advantage over the modified plane waves discussed in the previous section.

6.5 Exact Coulomb Waves

Exact Coulomb waves was first used for computing the cross sections of the electrodynamical processes described by the Feynman diagram in figure 1 by a

[7] A calculation that was first done by the originators of these wave functions, Sommerfeld and Maue (Olsen).

group in England in the mid-thirties. Because of the intractability of the required partial wave expansion and the absence of modern computing facilities, these calculations were only made for a few selected energies and target charges.
Thus, the numerical results were reported for the process of single-photon pair annihilation (Jaeger & Hulme 1936[a]), for the photoelectric effect (Hulme *et al*), free-free pair production (Jaeger & Hulme 1936[b]) and a number of other processes.
The analytical method applied by them was similar to the one used in the present thesis - they evaluated the partial wave matrix elements with the aid of the partial wave expansion (53) of the incoming photon, and expressed the radial integrals in terms of hypergeometric functions.

The photoelectric effect was later studied by Hultberg *et al* who, again, took essentially the same steps as taken by us in section 5 - these authors concentrated on the K-shell cross sections. They evaluated the integral (83) by expressing the spherical Bessel function in terms of the confluent hypergeometric function - the resulting integral of an exponential, a power and two confluent hypergeometric leads to Appell functions, hypergeometric functions of two arguments. This procedure avoids the finite sum expansion (84) of the Bessel function, but the Appell functions converge very slowly, so the method applied in the present work seems easier.

In 1965, Alling & Johnson made exact calculations of the photoelectric effect cross sections for the K and L-shells for photon energies up to 1.3 MeV.
These authors, again, divide the matrix elements in radial and angular parts and evaluate the former in exactly the same fashion that we have followed in section 5. Their approach to the angular integrals was somewhat different, however, so that their expressions for the differential and total cross sections are rather more complicated than (but, of course, equivalent to) those derived in section 4.

The same year, Johnson, Buss and Carroll carried out calculations of the cross sections of single-photon pair annihilation of K-shell electrons for energies up to 3.5 electron masses.
Like Alling & Johnson, they computed the radial integrals in the same way as described in subsection 5.3. They also derived a formula for the K-shell cross section, expressed in terms of the radial integrals.
In 1967, Johnson reported calculations of the K-shell differential cross sections for the same process. This time, he chose to evaluate the radial integrals numerically; the radial continuum functions were computed by means of a predictor-corrector routine.
Differential and total cross sections for single-photon pair annihilation for the L-shell were studied by Sheth & Swamy, who reported calculations for the $2s$-subshell.
The calculations for single-photon annihilation are of some interest for us, since they may be compared directly with those for bound-free pair production, the only difference being a factor of $\frac{p^2}{k_0^2}$ (as also argued by Olsen).

Exact numerical calculations for free-free pair production were reported by Øverbø *et al* in 1968, and is described in more detail in Øverbø's treatise. The numerical technique applied by these authors was quite similar to the approach of the present thesis, with the difference that they were concerned with two continuum wave functions, and after introducing the expansion (84) of the spherical Bessel function, the radial integrals still contain the product of two hypergeometric functions - these integrals thus lead to the very slowly converging Apple functions, and so the exact numerical cross section for free-free pair production is only available up to energies of about 6 MeV (Sud & Soto Vargas).

The cross sections for bound-free pair production with capture to the K shell was examined by Aste *et al* in 1994.
For their computations, they used the formula given by Johnson *et al*; the radial integrals were calculated using the power series representation of the radial continuum wave functions (Rose).

Part II
Photon-Impact Pair Production: Results

The cross sections discussed in part I have been calculated numerically; the total K-shell cross sections have been computed for seven values of Z (1,8,26,55,79,82,92) chosen for their experimental relevance (Pb,Au,U) or applicability for comparison with perturbation theory (H,O), those of the L shell for four (1,79,82,92).
The differential cross sections have also been computed for a variety of energies and target charges, as described below.

The calculations have been performed for photon energies ranging from ~ 2 to 50 mc^2, with an expected relative accuracy of 10^{-5}. After a short discussion of the implementation of the various formulae and the problems this entails, the results will be presented and compared to previous results.

7 Implementation

For the construction of the programs to take care of the numerical calculations the *c* programming language was chosen.

The implementation of the seemingly beautiful formulae for the cross sections and matrix elements poses several nontrivial problems. First of all, the expression (93) for the crucial matrix element integral requires the implementation of the Γ function for arbitrary complex arguments[8]. Secondly, the hypergeometric function is *in general* quite difficult to calculate. In our case, we may luckily (and, it turns out, most efficiently) always use the Gauss series.

$$F(a,b;c;z) = \sum_{n=0}^{\infty} \frac{(a)_n (b)_n}{(c)_n} \frac{x^n}{n!} \tag{120}$$

where as usual

$$(a)_n = a \cdot (a+1) \cdot \ldots \cdot (a+n-1), (a)_0 = 1 \tag{121}$$

It is, however, in no way at all clear that a straightforward summation of the series occurring in (93) would be numerically stable. Indeed, an example (described in Appendix A) has been found where this series for fixed values of all parameters except k (the parameter of the spherical Bessel function, which determines the number of terms to be computed in the expression (93)) contains terms, whose magnitude increase exponentially with k, while the result *de*creases

[8] Barring 0 and negative integers, of course !

exponentially. This is obviously the same as asking for trouble. For this reason, an alternative approach has been performed, described in Appendix A, which was numerically stable for this specific example. On applying this alternative (but not very efficient) calculation procedure to the cross sections, the results agreed within the expected accuracy of the new procedure for evaluating the integrals, that is, the procedure we have actually used was acquitted of being unstable for the cross section calculations.

7.1 Structure of the Implementation

Logically, the programs consist of several parts, which therefore are spread on a similar number of files, which will be described forthwith. For readers unfamiliar with the *c* programming language, I should mention that the files whose names end in ".h" are "specification modules" containing only the headers of the functions implemented in the corresponding ".c"-file. The idea is, that the .h-file may be included by other programs which must then be linked with the compiled version of the corresponding .c-file.

- *The files compl.h and compl.c* are an implementation of complex numbers, putting a number of simple operations and functions at the disposal of the programmer, which permits the formulae derived in the previous sections to be written almost exactly as they stand.

- *The files functions.h and functions.c* contain various necessary mathematical functions, including the confluent hypergeometric function, the hypergeometric function, the gamma function, and the like. They use the complex numbers mentioned above.

- *The file K.c.* This contains the (quite straightforward) implementation of the crucial integral (83). It also contains two function K1 and K2 which are similar to K, but may be used to avoid repeated computation of the integral with the same parameters. Each of them uses a 325×325 array to store the previous results. *This data structure must always be initialised when changing to a new energy or charge.* Uses the *compl* and *functions* files.

- *The files pairs.h and pairs.c* contain functions for computing the pair production matrix elements (51) and the radial integrals (76) and (77) and the total cross section (44). The program will include up to $L = 320$ in the expansion (44), which permits an relative accuracy of 10^{-6} up to impact photon energies of about 25 MeV. These files use *K.c*, and also the *compl* and *func* files.

- *The file K-cross.c* contains a main program which prompts the user for an atomic number and a file name, and then lists the cross section on the file

specified, in the format
(Positron energy) (Cross section) (estimated error)
where the estimated error is equal to the last term added to the cross section, divided by the cross section itself. The main program (of course) uses *all* the files mentioned above.

- *The file diff.c*, which computes the angular distribution for the K-shell at a specified target charge and positron energy from the expression (49) for the differential cross section.

Similar files exist, of course, for the L-shell.

The programs are not heavily commented, but clearly written. The pair production files are written using a notation as close as possible to the one used in the present work.
The programs used to compute the K-shell total cross sections may, as an example, be found in Appendix B. An electronic version is available upon request.

7.2 Testing the Program

The implementation of the formulae were submitted to a number of tests, which will be described in the following. First of all, a few general remarks:
When testing a program, it is important to remember that tests may only prove the program to be wrong; this is because most interesting programs have *infinitely* many possible inputs, and it is only possible to actually test them on a finite subset.
Obviously, the demonstration that the program in question returns the correct result on one particular input does not allow one to conclude that it is correct for all inputs.

In principle, this may be remedied by defining a formal semantics for the programming language in question and then perform a mathematical proof that the program will yield the correct output on all possible inputs. Although there *has* been some interest in applying such techniques to real-sized programs, this is normally considered infeasible. [9]

As regards scientific computing, the situation is even worse, since we might construct a proof that a program is correct assuming we had the real numbers at our disposal. But since what we do have is only finite-precision floating point numbers, a program may be "mathematically" perfectly correct, and yet fail disastrously when applied to an actual problem (an example has already been mentioned). So a mathematical proof of the correctness of a numerical algorithm

[9] Especially, there has been some interest in applying automatic program verification in the realm of micro-chip construction, thus providing each chip with a machine-computed proof of its correctness - within limits, as many problems of that kind are undecidable. But use of these techniques might have spared a certain major micro-chip producer a serious embarrassment.

would not consist in proving that the steps performed by the computer would, idealised, give the correct result, but that the result will not deviate too much from the floating point representation of the "real" result.
So if testing is no use and mathematical proof out of reach, what *does* one do? Well, one tests the program, and tries to do it systematically. A systematic test program has three objectives:

- Internal test. The program is given a specific input, designed so that all branches are taken and all program lines executed, with the desired result.
- External test. The program is given a variety of different inputs with different parameters, designed to correspond to the various different kinds of input that actually occur, with particular emphasis on especially difficult cases. In the case of scientific computing, this may also produce variations in the results valuable for the assessment of the numerical accuracy of the result.
- Special cases. Cases like zeroing one or more parameter, inputs that give trivial or easily-controlled results, or ought to produce errors like dividing by zero and the like.

These criteria have been met - a careful test of the complex arithmetic routines and special functions (logarithm, exponentials, etc.) implemented in *compl.c* has been performed.
The hypergeometric function has both been implemented as the Gauss series, and as the analytical continuation of the Gauss series, calculated by direct integration in the complex plane (as described by Press *et al*). These functions have been tested both by comparison of the results obtained by the two methods, and by comparing to a number of formulae (found in Abramowitz & Stegun) for special values of the parameters.

In the calculations we have performed for the present work, the Gauss series turns out to be faster and more accurate - for the calculations described in Appendix A, however, the analytical continuation was necessary. For the testing of the above functions, the condition that all branches be taken (internal test) followed automatically from the external testing.

The other special functions which we have needed, the Legendre polynomials, Γ function and Bessel functions have all been implemented according to the prescription given by Press *et al*, and tested according to the prescriptions given above.

As a check of the accuracy of the program used for computing total cross sections for the K-shell, we can also compare directly with the data published by Aste *et al* and the tables given for low energies by Johnson *et al*.

Johnson *et al* computed the cross sections up to $E = 3.5$ (where E denotes the positron energy) for single-photon pair annihilation. By limiting the maximum

number of partial cross sections, the program used for the present calculations reproduce their data exactly to four digits (out of four) below $E = 1.5$, and to three above. The reason for the last small discrepancy may be that while Johnson *et al* effectively perform the partial wave expansion over the total angular momentum quantum number J, we perform the summation over the orbital angular momentum quantum number L.

Figure 5, presented below, also shows total agreement with the curve published by Aste *et al*.

Agreement with previously published results is of course no proof of correctness, but it surely helps, especially since the results in the three cases are obtained by rather different means, as described in section 6.5.

Another check of the program is the behaviour of the cross sections for very low Z, where the Born approximation result is available. The agreement between the Born approximation and the results for $Z = 1$ is striking, as seen on figure 6. The same thing is seen on figures 30-32, where the differential cross sections for Z=1 are compared with the Born approximation; once again, the agreement is excellent.

The programs for calculating differential cross sections were also checked by integrating the results numerically over all angles - in this way, we were able to recuperate the first 4 digits of the total cross section (the last discrepancy is probably introduced by the numerical integration).

After these optimistic conclusions, two inconveniences in the existing programs should be mentioned:

First of all, a glance at equation (93) reveals that as the energy increases, the arguments $\frac{2p}{p+k_0 \pm ip_0}$ of the hypergeometric function will approach its singularity at $z = 1$ - at the same time, the number of partial waves needed for the computation also increases with the energy. This means, that while the low energy cross sections can be computed in seconds or minutes, at high energies the calculations become very labourious indeed. Furthermore, it has been found that the program will not work if one attempts to take the summation over partial waves higher than $L = 325$, and this means that at energies above 50-60 electron masses, an estimate of the remainder should be performed.

Secondly, the differential cross section curves display discontinuities or "glitches" at certain angles - see, for instance, figure 33 below. This phenomenon seems to imply that the implementation of the sum in (49), which involves successive cancellation of terms with different phase, fails to converge at these angles.

The ability of our program to reproduce the Born approximation as well as the correct total cross sections leads to the conclusion, however, that these problems are limited to the angles for which the glitches appear, so the curves displayed below may be considered accurate except in the "glitch points."

8 Total Cross Sections

The results of the calculations of the total cross sections for pair production with capture to the K- and L-shells are presented in this section.
It has been decided not to include tables, in the understanding that programs producing such tables are available on request, and because the graphical presentation gives a much better presentation of the data and a much better impression of the asymptotics and particular traits of the spectra.

8.1 K shell

The total cross sections for bound-free pair production with capture to the ground state were computed, as stated above, for the seven elements we choose as our examples. We would expect these cross sections to increase rapidly for low energies, reach a maximum close to zero and afterwards decrease, asymptotically as E^{-1}, as discussed in Section 6.

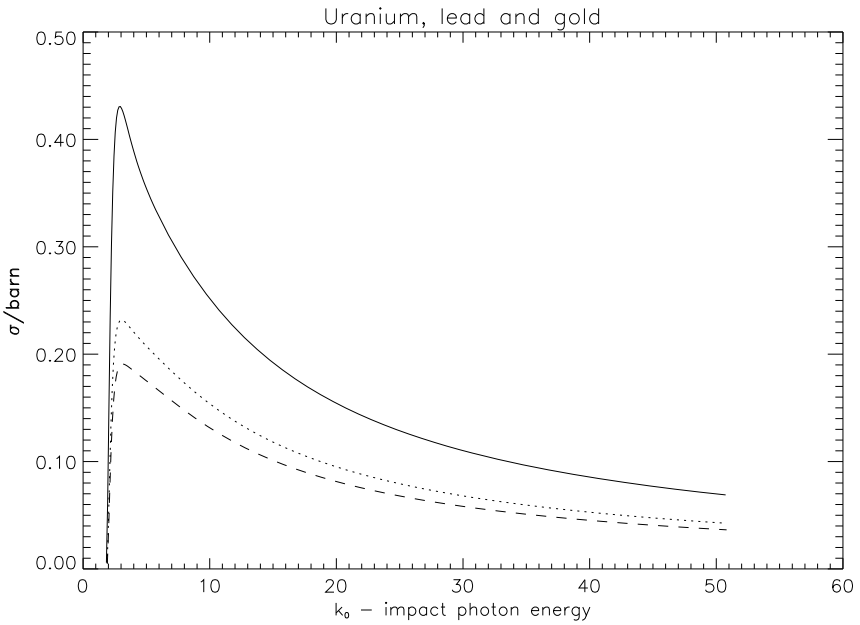

Figure 5: Total cross sections for bound-free pair production with capture to the $1s$ state for U (full curve), Pb (dotted) and Au (dashed).

In figure 5, we show the cross sections for uranium, lead and gold as a function of the photon energy. We note the rather sharp peak, after which the cross section starts falling off, displaying the the asymptotic E^{-1} behaviour.

The exact, numerical results must of course be expected to agree with those of the Born approximation (104) if $\alpha Z \ll 1$.
In figure 6, this is illustrated for hydrogen - the two curves are seen to be in

very good agreement, and the Born approximation is very nearly equal to the exact result. In figure 7 we show the cross sections of our seven example atomic

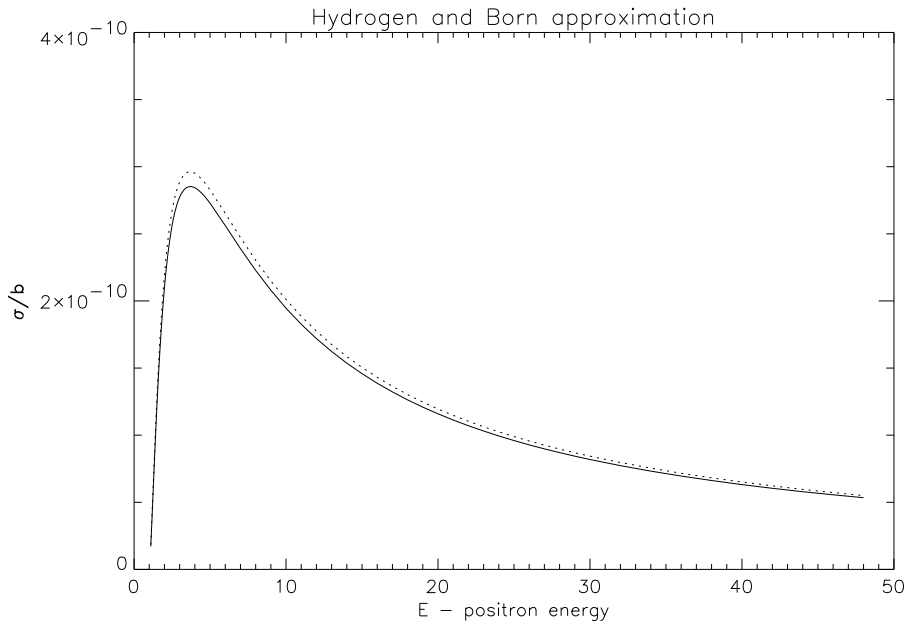

Figure 6: K-shell cross section for hydrogen, compared to the Born approximation (104) (dotted curve).

numbers, scaled by Z^5. Even though the curves corresponding to different target charges actually do cross, apparently because the cross sections tend to become more "peaked" at higher charges, their high energy limit is seen to decrease steadily with increasing Z. This is further illustrated in figure 8, which shows the same cross sections, this time in units of the Sauter cross section (105).
We see that at high energies these curves become straight, horizontal lines, so that, following Pratt and Milstein & Strakhovenko, we can give the cross section at high energies as

$$\sigma_K = \sigma_0 f(Z), \qquad k_0 \to \infty \tag{122}$$

where $f(Z)$ is a decreasing function of Z, and σ_0 is the Sauter cross section.

We note that at $k_0 = 50$ (that is, of course, about 25 MeV) the high energy limit is nearly reached.

Now, since the Sauter cross section is the asymptotic limit of the Born approximation, and since the exact K-shell cross section is, therefore, *asymptotically* equal to the Born approximation times a slowly decreasing function of Z, it might be feasible to make a "modified Born approximation" (MBA) by assuming that

$$\sigma \sim \sigma_{MB} = f(Z)\sigma_B \tag{123}$$

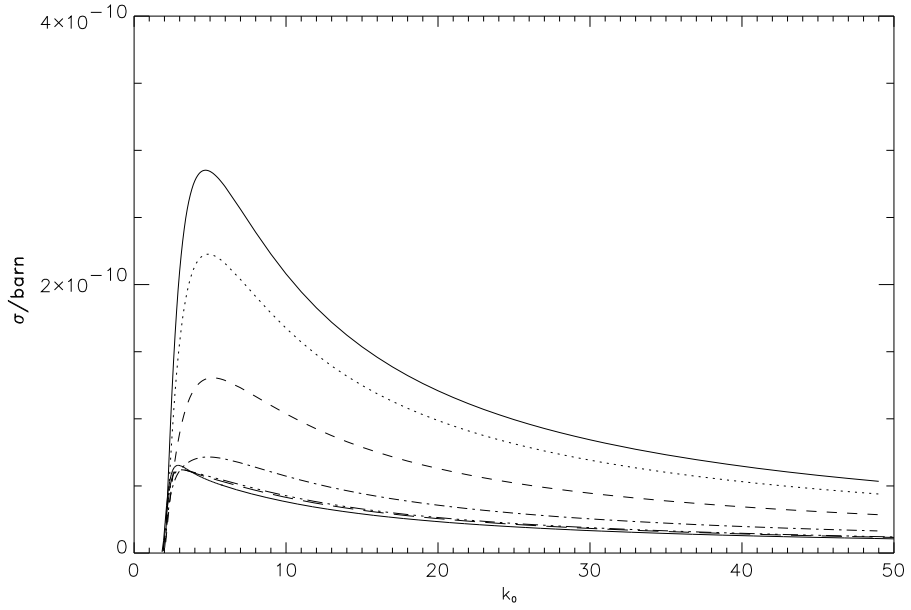

Figure 7: Total cross sections for our seven example elements, scaled by Z^5. The full line on top is H, then follows O (dotted), Fe (dashed), etc.

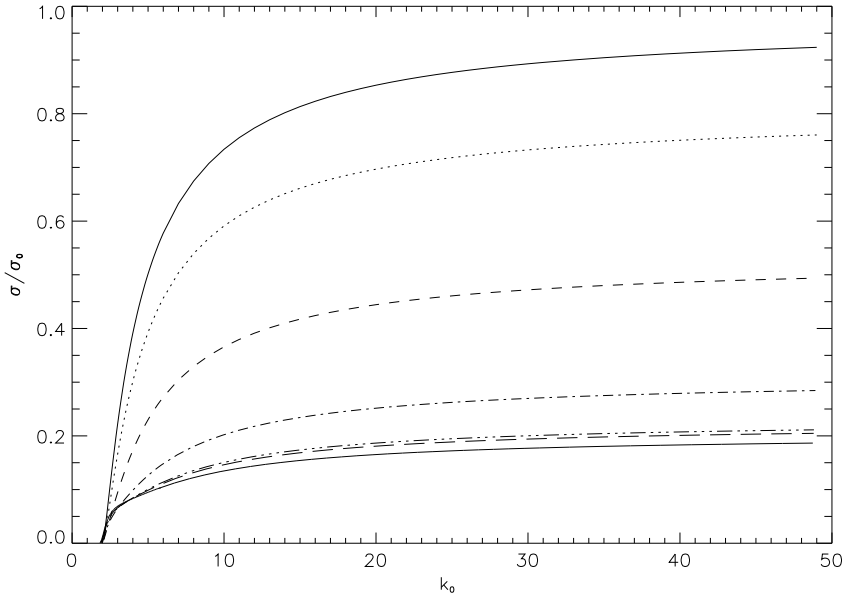

Figure 8: Total cross sections for our seven example elements in units of the Sauter cross section. The uppermost full line is H, then follow O (dotted), Fe (dashed), Cs (chained), Au (chained with three dots), Pb (dashed) and U (full).

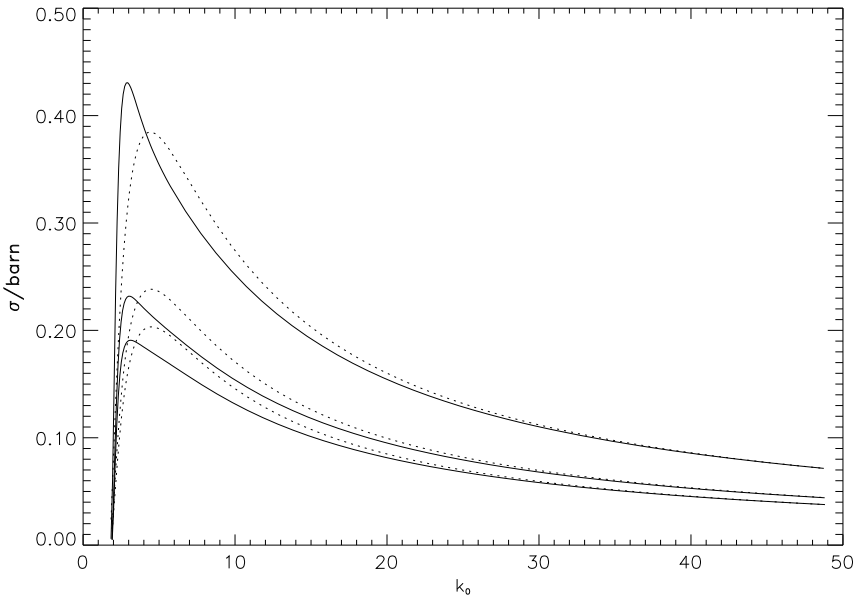

Figure 9: Total cross sections for U, Pb and Au compared to the modified Born approximation (123).

where $f(Z)$ is the function mentioned above.
In figure 9, we show the resulting MBA; we see that while the exact cross sections are more peaked at low energies, the MBA is nearly exactly valid for $k_0 \geq 20$.

The modification factors $f(Z)$ have been obtained by extrapolation of the high-energy region of the present calculations; Aste *et al* suggest as $f(Z)$ the, as they say, "purely heuristic" factor

$$f(Z) = (\tfrac{1}{2} + \frac{\alpha Z}{4})^{2\pi\alpha Z} \tag{124}$$

Even though our results, as has been mentioned, are in good agreement with those of Aste *et al*, this formula turns out to be somewhat below the mark (5-10 %).
The reason for this discrepancy may be that Aste *et al* may not have taken their calculations to sufficiently high energies or have not included sufficiently many partial waves. Or, perhaps more likely, they have preferred to have a compact (if not quite exact) formula for estimating the cross sections at high energies, and so chose to sacrifice some accuracy. The results of Pratt (1960[a]) are in better agreement with the present calculations.
Another useful approximation formula is the modified Hall formula mentioned above, equation (108). Once more, it should be emphasised that the unmodified Hall formula (107) quoted by some authors is *not* a good approximation to the high-energy behaviour.

Z	Present calc.	Pratt	(124)	(108)
92	0.196	0.203	0.182	0.175
82	0.216	0.223	0.197	0.201
79	0.222	0.228*	0.203	0.209
55	0.293	0.310*	0.271	0.305
26	0.518	0.532*	0.4875	0.529
8	0.798	0.793*	0.784	0.805
1	0.971	-	0.969	0.972

Table 1: Table comparing the high energy limits of $\frac{\sigma}{\sigma_0}$ for the K shell extrapolated from the present work with the work of Pratt,the high-energy approximation (124) obtained by Aste *et al* and the modified Hall formula (108). The numbers marked with an asterisk are extrapolated from the data given in Pratt *et al*.

The various high energy limits are compared in table 1. The formulae (124) and (108) are seen to be of nearly the same quality. The discrepancies between our high-energy limits and those given by Pratt *et al* may either be caused by numerical or analytical inaccuracies in the original calculations of Pratt (1960[a]) - as mentioned in section 6, a lot has happened in the realm of electronic computers since 1960, and an attempt to repeat the computation of the exact high-energy limit might not be superfluous, especially since the method used by Pratt did not permit him to perform the calculations in the low-Z limit.
On the other hand, it might be possible that the present calculations have not been taken to sufficiently high energies, so that the results do not permit the extraction of the correct high energy limit. This appears, however, to be improbable considering the striking agreement between the present results and those of the MBA for energies above 20 electron masses.

On figure 10, we compare the cross sections for the process of pair production with capture to the 1s-state with the cross section for the creation of a positron and a free electron near threshold.
We see that near threshold the cross section for bound-free pair production actually exceeds that of the creation of a free pair; the latter does not decrease with increasing energy, and away from threshold the former is completely insignificant by comparison.

8.1.1 Partial Wave Cross Sections

The total cross sections are, as we know, sums of partial cross sections corresponding to different angular momentum quantum numbers.
In figures 11-13 we display the distribution of the partial cross sections of the total angular momentum quantum number J for three different energies. We see that for increasing energy, the number of partial waves that contribute to the

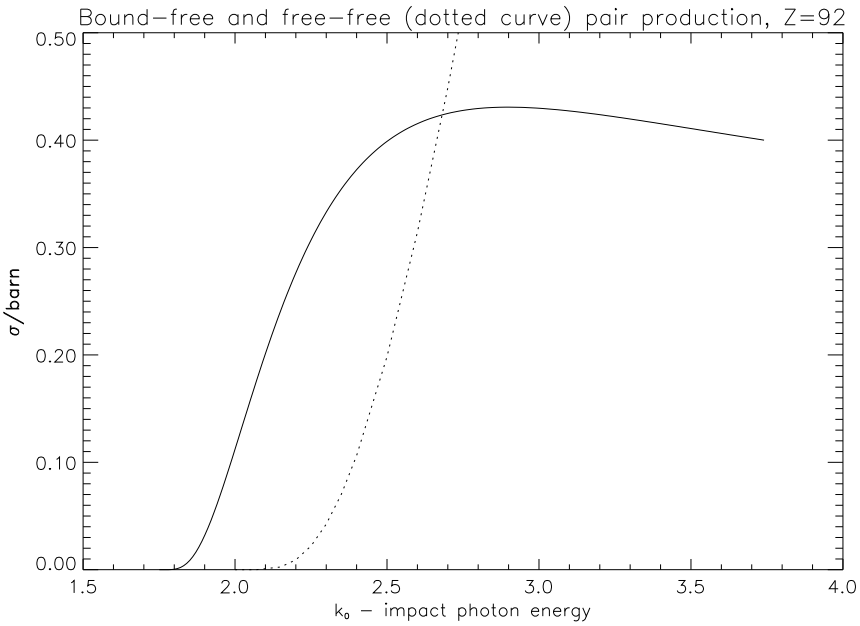

Figure 10: Total cross section for K-shell bound-free (full curve) and free-free (dotted curve, data from Øverbø) near threshold.

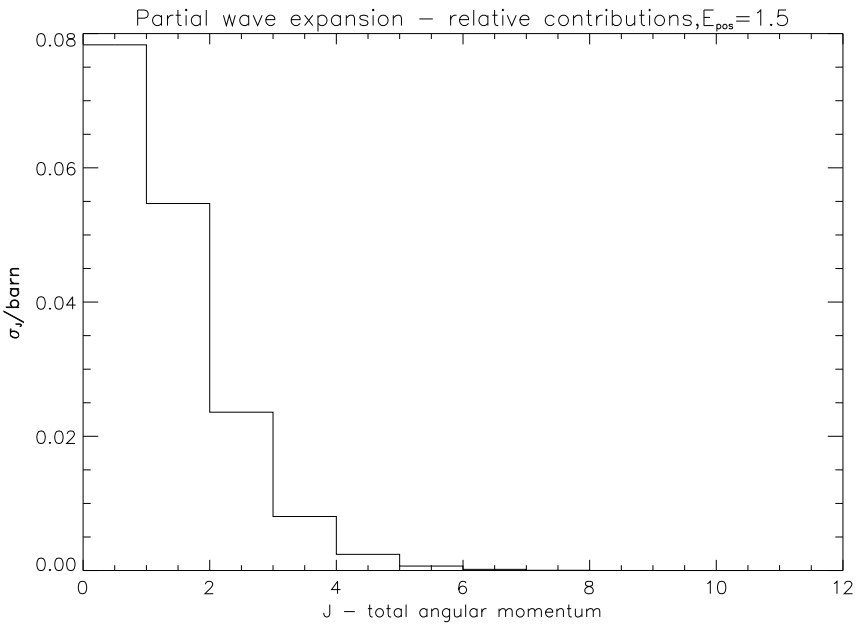

Figure 11: In this figure we display the distribution of the partial cross sections for $Z = 82$ on the total angular momentum quantum number J of the emitted positron, for the positron energy $E = 1.5$.

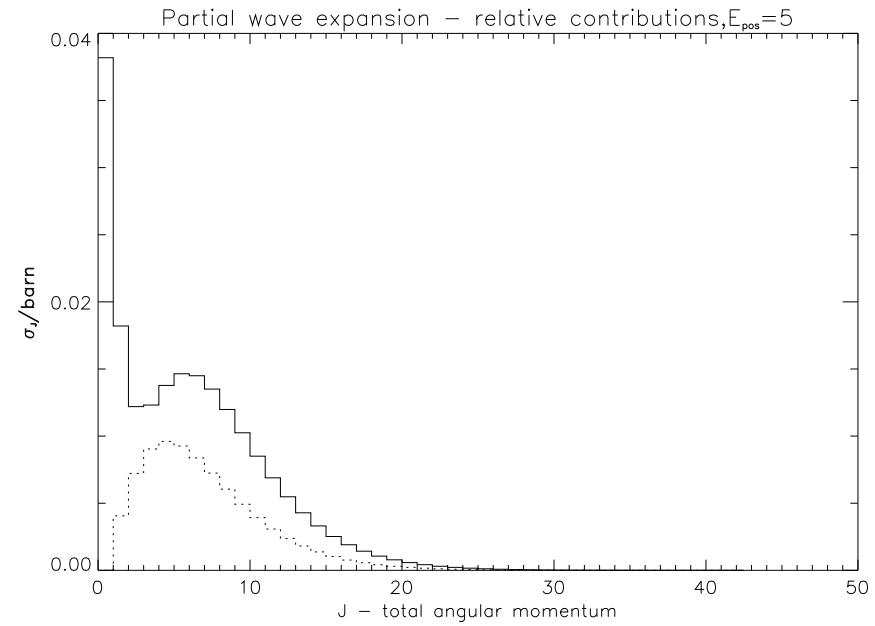

Figure 12: As in figure 11, only $E = 5$ - in this figure, the dotted curve corresponds to the cross section for the final state electron to have $m = -\frac{1}{2}$, if the photon has helicity $\lambda = +1$.

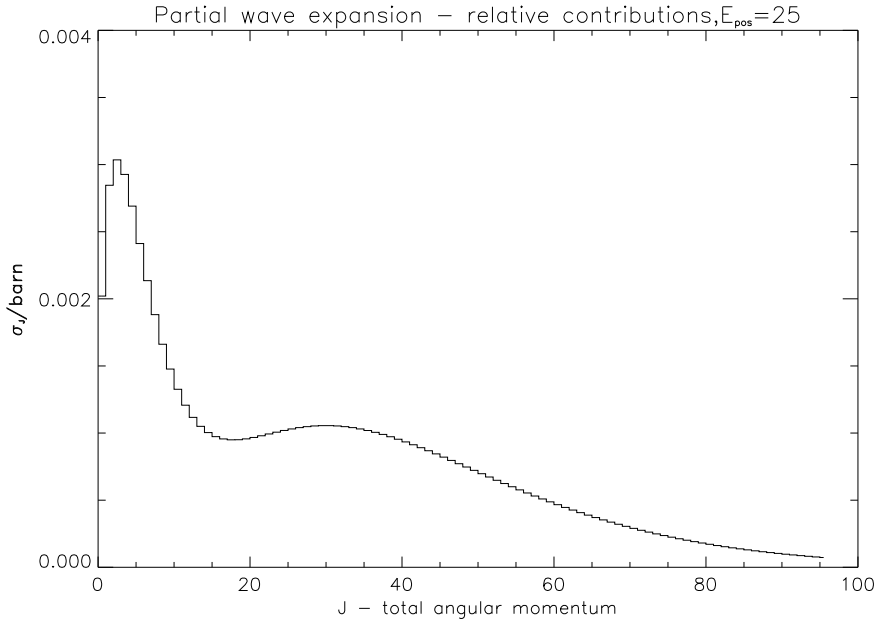

Figure 13: As in figure 11, but this time with $E = 25$. Note the characteristic structure with a peak at low J and a "hill" at higher J.

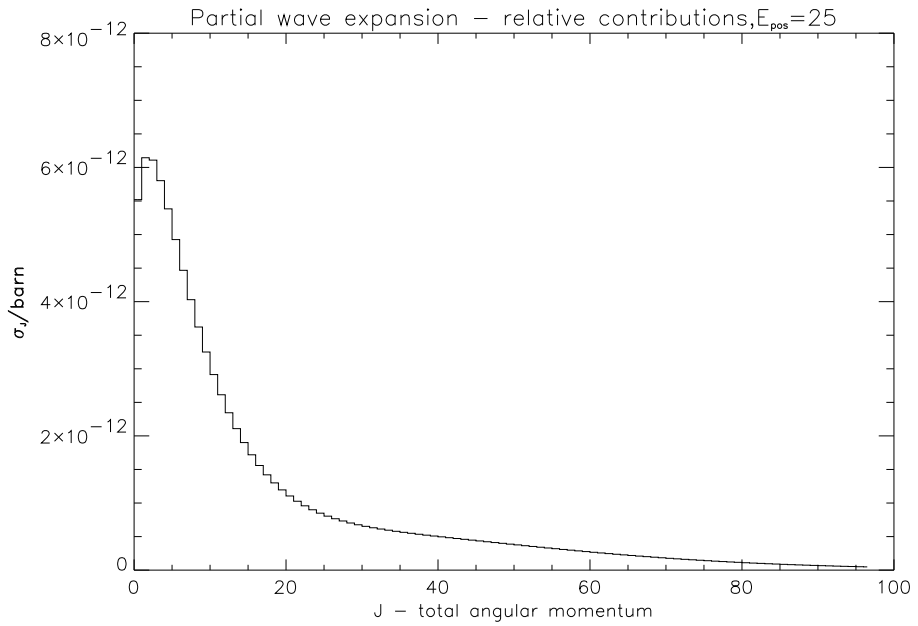

Figure 14: Here, for comparison, the same distribution as in figure 13 for the case $Z = 1$. Note the diminished "hill" at higher J.

sum gets higher and higher - on figure 13 we show the contributions for $J \leq 100$, but actually it is necessary to include the contributions up to $J = 202.5$ in order to get a sufficiently accurate result.
The distributions are drawn as histograms; for higher energies they might also have been drawn as continuous curves, but the histograms are retained in order to emphasise the discrete nature of the angular momentum. These distributions are, of course, what we will expect to see experimentally if, upon detection, the total angular momentum and not the cross section in a particular solid angle interval is measured.
A very conspicuous feature of the distribution of the cross section on the angular momentum quantum numbers at high energies is (as seen on figures 12 and 13) the sharp peak at low J, followed by a decrease and a new increase at higher J, rather resembling a hill or a mountain.
The peak at low J is the contribution from the radial integral I_1 containing the large components of the wave functions, whereas the "mountain" stems from the integral I_2 containing the small components.
This may be appreciated if we look at figure 12, where the dashed curve displays the partial cross sections for going (supposing the incoming photon is polarised with helicity $\lambda = +\frac{1}{2}$) to the substate where the ground state electron has projection quantum number $m = -\frac{1}{2}$ and recall that only the small components contribute to that matrix element (cf. equation (70). It may also be seen by comparing figures 13 and 14, which shows the same distribution for the same energy,

but this time for hydrogen. In the low-Z limit the contribution from I_2 tends to vanish, and the "mountain" is, indeed, very much diminished.

It should be noted, however, that even though the small components of the wave functions tend to vanish for $\alpha Z \to 0$, the high-energy behaviour will be determined by the contributions from the small components, because the importance of the peak at low Z will tend to vanish, since the hill caused by the small components cover a much broader range of angular momenta (Erber).

8.2 L shell

As we know, the cross sections for the L shell are expected to be smaller than the K-shell cross sections. As was also proved by Pratt (1960[b]), to first order in αZ the ns-shell cross sections obey a scaling law, so that

$$\sigma_{ns} = \frac{1}{n^3}\sigma_K \tag{125}$$

In agreement with this result, Gavrila's second order Born approximation for the $2s$-state yielded identically $\frac{1}{8}$ of his second-order K-shell cross section (Gavrila 1961).

As a consequence of this, the $2s_{\frac{1}{2}}$ cross section must of course be expected to be $\frac{1}{8}$ of the K-shell cross section at low target charges. The calculations of Pratt showed that in the high energy limit, this scaling property continues to be very close to the exact result at all target charges.

The $2p$-states, on the other hand, have quite insignificant cross sections at low target charges while at high target charges they will be of the same order of magnitude as the $2s$-cross sections (though they will still be smaller). The result is that the cross section for bound-free pair production with capture to the L shell is approximately 12.5% of the K-shell cross section for low target charges, where the Born approximation is valid, and about 20 % for high target charges (see also figure 26 below). As we shall see, the present calculations show that this prediction, which was originally based on Pratt's high-energy calculations, is valid at practically all energies away from threshold.

The reason for this is that the p-cross sections increase more rapidly with Z; in the Born approximation, that is, to lowest order in αZ, they are expected to increase as Z^7 (*versus* Z^5 for s-states, Gavrila 1961). Comparing figures 15 and 16, we see that for these examples, the contributions from the $2p_{\frac{1}{2}}$-states are about half those of the $2s$-states. On figure 17, we show the $2p_{\frac{3}{2}}$-cross sections for the same three elements.

In figure 20, the three sub-shells are displayed in the case of uranium - we may compare with figure 21 and 22, where the same thing is done for lead and gold, and note the increased importance of the p-states at higher Z. In the case

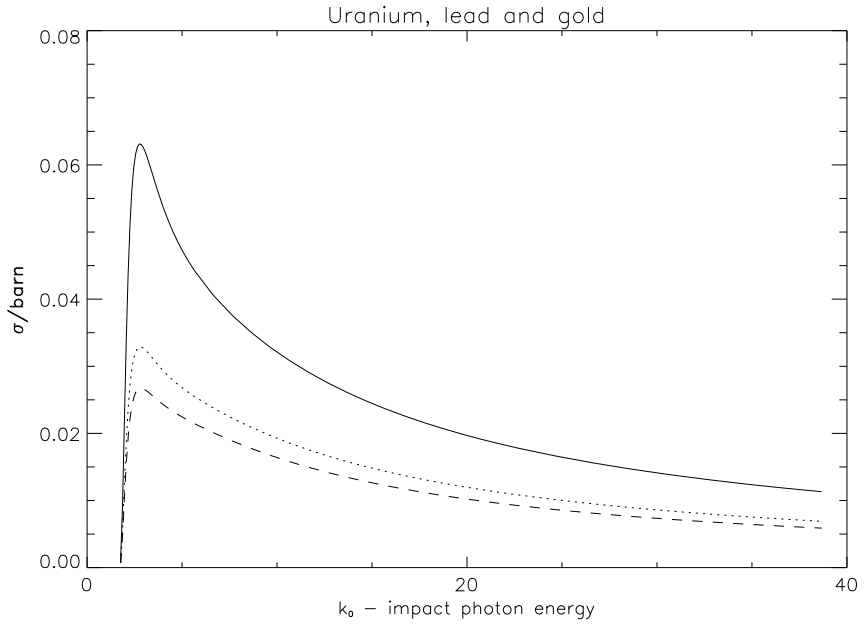

Figure 15: Cross sections for pair production with capture to the $2s_{\frac{1}{2}}$ shell for U (full curve), Pb (dotted) and Au (dashed).

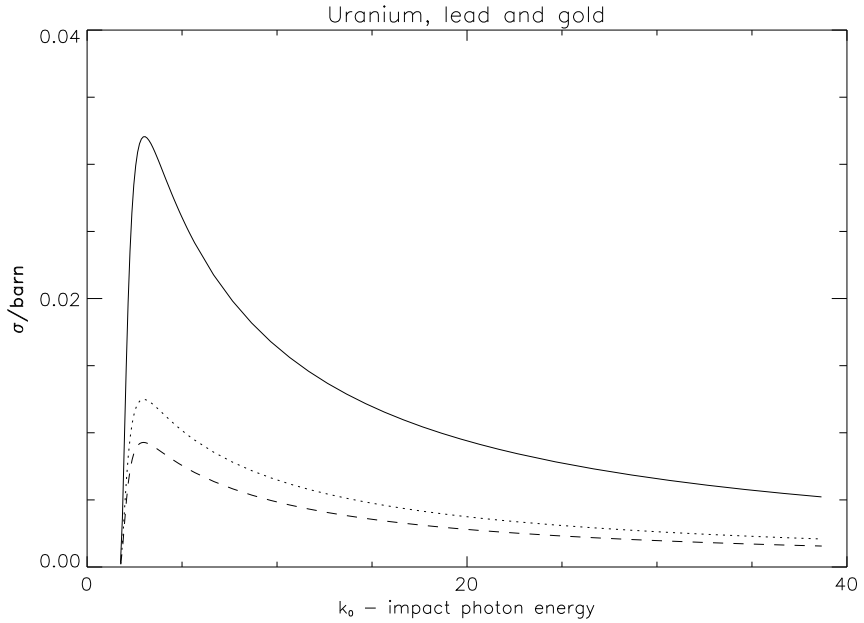

Figure 16: Cross sections for pair production with capture to the $2p_{\frac{1}{2}}$ shell for U (full curve), Pb (dotted) and Au (dashed).

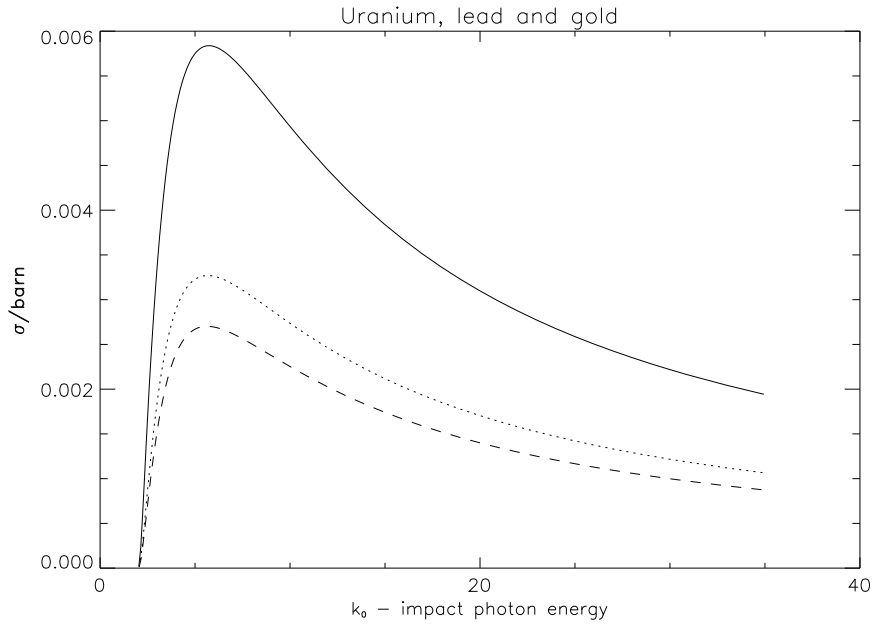

Figure 17: Cross sections for pair production with capture to the $2p_{\frac{3}{2}}$ shell for U (full curve), Pb (dotted) and Au (dashed).

of hydrogen, there would be no point in making a similar figure, since the p-states would not show at all.

Instead, on figure 18 we show the cross section for H with capture to the $2p_{\frac{1}{2}}$-state compared with Gavrila's (1961) Born approximation. As in figure 6, we note a striking agreement between the Born approximation and the present calculations.

Figure 19 is similar, here we display the cross section for $Z = 1$ and with capture to the $2p_{\frac{3}{2}}$-shell. Here, the agreement with the Born approximation is somewhat less striking, but nevertheless still good.

The $2s$-curves are seen to be very similar to the $1s$-curves, and indeed we find that $\frac{\sigma_{2s}}{\sigma_K}$ is very close to $\frac{1}{8}$ for all energies and target charges.
This is further illustrated by figure 23, where we display the ratios of the different L-shell cross sections to the K-shell cross section for U, and on figures 24 and 25 we do the same for Pb and Au. We do not do it for hydrogen, since the curves for the p-states would be to small to show.
It is interesting to see that away from threshold, these ratios are very nearly independent of the energy even at relatively low energies.

This is further illustrated on figure 26, where we compare the ratio $\frac{\sigma_L}{\sigma_K}$ for our four example elements. We note that even at quite low energies it appears to be constant, so that the high-energy limit of the L-shell cross sections may be predicted from knowledge of the high-energy limit of the K-shell cross sections.

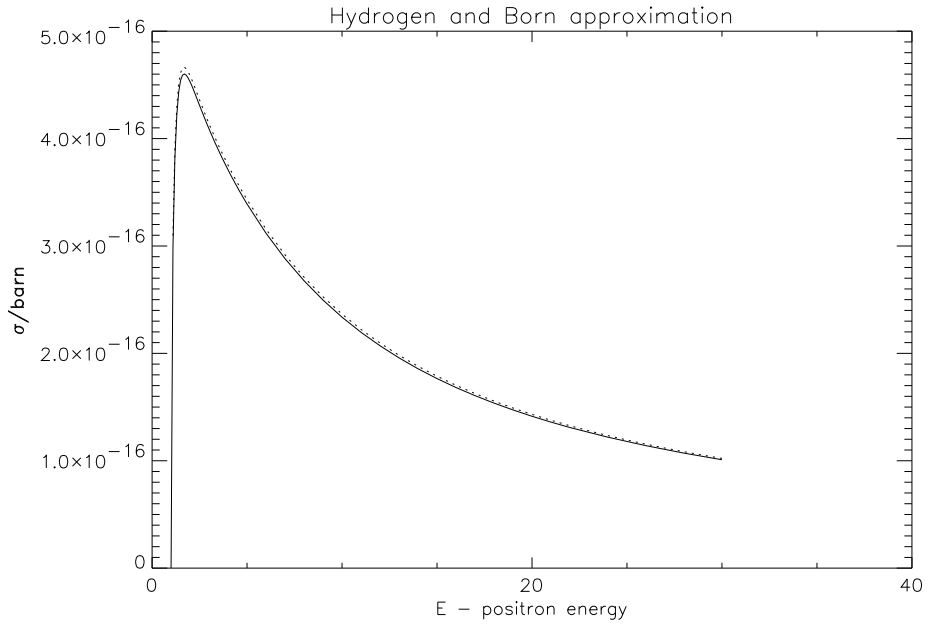

Figure 18: Cross section for H with capture to the $2p_{\frac{1}{2}}$ shell, compared to the Born approximation (dotted curve taken from Gavrila 1961).

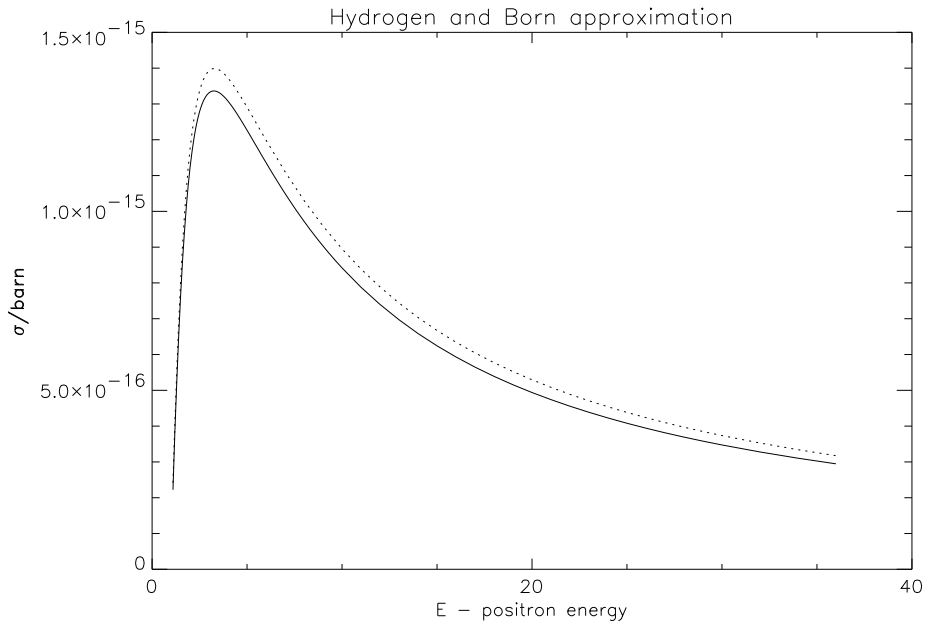

Figure 19: As in figure 18, but with capture to the $2p_{\frac{3}{2}}$-shell.

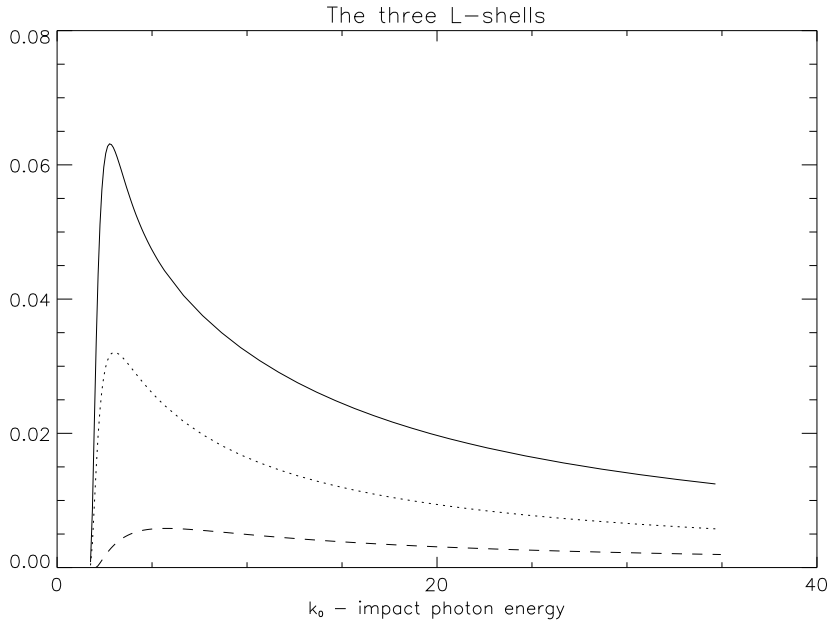

Figure 20: Cross sections for pair production with capture to the $2s_{\frac{1}{2}}$ (full curve), $2p_{\frac{1}{2}}$ (dotted) and $2p_{\frac{3}{2}}$ (dashed) states for $Z = 92$.

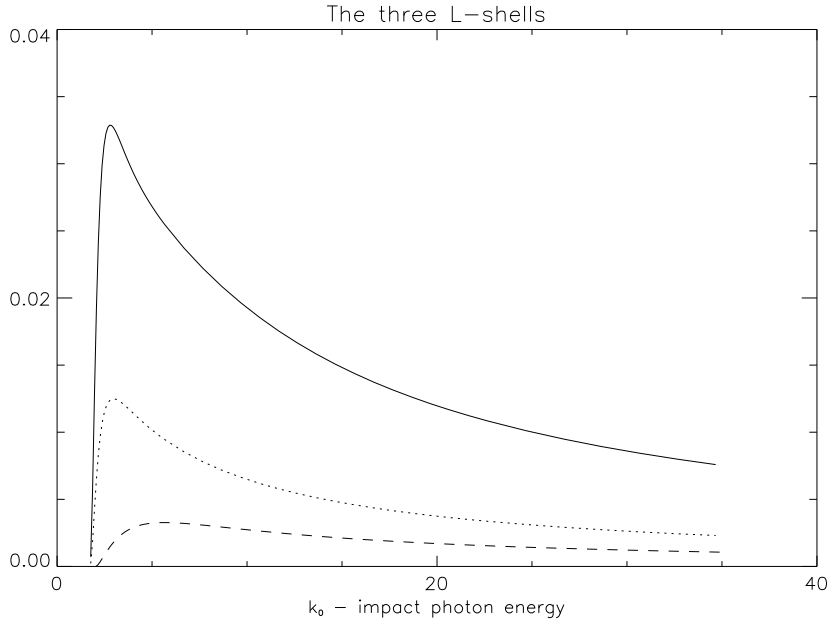

Figure 21: As in figure 20, but for $Z = 82$.

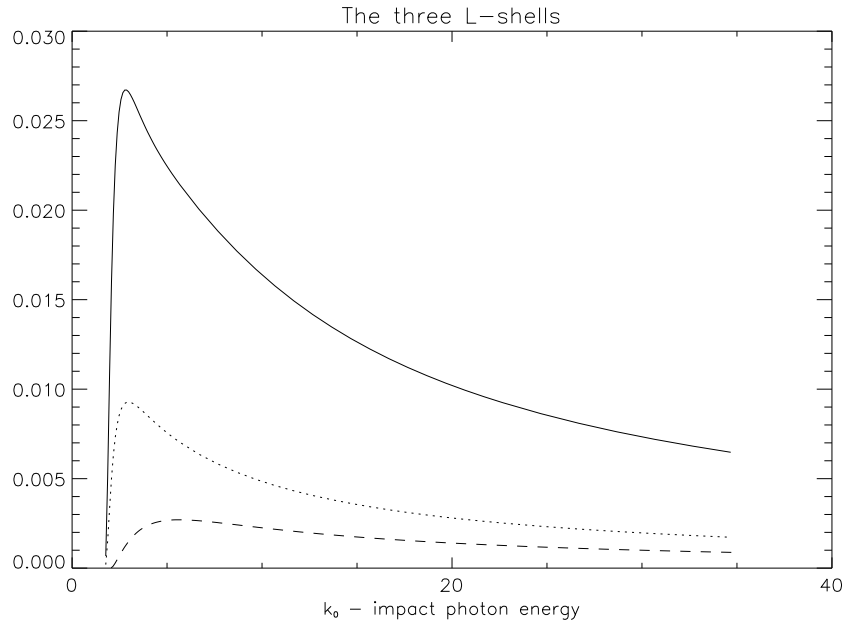

Figure 22: As in figure 20, but for $Z = 79$.

We also notice that the L-shell contribution for hydrogen is almost exactly $\frac{1}{8}$ at all impact energies - this was of course to be expected, since the only appreciable contribution comes from the $2s$-state.

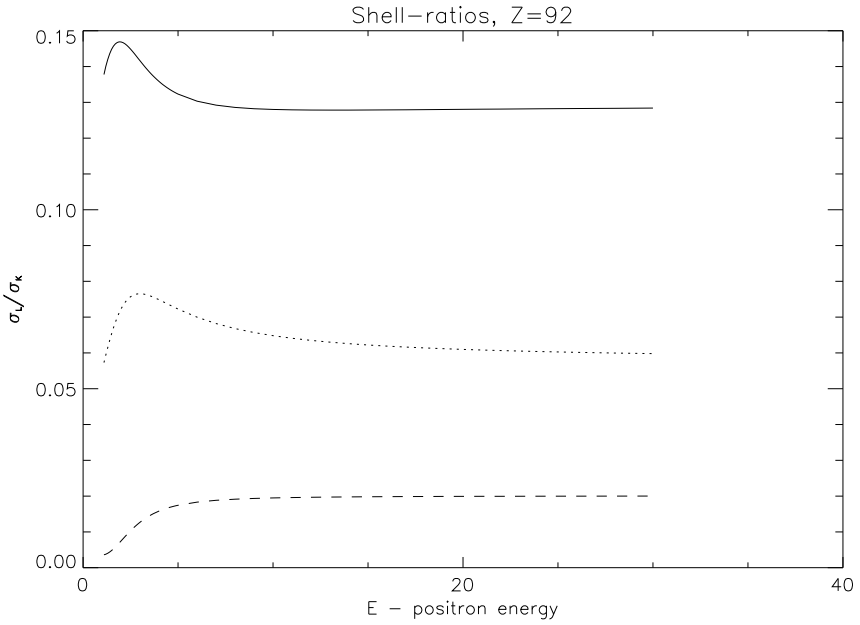

Figure 23: Ratios $\frac{\sigma_{2s}}{\sigma_K}$ (full curve), $\frac{\sigma_{2p_{\frac{1}{2}}}}{\sigma_K}$ (dotted) and $\frac{\sigma_{2p_{\frac{3}{2}}}}{\sigma_K}$ (dashed) for $Z = 92$

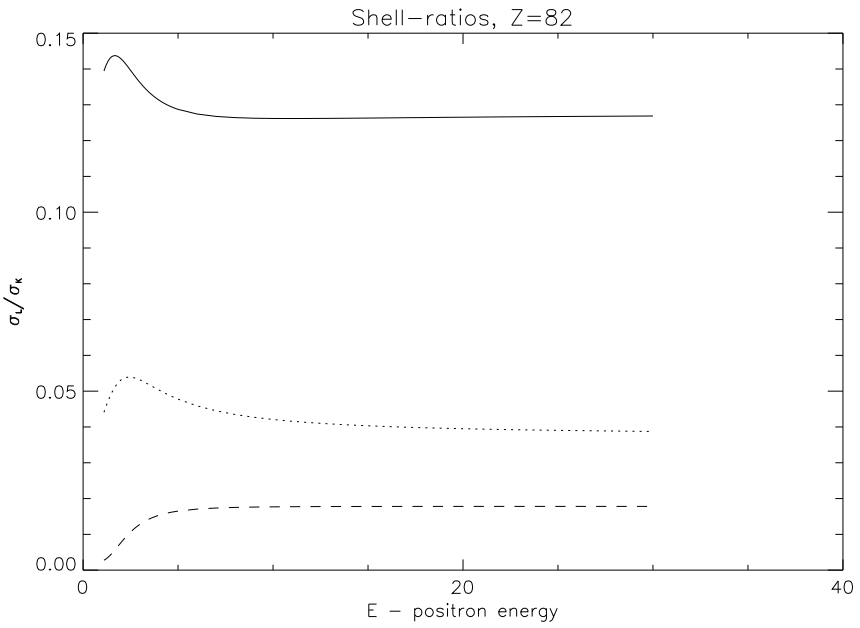

Figure 24: Ratios $\frac{\sigma_{2s}}{\sigma_K}$ (full curve), $\frac{\sigma_{2p_{\frac{1}{2}}}}{\sigma_K}$ (dotted) and $\frac{\sigma_{2p_{\frac{3}{2}}}}{\sigma_K}$ (dashed) for $Z = 82$

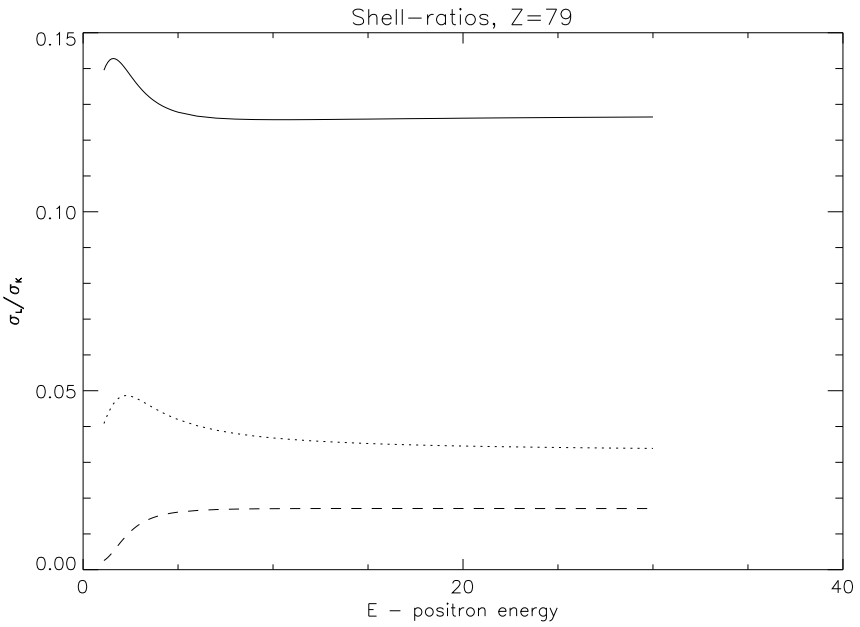

Figure 25: Ratios $\frac{\sigma_{2s}}{\sigma_K}$ (full curve), $\frac{\sigma_{2p_{\frac{1}{2}}}}{\sigma_K}$ (dotted) and $\frac{\sigma_{2p_{\frac{3}{2}}}}{\sigma_K}$ (dashed) for $Z = 79$

The high energy limit for the L-shell cross sections is easiest obtained by extrapolating the high energy limit for the shell ratios - the high energy limits

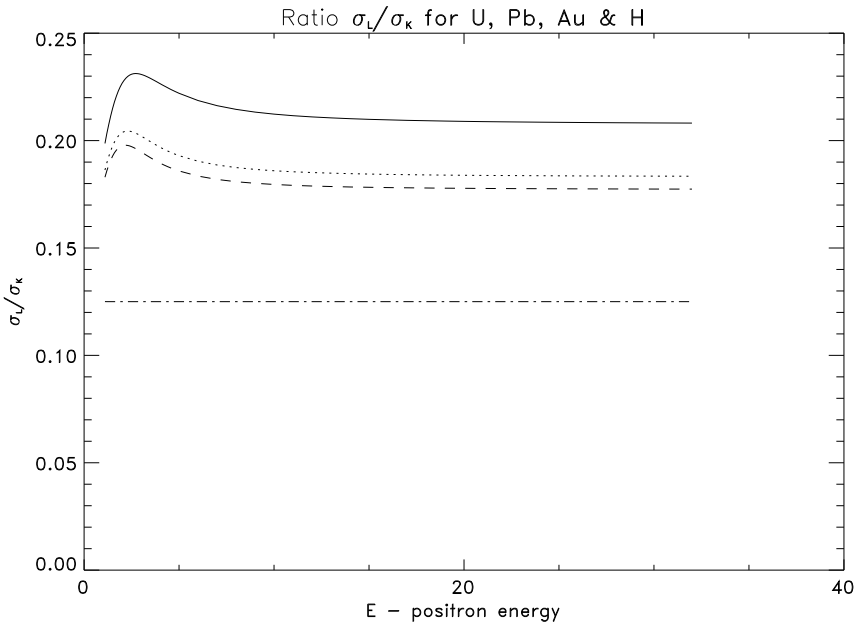

Figure 26: The ratio $\frac{\sigma_L}{\sigma_K}$ as a function of the energy of the emitted positron for Z=92 (full curve), 82 (dotted), 79 (dashed) and 1 (chained).

displayed in table 1 may then be used to compute the cross section at a given (high) energy. These shell ratios are displayed in table 2 for the four elements for which calculations were done, and compared to the results obtained by Pratt (1960^b).

Z	$2s$	$2s^P$	$2p_{\frac{1}{2}}$	$2p^P_{\frac{1}{2}}$	$2p_{\frac{3}{2}}$	$2p^P_{\frac{3}{2}}$
92	0.129	0.130	0.0598	0.0576	0.0201	0.0212
82	0.128	0.128	0.0385	0.0374	0.0178	0.0179
79	0.127	0.127*	0.0340	0.0331*	0.0171	0.0165*
1	0.125	0.125	$1.24 \cdot 10^{-6}$	$1.25 \cdot 10^{-6}$	$4.24 \cdot 10^{-6}$	$4.44 \cdot 10^{-6}$

Table 2: High energy limits of the ratios $\frac{\sigma_L}{\sigma_K}$.The results marked with ^{P} are Pratt's high-energy results, except for the case $Z = 1$, where the high energy limit of Gavrila's Born approximation is used. As in table 1, the asterisk indicates that the results are extrapolated from the data given by Pratt *et al.*

9 Differential Cross Sections

The angular distribution of the emitted positrons depends strongly on the target charge and the photon energy.
Regarding the latter, the spectra are, as might be expected, strongly contracted as the energy increases. As for the former, it will be seen that the non-perturbative character of the process is very evident, since the angular distributions at high target charges are very different from the (Born-compatible) low-charge result.
It should be mentioned that since the distribution of the emitted positrons are expected to be a function of the positron energy, different elements are compared at the same value of the positron energy as opposed to the energy of the incoming photon.

9.1 Angular Distribution for the K shell

In figure 27 we see a typical example, the angular distributions for three heavy elements at a quite low energy (1.5 mc^2). The emission is strongest in the forward direction and decreases steadily until about 90 degrees, after which it stays essentially constant.
At these relatively low energies, the distribution is rather broad and the cross section for emission in the backward direction is non-vanishing. At higher energies, the spectrum contracts and falls of rapidly with a virtual cutoff at around $\vartheta = \frac{3}{E}$.

This is seen on figures 28 and 29, where the angular distributions for $E = 5$ and $E = 10$ are seen to be of nearly the same shape, apart from the contraction. Indeed, at high energies the differential cross sections obey a *scaling law*, which will be investigated below.

At low target charges (and not too low energies) the Born approximation is valid, and it predicts that the differential cross section vanishes in the forward direction and attains a maximum around $\vartheta \sim E^{-1}$.

It is noteworthy, that this angular distribution is different from that of free-free pair production, which has a maximum in the forward direction (cf. the result given by Heitler).
This may be compared to the related processes of the photoelectric effect and bremsstrahlung, where the former in the Born approximation is zero at $\vartheta = 0$ while the latter has its maximum there.

This asymmetry of the bound-free and free-free processes has, historically speaking, caused some concern; some investigators, among them Fano *et al*, saw a problem in this and tried to apply a detailed balance argument to show that the photoelectric effect must have the same angular distribution as the low-energy tip of bremsstrahlung, [10] so the first Born approximation must be invalid, but

[10] That is, with a final-state electron momentum equivalent to that of the ground state.

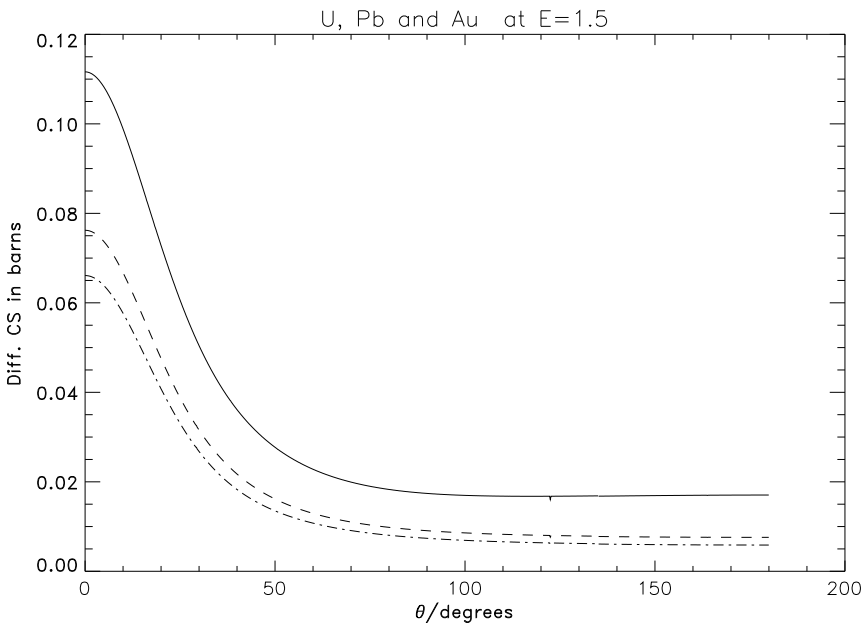

Figure 27: Differential cross section for bound-free pair production as a function of positron emission angle for U (full line), Pb (dashed line) and Au (chained line) at positron energy E=1.5.

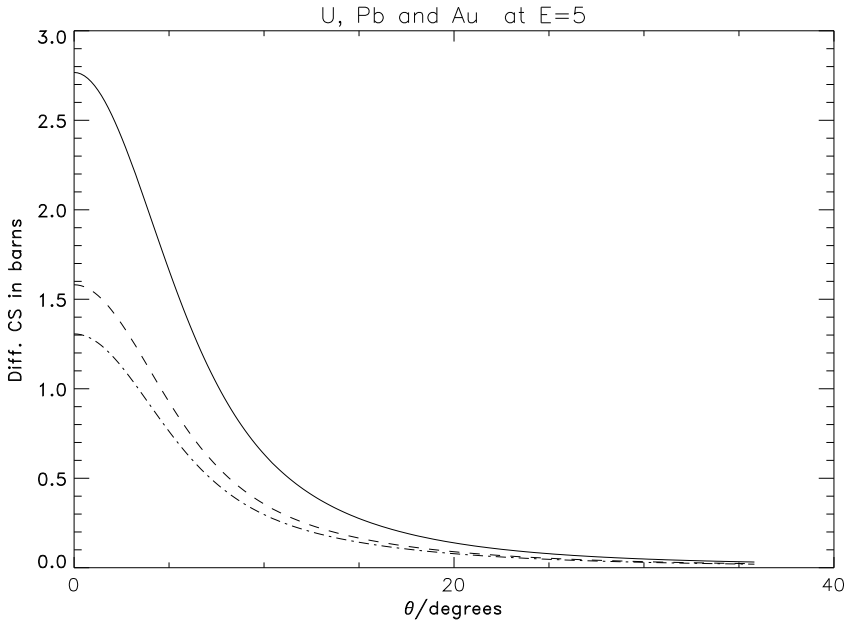

Figure 28: As in figure 27 for $E = 5$.

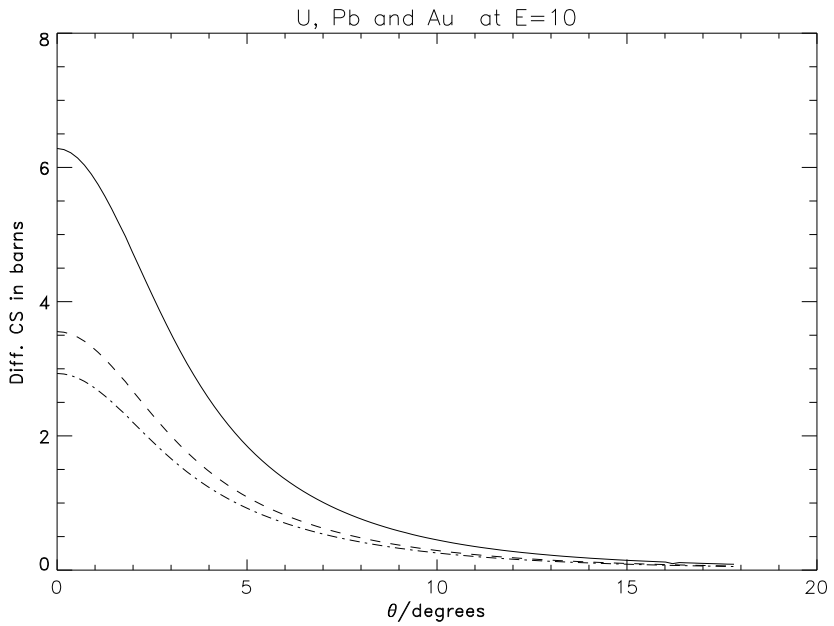

Figure 29: As in figure 27 for $E = 10$.

the argument did not hold: Gavrila's second order Born approximation also vanishes in the forward direction (Gavrila 1961 - note that he erroneously states the contrary in (1959)), and the present exact calculations also give results in good agreement with the Born approximation.

This is seen in figures 30-32, where the angular distribution for hydrogen is shown at three different energies. On these figures, we also show the Born approximation (106) for comparison. As expected (and as in the case of the total cross sections), the results are in good agreement with the Born approximation, especially at high energies. It seems that the small difference between the total cross sections and the Born approximation (as shown on figure 6) at low energies mainly comes from the area near the peak, since the Born approximation differential cross section is seen to be somewhat higher in this region.[11]

In figure 33-35, the corresponding distributions are shown for $Z = 8$. In this case, we note that the relative importance of the contribution to the cross section for $\vartheta = 0$ is non-vanishing, so the transition towards the behaviour of the differential cross section at higher energies has begun.

This is further illustrated on figure 36, which displays the angular distributions for five values of Z, scaled by Z^5, at E=1.5. Here, we can follow the steady breakdown of the Born approximation (whose angular distribution vanishes in

[11]At low Z, our angular distribution is quite similar to that of the photoelectric effect - at high Z, it is very different, since the K-shell photoelectric effect cross sections always have a local minimum at $\vartheta = 0$ (Alling & Johnson), and our results (and those obtained by Johnson for single-quantum annihilation) display a maximum in the forward direction at high Z.

the forward direction and corresponds to our results for hydrogen).

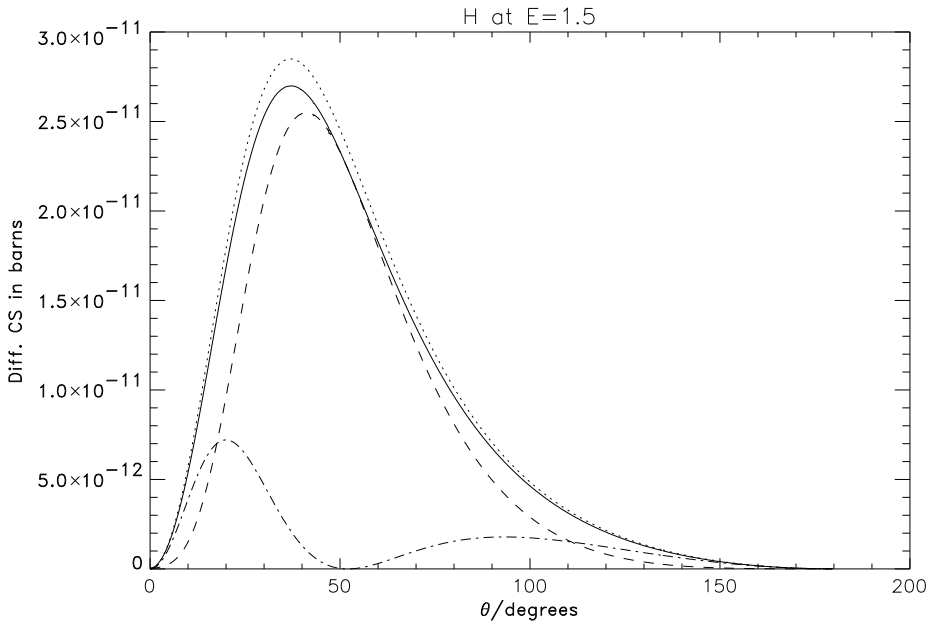

Figure 30: Differential cross section as a function of emission angle for H and positron energy $E = 1.5$. The full curve is summed over spin states - we also show the Born approximation (106) (dotted) and the contributions corresponding to $\sigma\lambda = 1$ (dashed curve)and -1 (chained), respectively, where λ is the helicity state of the initial photon.

It is curious to note that while the *total* cross section decreases approximately as E^{-1} with increasing energy, the *differential* cross section in the forward direction (or - generally speaking - at its maximum) keeps *in*creasing. But this is as it should be:
Indeed, at high energies we would expect the differential cross section to increase *linearly* with energy near its maximum. To see why this is so, we remember that the differential cross section is concentrated at $\vartheta \leq 3E^{-1}$.
According to the mean value theorem, this means that for some angle ϑ_0 in this region, the differential cross section will attain the value σ_0, so that

$$\sigma \sim 2\pi \int_0^{3E^{-1}} \sin\vartheta d\vartheta \frac{d\sigma}{d\Omega} = 6\pi E^{-1}\vartheta_0\sigma_0 \tag{126}$$

If we assume that the angular dependence scale *exactly* with the energy, ϑ_0 must be a universal fraction of E^{-1}, say, $\vartheta_0 = aE^{-1}$, so that we have

$$\sigma = \frac{f(Z)}{E} = \frac{6\pi a\sigma_0}{E^2} \Rightarrow \sigma_0 = \frac{f(Z)}{6\pi a}E, \tag{127}$$

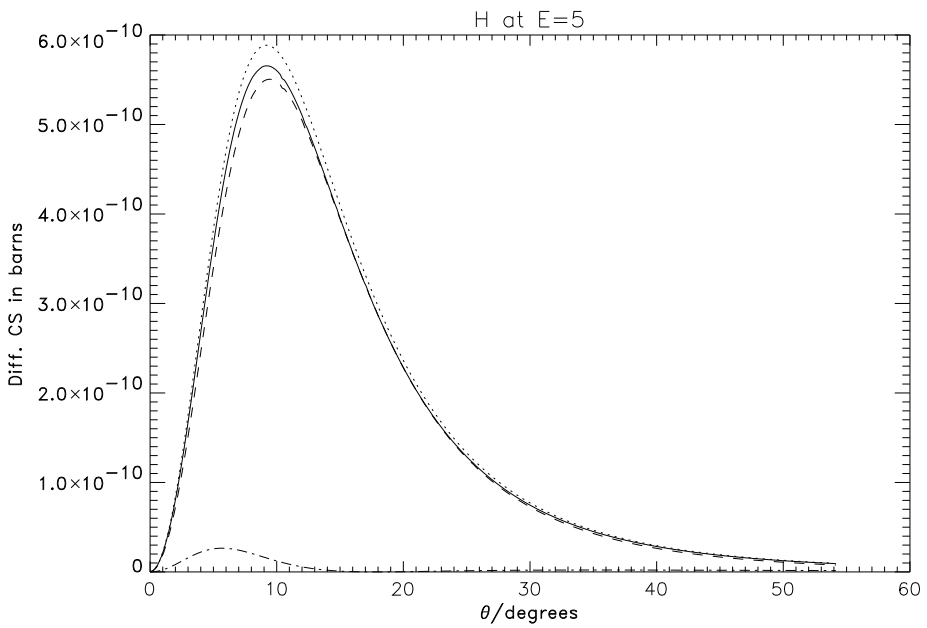

Figure 31: As in figure 30, this time for $E = 5$.

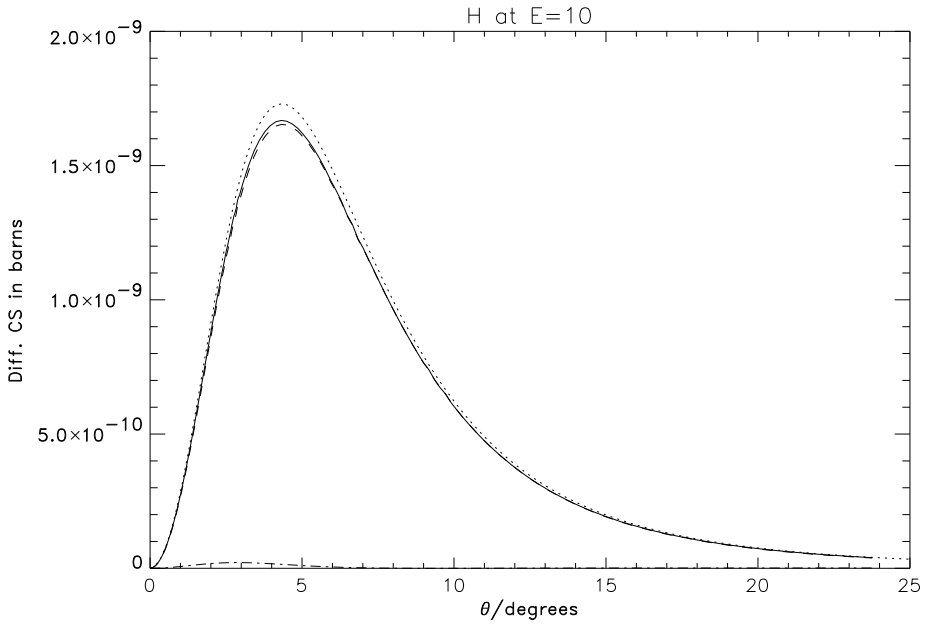

Figure 32: As in figure 30 but with $E = 10$. In this figure, and in figure 31, we note the violent decrease of the "spin-flip" contribution $\sigma\lambda = -1$ with increasing energy.

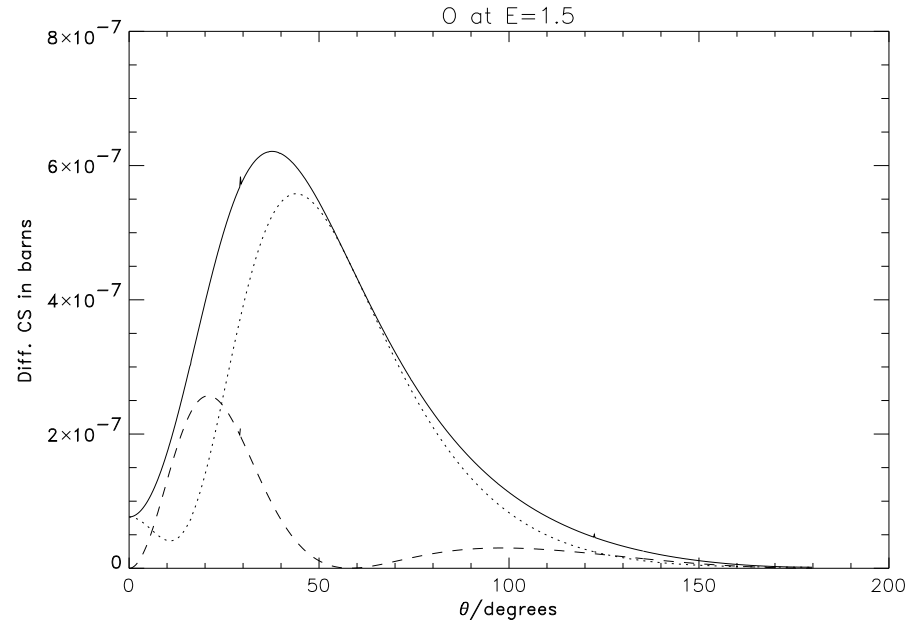

Figure 33: Differential cross section as a function of positron emission angle as in figure 30 for $Z = 8$ and $E = 1.5$. Once again, we display the contributions for $\sigma\lambda = +1$ (dotted curve) and -1 ("spin-flip", dashed).

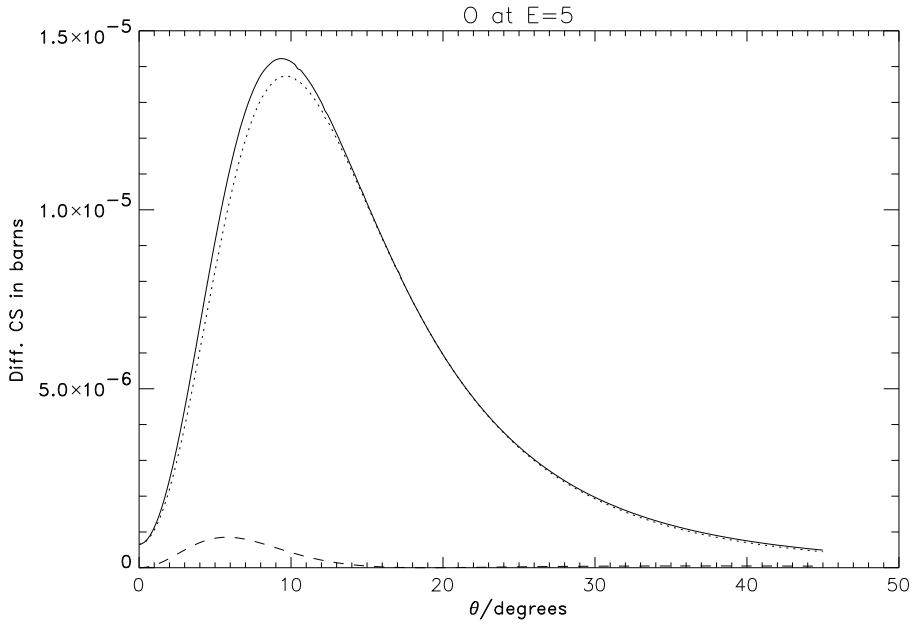

Figure 34: As in figure 33, for $E = 5$.

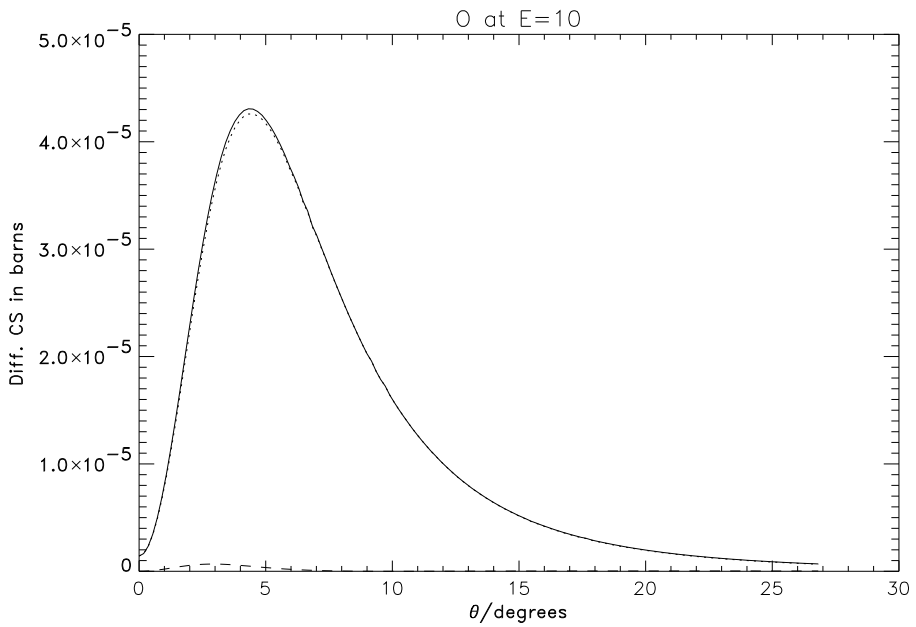

Figure 35: As in figure 33, for $E = 10$.

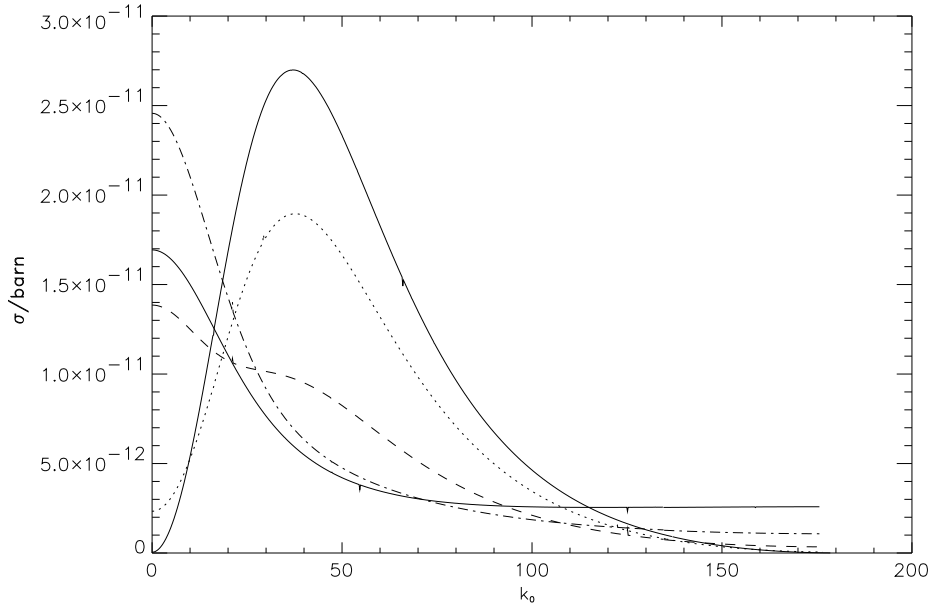

Figure 36: The differential cross section as a function of emission angle at $E = 1.5$ for Z=1 (full curve), 8 (dotted), 26 (dashed), 55 (chained) and 92 (full, with a maximum in the forward direction), scaled by Z^5.

that is, as stated above, the maximum value of the differential cross section is expected to increase linearly with the energy.

This is illustrated on figure 37, where $\frac{1}{E}\frac{d\sigma}{d\Omega}$ is shown as a function of $E\vartheta$ for $Z = 92$. We note that while equation (127) does not appear to be completely true in the region we have considered, it certainly does contain a great deal of the truth and may be expected to hold good for higher energies. This scaling property expressed in equation (127) is, of course, valid for all target charges. For H, it is illustrated on figure 38. Note how the scaled maximum becomes higher and more peaked - again we note that while the scaling law is not exact, it certainly does contain some truth, and may be used for estimating the cross section near its maximum at higher energies

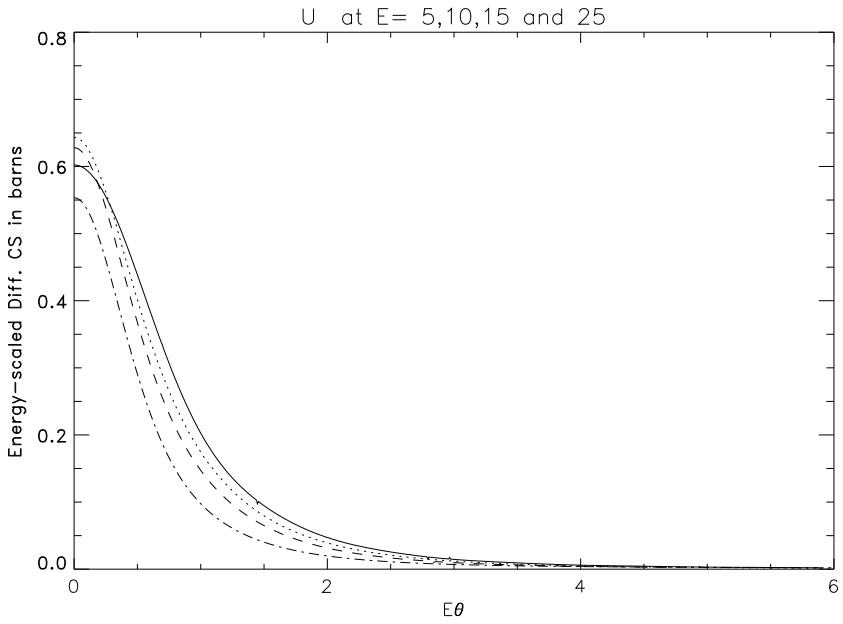

Figure 37: $\frac{1}{E}\frac{d\sigma}{d\Omega}$ as a function of $E \cdot \vartheta$ (ϑ in radians) for $Z = 92$ and E= 25 (full), 15 (dotted), 10 (dashed) and 5 (chained).

9.1.1 Polarisation Effects

If the incoming photon is polarised so that it is assumed to have, say, circular polarisation corresponding to positive helicity, the resulting positrons will be more or less polarised. The *polarisation* $P(\vartheta)$ of the produced positrons is defined by

$$P(\vartheta) = \frac{d\sigma(\sigma = 1) - d\sigma(\sigma = -1)}{d\sigma(\sigma = 1) + d\sigma(\sigma = -1)} \tag{128}$$

This polarisation function is the component of the polarisation vector in the direction of the momentum of the emitted positron. If this component is 1 or -1,

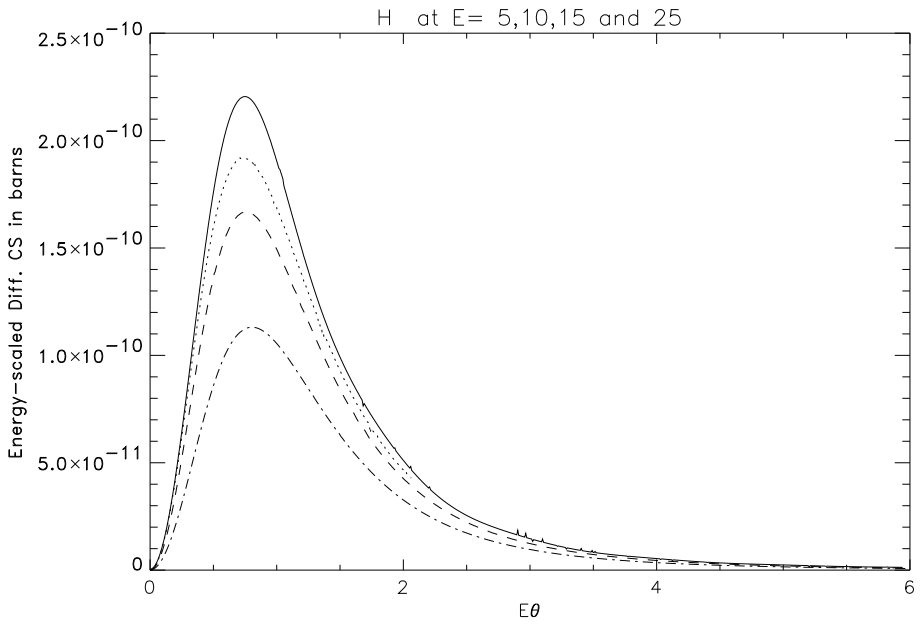

Figure 38: As in figure 37, but for $Z = 1$.

the emitted positron is completely polarised in the direction (or in the opposite direction) of the momentum. We may also say that if $P(\vartheta)$ is equal to 1 or -1, the incoming photon in a pure spin state will result in a positron emitted in a pure state - if it is between 1 and -1, the emitted positron is in an incoherent state. Because of the angular momentum selection rules, the positrons emitted in the forward and backward directions are always completely polarised. On figures 39 and 40, we see the polarisation function for a light element (H) and a heavy element (U), respectively.

Note that the hydrogen polarisation becomes complete for ϑ about 50 degrees for $E = 1.5$, and for ϑ about 10 degrees for $E = 10$. This is, as noted by Olsen, predicted by the Born approximation: we should expect the polarisation transfer to be complete at an angle approximately given by

$$k_0(k_0 - 1)(1 - \beta \cos \vartheta) = 2 \tag{129}$$

And this formula indeed predicts that the complete polarisation transfer should occur at $\vartheta = 51.5$ degrees for $E = 1.5$, and for $\vartheta = 9.3$ degrees for $E = 10$. Upon inspection in the data files, it appears that the maxima occur at 52.0 and 9.3 degrees, respectively.

And this leads to three observations: first of all, we note with satisfaction how our predictions reproduce those of the Born approximation in the low-Z limit. Secondly, the better agreement at the higher energy reflects the well-known fact that the Born approximation is more accurate at higher energies. And finally, that the complete absence of such phenomena in the polarisation functions for

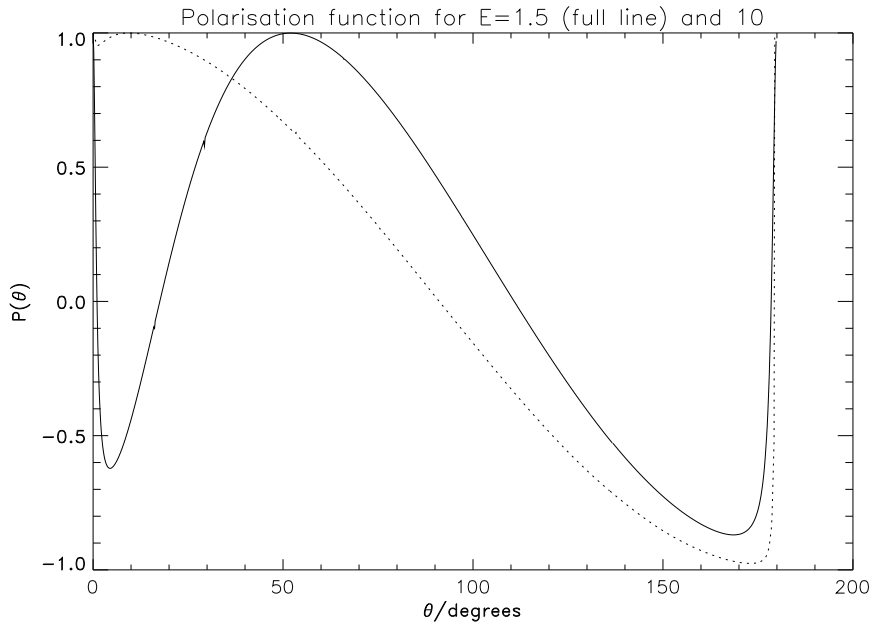

Figure 39: The polarisation function (128) for $Z = 1$ and $E = 1.5$ (full) and 10 (dotted).

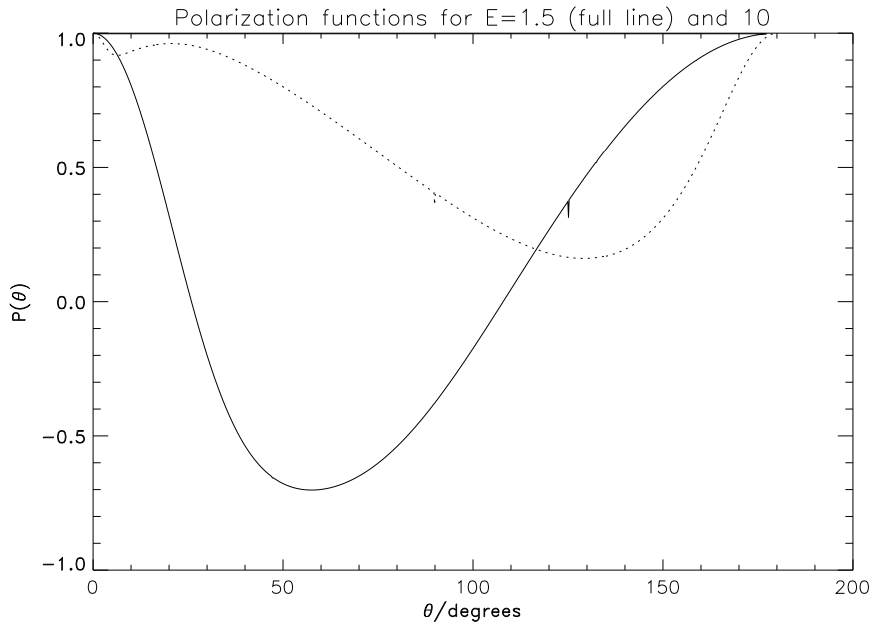

Figure 40: As in figure 39, this time for $Z = 92$.

U further demonstrates the complete breakdown of the Born approximation at high target charges.

9.2 Angular Distribution for the L shell

The angular distribution from the $2s$ subshell is almost exactly equal to that of the K shell, apart from the fact that it is reduced to about $\frac{1}{8}$ for all elements. The polarisation correlations etc. are practically the same, which is also not very surprising, since both states have spherical symmetry and the energy dependence of the total cross sections is also similar (apart from the factor of ~ 8). We shall thus have little to say about this subshell.

As an example of the above statements, the differential cross sections for $E = 1.5$ are displayed on figure 41. Furthermore, on figure 42 we compare the differential cross section for capture to the $2s$ shell for $Z = 92$ with $\frac{1}{8}$ of the K shell cross section. Once again, we note that even at high Z, the $\frac{1}{n^3}$ scaling law is very close to the truth.

On figure 43, we show the differential cross sections corresponding to emission of a positron of $E = 1.5$ and capture into the $2p_{\frac{1}{2}}$ state. Their form is very similar to that of the s-state differential cross sections (though a little broader), but it is easily seen that these cross sections increase more rapidly with Z.

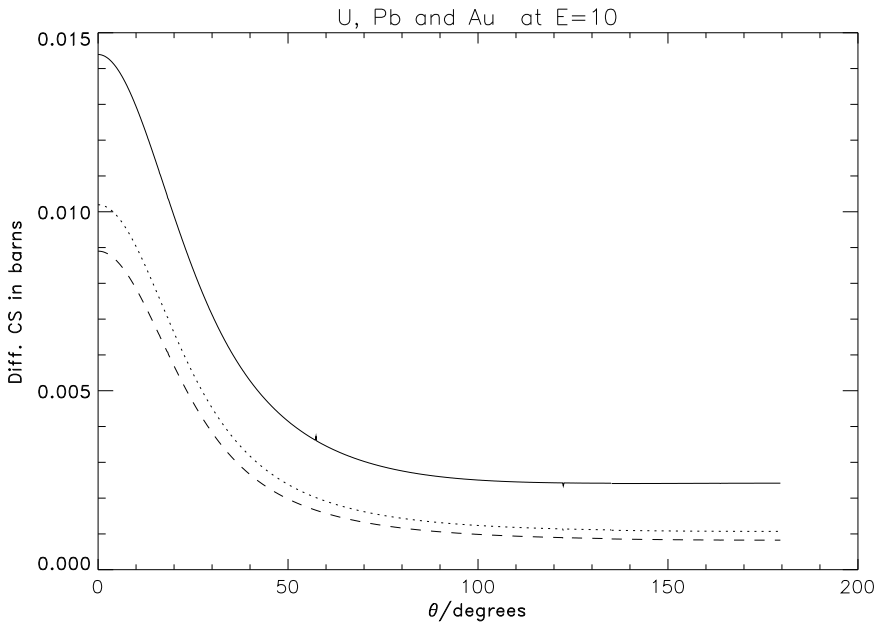

Figure 41: Differential cross sections for capture into the $2s$ subshell at $E = 1.5$ for our three heavy example elements

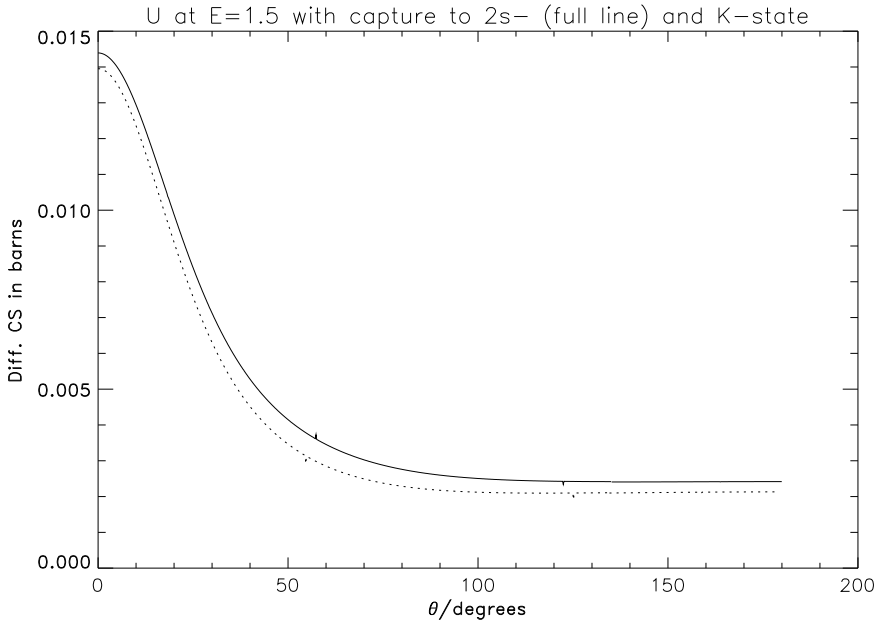

Figure 42: Differential cross section for capture into the $2s$ subshell for $Z = 92$ at $E = 1.5$, compared to $\frac{1}{8}$ of the corresponding K-shell cross section (dotted).

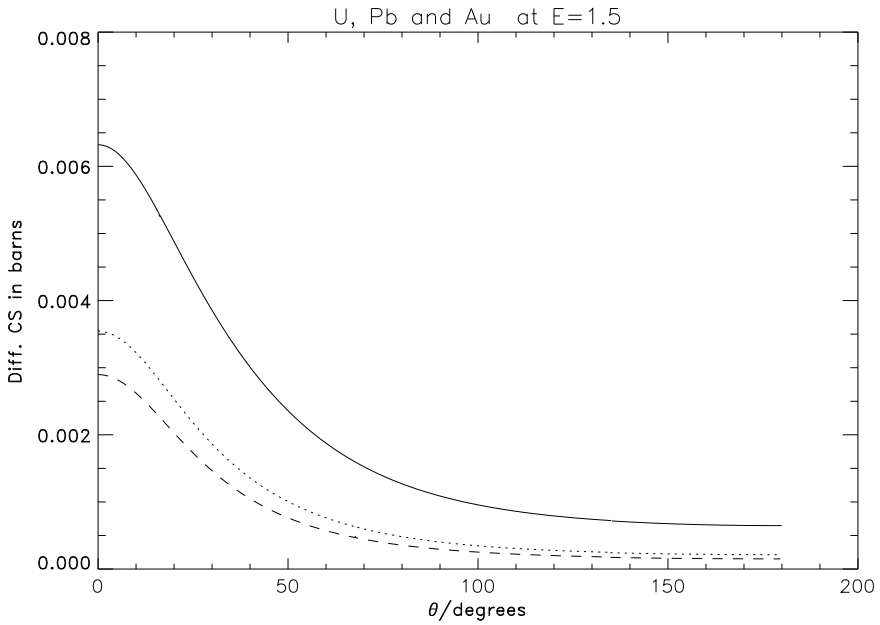

Figure 43: As in figure 41, but this time with capture to the $2p_{\frac{1}{2}}$ subshell.

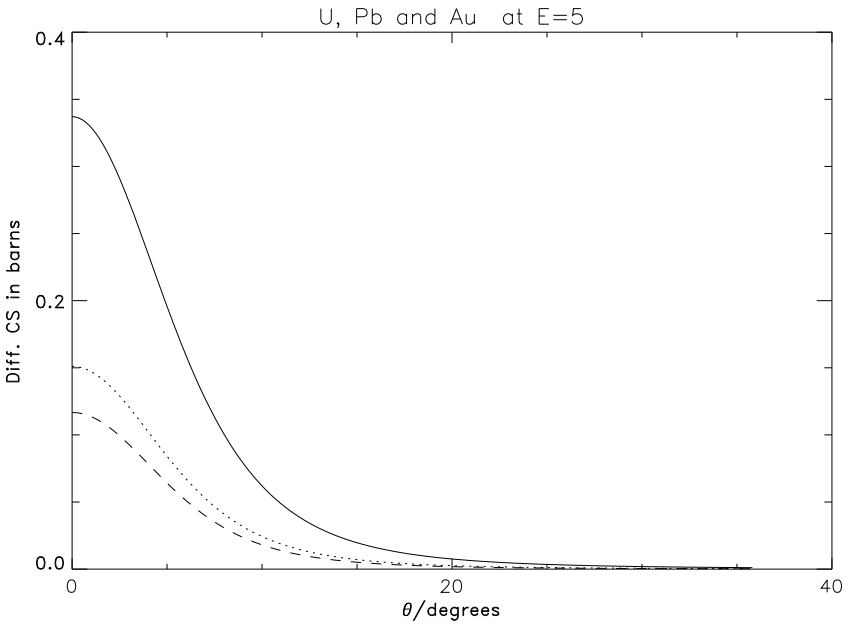

Figure 44: As in figure 43, but for $E = 5$

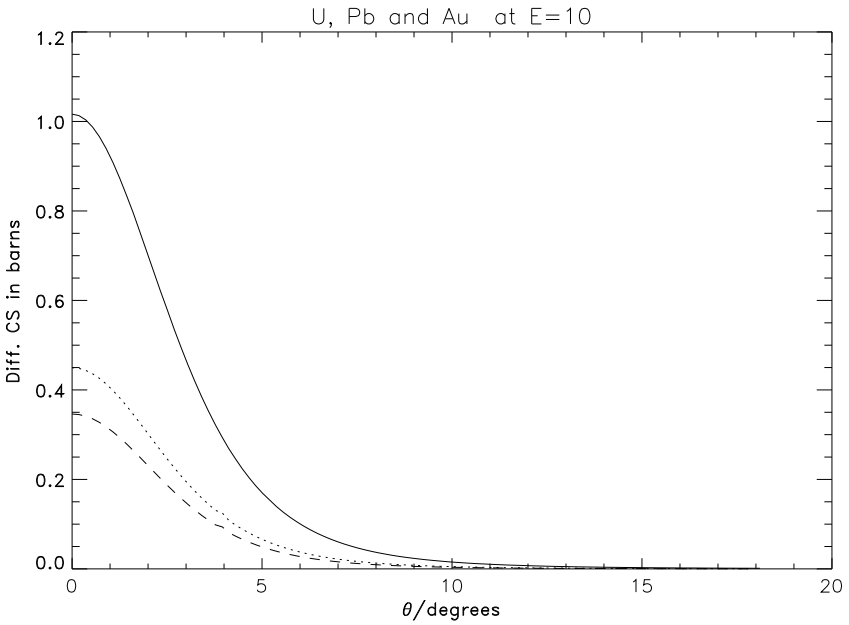

Figure 45: As in figure 43, but for $E = 10$

It is interesting to note that the angular distribution at $Z = 1$ is entirely different from that of the s-states. As we see on figure 46-48, the cross section for this shell has its maximum in the forward direction even for low Z.
This is in good agreement with Gavrila's perturbation result (1961), which predicts a narrower distribution than for the K shell with a maximum at $\vartheta = 0$.

The fact that the angular distribution of the $2p_{\frac{1}{2}}$ shell has its maximum at $\vartheta = 0$ while the K- and $2s$-shell distributions nearly vanish there does *not*, however, mean that the contribution of the $2p$-states to the differential cross section in the forward direction is larger than that of the $1s$ and $2s$ states for low Z - even though the latter have a minimum there, they do not exactly vanish, and they are still about two orders of magnitude larger than the maximum of the $2p_{\frac{1}{2}}$-state. The polarisation functions for $Z = 1$, displayed on figure 49,

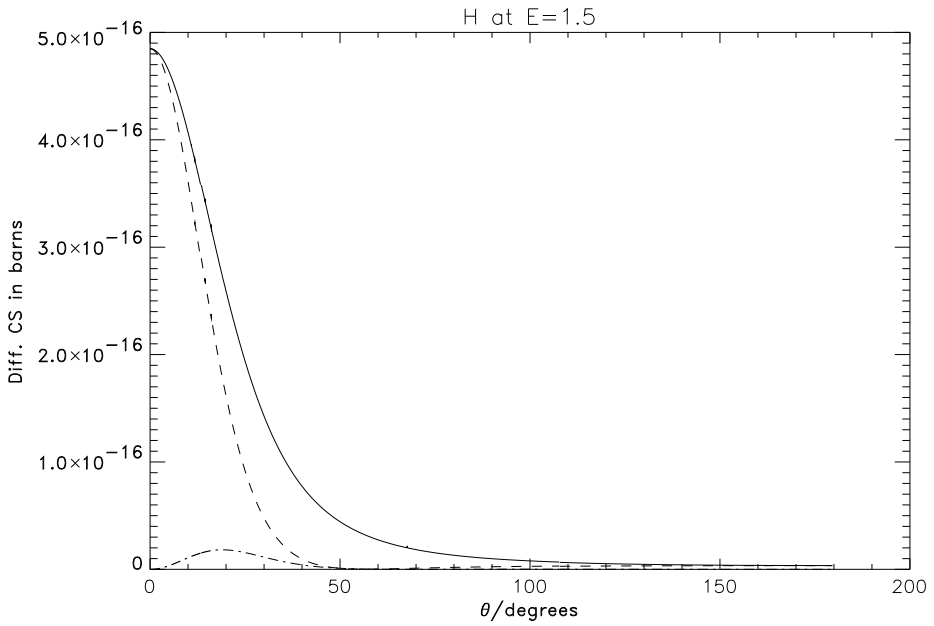

Figure 46: Differential cross section for pair production with capture to the $2p_{\frac{1}{2}}$ state as a function of emission angle for H and positron energy $E = 1.5$. The full curve is summed over spin states - as in figure 30, we also give the contributions corresponding to $\sigma\lambda = 1$ (dashed line)and -1 (chained curve), respectively, where λ is the helicity state of the initial photon.

are also completely different from the corresponding s-state polarisation function shown on figure 39. Note that we do not, as were the case for the K shell, have complete polarisation transfer - instead, we have complete polarisation *reversal* (complete spin-flip) at a certain angle.
On figure 50, we show the polarisation function for the case $Z = 92$ - as for

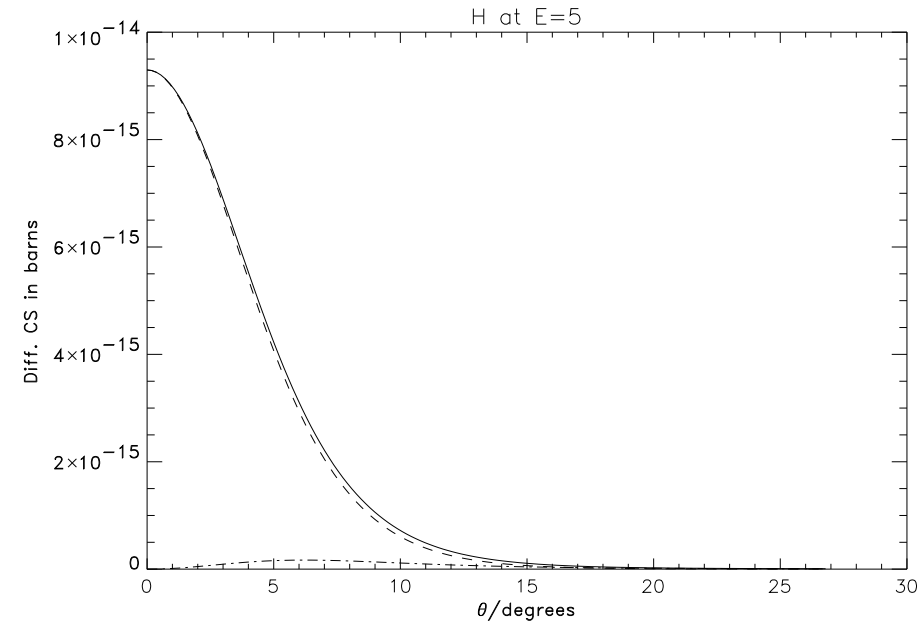

Figure 47: As in figure 46, this time for $E = 5$.

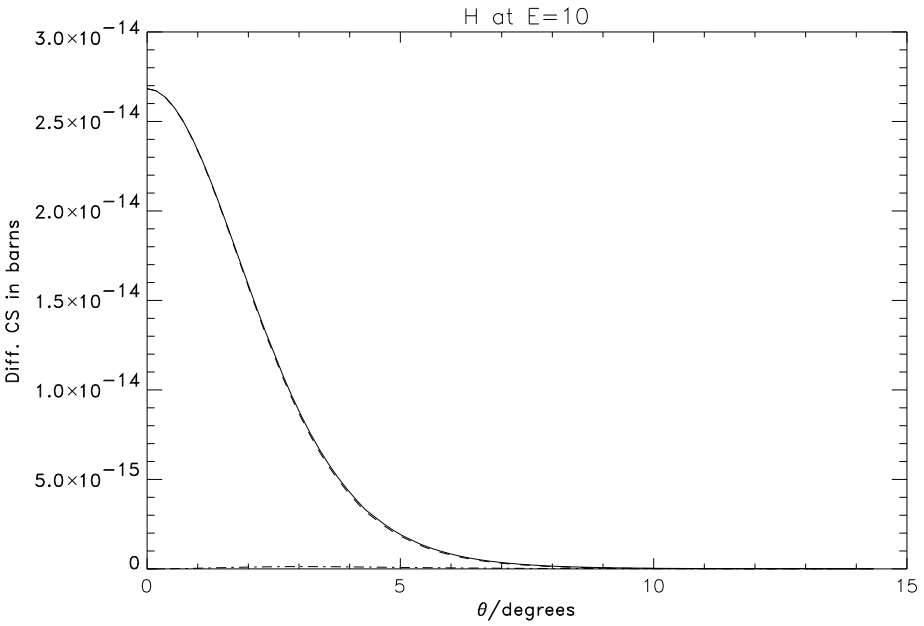

Figure 48: As in figure 46 but with $E = 10$.

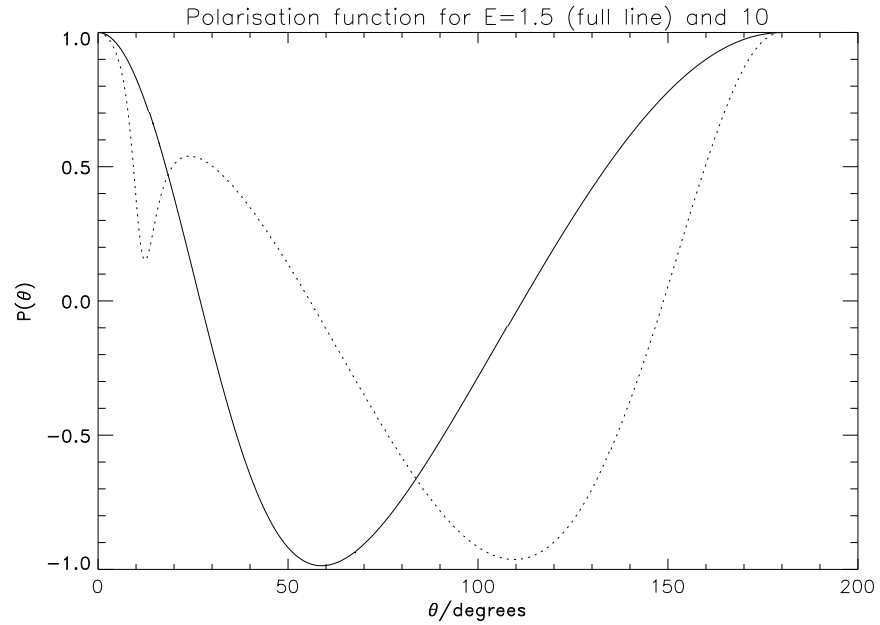

Figure 49: The polarisation function (128) for $Z = 1$ and $E = 1.5$ (full line) and 10 (dotted line) for capture to the $2p_{\frac{1}{2}}$ subshell.

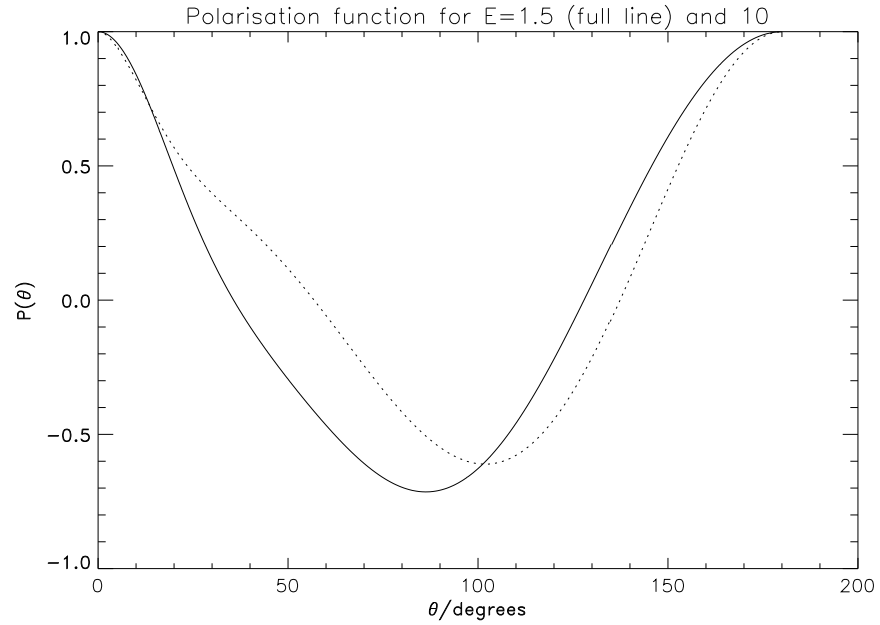

Figure 50: As figure 49 , this time for $Z = 92$.

the K shell, this is completely different from the case $Z = 1$, which once again emphasises the breakdown of the Born approximation.

Part III
Pair Production in Relativistic Ion Collisions

10 The Impact Parameter Model

Direct pair production may occur in relativistic collisions of charged particles. The cross sections for these processes are easily calculated in perturbation theory, as given, for instance, by Feynman for a muon incident on a nucleon. In this case, we have two Feynman diagrams of the type shown in Fig 51.

In the case of collisions of heavily charged ions, these perturbation results become invalid, and an exact calculation is needed (see, for instance, Eichler (1990), Momberger *et al* (1996), and Baltz *et al*, and references therein.)
This process is, however, very difficult to calculate exactly, so that we shall make the following approximations, arriving at the situation described in Figure 52. Let us for simplicity consider the process of excitation or ionisation, and imagine the target to be a hydrogen-like system of arbitrary charge Z and the projectile to be a fully stripped ion of charge Z_p (in units of the elementary charge e). The approximations and definitions to be used are

- Any influence of the electron on the motion of the ions is neglected, which amounts to considering the ions as very much heavier than the electron.
- The target nucleus is treated as an infinitely heavy point charge located at the origin.
- The projectile is treated as a classical particle moving with velocity β - furthermore, the influence of the Coulomb field from the target ion on the particle is neglected, and the hyperbolic motion displayed by a charged particle in a Coulomb field is replaced by the corresponding straight-line trajectory.
- The motion of the particle is taken to be parallel to the z-axis, passing the origin at the minimum distance b (b thus being the *impact parameter*), which offset is taken to be along the x-axis in the calculations.

The calculation of ionisation or excitation cross sections is now reduced to computing the probability for the target electron of going to a given final state in the time-dependent electromagnetic field of the particle ion for arbitrary impact parameters, and subsequently integrate this result over the impact parameter plane.

Figure 51: One of the Feynman diagrams needed for perturbation calculations of pair production in ion collisions (from Feynman).

The main result of these approximations is that we have succeeded in reducing an extremely difficult quantum mechanical three-body problem to the merely very difficult problem of calculating the time development of the electronic wave function in the time-dependent field of the particle - thus ensuring that the probability of the process can be given in terms of single-electron matrix elements. Since the ions are so much heavier than the electron, the impact parameter approximation is valid, and the difficulty of calculating the process exactly arises solely from the intractability of the time-dependent one-electron problem in the relativistic case.
Turning our attention to pair production, the initial state is now taken to belong to the negative energy continuum, while the wave function of the resulting electron is taken to be the final state, as discussed in section 3.5. That is, once more the process of pair production is viewed as an "ionisation from the negative-energy continuum", and the treatment is completely analogous to that of ionisation.

Extensive reviews of relativistic heavy ion collisions (RHIC) in the impact parameter model (by some also called the semi-classical approximation, often abbreviated SCA) are given by Eichler (1990) and Bertulani & Baur.

Figure 52: Ion collisions as considered in the impact parameter model

11 Calculation of Transition Probabilities

As we have seen, by applying the impact parameter model we have reduced the problem of finding the cross sections for the various cross section to that of calculating the transition amplitudes for a one-electron system in a time-dependent potential.

The theory for these processes may then be based on time-dependent quantum theory, which will permit us to write up relations which are, in principle, exact. In order to compute transition probabilities, however, it may be necessary to introduce various approximations, of which the most popular is the Born approximation.

We shall also examine another approximation, the "sudden collision" or *Magnus* approximation, which has been used many times in problems from nuclear and nonrelativistic atomic physics. Recently, it has been attempted to use it in the relativistic regime (Ionescu), and an attempt has also been made to use it in connection with the present work. Later, however, we shall see that the first Magnus approximation is not very convenient in RHIC or in relativistic atomic physics in general.

11.1 The Transition Operator

Let us imagine we have a quantum-mechanical system whose wave function at $t = -\infty$ and $t = +\infty$ (that is, its initial and final states) are solutions of a time-independent Hamiltonian H_0. Let us also imagine that we want to compute the probability for going from an initial state characterised by the quantum numbers i to a final state, characterised by the quantum numbers f. These states will be assumed to be stationary solutions of H_0, so that

$$H_0\Psi_i^0 = E_i\Psi_i^0, H_0\Psi_f^0 = E_f\Psi_f^0 \tag{130}$$

Furthermore, we may imagine the system to be perturbed by a time-dependent interaction potential $V(t)$, so that for arbitrary times the time development is given by [12]

$$i\frac{\partial\Psi^0(t)}{\partial t} = \left[H_0 + V(t)\right]\Psi^0(t) \tag{131}$$

Defining some new wave functions $\Psi(t)$ by

$$\Psi(t) = e^{iH_0t}\Psi^0(t) \tag{132}$$

we find that they fulfil the "reduced" equation

$$i\frac{\partial\Psi(t)}{\partial t} = \bar{V}(t)\Psi(t) \tag{133}$$

where the interaction potential is transformed, so that

$$\bar{V}(t) = e^{iH_0t}V(t)e^{-iH_0t}. \tag{134}$$

In the new representation (the *interaction representation*) the operators from the normal representation (where the state vectors obey (131)) must undergo a similar transformation in order to conserve the values of all scalar products.
(133) has the formal solution

$$\Psi(t) = \Psi_i - i\int_{-\infty}^{t} dt'\bar{V}(t')\Psi(t'), \Psi_i = \Psi(t=-\infty) \tag{135}$$

Defining the *time evolution operator* (actually a Green's function) $O(t,t')$ by

$$\Psi(t) = O(t,t')\Psi(t'), \tag{136}$$

it is clear by insertion and iteration of (135) that

$$\Psi(t) = O(t,-\infty)\Psi_i \tag{137}$$

where[13]

$$O(t,-\infty) = 1 - i\int_{-\infty}^{t} dt'O(t',-\infty) \tag{138}$$

$$= 1 - i\int_{-\infty}^{t} dt'\bar{V}(t') + i^2\int_{-\infty}^{t} dt'\bar{V}(t')\int_{-\infty}^{t'} dt''\bar{V}(t'') + \ldots$$

[12]It might be argued that (131) looks conspicuously like a Schrödinger equation, while we are mainly concerned with the Dirac equation in this work. But relations of the type $i\frac{\partial\Psi(t)}{\partial t} = H\Psi$ is true for the time development of *any* quantum system; it is *the* dynamic equation of quantum theory. The Schrödinger, Pauli or Dirac equations are thus all special cases, corresponding to different kinds of wave functions (in relativistic quantum theory, different representations of the Lorentz group).

[13]Yes, I am certainly skipping some details here. The process of matching the number of terms with factorials in the denominator is described in some detail in Weissbluth, chapter 9.

$$= Te^{-i\int_{-\infty}^{t} dt\bar{V}(t)}$$

In this equation, T denotes the *time ordering operator* defined by

$$T\{A(t)B(t')\} = \begin{cases} A(t)B(t'), & t > t' \\ B(t')A(t) & t < t' \end{cases} \tag{139}$$

Comparing (130) to (138) finally yields

$$\Psi(t = +\infty) = S\Psi_i = \left\{ Te^{-i\int_{\infty}^{\infty} dt\bar{V}(t)} \right\} \Psi_i \tag{140}$$

where we have defined the *scattering matrix* or *S-matrix*

$$S = O(\infty, -\infty). \tag{141}$$

The amplitude for going from the initial state with quantum numbers i to the final state with quantum numbers f is thus given by

$$S_{fi} =< f|S|i >=< f|Te^{-i\int_{-\infty}^{\infty} dt\bar{V}(t)}|i > \tag{142}$$

In perturbation theory one *usually* expands (142) from the assumption that the interaction potential is weak; in many cases one thus only retains the first term, which yields

$$< f|S - 1|i >= -i < f| \int_{-\infty}^{\infty} \bar{V}(t)dt|i > \tag{143}$$

This is, of course, the *first Born* approximation, which is valid to first order in the (supposedly weak) interaction potential. In the *sudden collision approximation* (SA), on the other hand, the expansion is not in the magnitude of the interaction, but in the duration of the process, which is equivalent to assuming that only a small time interval contributes substantially to the sum (138), or, alternatively, that the interaction potential commutes at different times[14]. The method is described by Eichler (1976) and also in some detail by Bransden and McDowell. The point is that, departing from (142) we introduce the expansion

$$S_{fi} =< f|e^{-i\int_{-\infty}^{\infty} \bar{V}(t)dt + \frac{1}{2!}i^2 \int_{-\infty}^{\infty} dt \int_{-\infty}^{t} dt' \left[\bar{V}(t), \bar{V}(t')\right] + \cdots}|i > \tag{144}$$

If only a very narrow range of times actually contribute to the integrals, one may retain only a few terms. The first term of this expansion (and the only one we will retain) is

$$< f|S - 1|i >=< f|e^{-i\int_{-\infty}^{\infty} \bar{V}(t)dt}|i >, \tag{145}$$

and this will correspond to regarding the collision process as instantaneous; this approach is also called the *Magnus approximation*. If the interaction potential

[14]This is *not* the case for RHIC in the impact parameter model, which we will discuss in the next section.

should happen to commute at different times, the first Magnus approximation is of course exact.
A thorough derivation of the Magnus expansion (144) and a discussion of its convergence properties including the conditions for using (145) is given by Pechukas & Light.

11.2 Coupled Channel Equations

A formulation of the time-propagation problem which is wholly equivalent to the derivation of the S-matrix given in the preceding section leads to the so-called *coupled channel equations*. Since this formulation is very much used, and since coupled channel calculations have frequently been used in the calculation of probabilities of the various processes in RHIC, we shall include a short discussion of these.
The starting point is, once again, the time-dependent equation in the interaction picture,

$$i\frac{\partial\Psi(t)}{\partial t} = \bar{V}(t)\Psi(t) \tag{146}$$

We may, of course, expand Ψ on a basis of stationary states, so we can write

$$\Psi = \sum_n a_n(t)|n>, \tag{147}$$

which upon insertion in the above equation reduces to equations for the coefficients a_n, that is,

$$i\frac{da_n(t)}{dt} =< n|\bar{V}|\Psi >= \sum_k a_k(t)V_{nk}e^{i(E_n-E_k)t}, \qquad V_{nk} =< n|V|k > \tag{148}$$

In coupled channel calculations, these equations are integrated numerically with the limiting condition

$$\lim_{t\to-\infty} a_n(t) = \delta_{ni} \tag{149}$$

and at plus infinity (practically speaking, at some advanced, finite time) the resulting wave function Ψ is to be projected on the final state, so that the probability of the transition becomes

$$|<f|\Psi>|^2 = |a_f(\infty)|^2 \tag{150}$$

It should be noted that the equations (148) also serve as the starting point for time-dependent perturbation theory. Thus, the Born approximation (143) may be obtained by setting the a_k on the right-hand side of (148) equal to δ_{ki}.
In actual calculations, the basis of stationary states must of course be *finite*, and this truncation of the basis may severely limit the precision of the calculations, as discussed by Baltz *et al* - see also the discussion in Momberger *et al* (1996).

12 Transition Probabilities in RHIC

12.1 Born Approximation

In the impact parameter model, the formalism of the preceding section may be implemented with the Coulomb potential of the target as the time-independent potential H_0, while the interaction potential is represented by the Lorentz-contracted Coulomb potential of the particle (as described by Eichler (1990) and Bertulani & Baur). This must be introduced in the Dirac equation by minimal coupling, so that the resulting potential becomes[15]

$$V_p(\mathbf{r},t) = -\gamma(1-\beta\alpha_z)\frac{\alpha Z_p}{\sqrt{(x-b)^2+y^2+\gamma^2(z-\beta t)^2}} \tag{151}$$

The process of bound-free pair production may be described by the use of this potential, and this is exactly what has been done by a number of authors, albeit with rather different approaches.

In the Born approximation (143), the transition probability becomes

$$P(b) = |S_{fi}|^2 = |<1s|\int_{-\infty}^{\infty} e^{i(E_{1s}+E_p)t}V_p(\mathbf{r},t)dt|-E_p>|^2, \tag{152}$$

where $|1s>$ of course is to be interpreted as the electronic state corresponding to the ground state of the unperturbed target, while $|-E_p>$ is the wave function of the negative continuum corresponding to the energy E_p of the emitted positron.

Upon taking the time integral in (152), the corresponding probability amplitude becomes

$$a_{fi} = -2i\frac{\alpha Z_p}{\beta}<1s|e^{i\frac{E_{1s}+E_p}{\beta}z}(1-\beta\alpha_Z)K_0\left(\frac{(E_{1s}+E_p)}{\beta}\frac{\sqrt{(x-b)^2+y^2}}{\gamma}\right)|-E_p> \tag{153}$$

where K_0 is a modified Bessel function of the second kind.
In order to obtain the total cross sections for pair production in the Born approximation, "all" one has to do is compute these matrix elements, square them, sum them over partial waves, integrate them over the positron energy and, finally, take the integral over the impact parameter plane.

The calculations in the Born approximation for bound-free pair production were done by Becker *et al* in 1986.

12.2 Coupled channel calculations

Coupled channel calculations may be implemented as described in the preceding section, in analogy to the Born approximation procedure. Such calculations were

[15]In this and the following equations, α_z is the z component of the matrix vector defined by equations (5) and (7).

reported in 1991 by Momberger *et al* (1991) and by Rumrich *et al*. Rumrich *et al* calculated the transition probabilities for a number of of different projectiles on a $Z = 82$ target. For this purpose, they used a basis set consisting of 334 states, including the 22 lowest bound states. They reported a considerably higher transition probability at low impact parameters than predicted by perturbation theory (about two orders of magnitude larger than those obtained using the Born approximation discussed above), which led them to conclude that the perturbation theory underestimates the total cross section by as much as a factor of 5.

Later calculations by Baltz *et al* using larger basis sets (which was not feasible for the authors mentioned above) showed a considerable reduction of the nonperturbative enhancement, and by varying the size of their basis they were able to show that the enhancement behaved like a decreasing function of the size of basis - and this definitely indicates that the calculations of Rumrich *et al* were not sufficiently accurate due to the truncation of the basis set.

Recent calculations by Momberger *et al* (1996) which did not involve coupled channel calculations also denies the appearance of this so-called "nonperturbative enhancement" and ascribe the results of Rumrich *et al* to failure of convergence due to the truncation of the basis set.

12.3 Magnus Approximation

The SA was introduced in ion-atom collisions in the non-relativistic regime by J. Eichler in 1977, who introduced it for the study of ionisation in ion-atom collisions.
Eichler started with the expansion (144), and argued that if only the collision time was very much smaller than the typical orbit times of the system, the time structure of the process might be wholly ignored, and the transition operator for the process would to a good approximation be given by (145)
He further argued that if this was the case, then the effect of the transformation (134) to the interaction picture was negligible, so that he might simply take $\bar{V} = V$.
These two steps, however, actually represent two *different* assumptions, which it is convenient to spell out.

- First of all, the collision time must be very much smaller than the characteristic orbit times of the perturbed system.
  The appropriate collision time must here be taken as the duration of the interaction at a single point; in RHIC, this is the passage time $\frac{b}{\gamma\beta}$ of the Lorentz-contracted Coulomb field of the particle. This is so, since the terms in the exponent in the expansion (144) will contain powers of the interaction potential, which falls of with time, so that it is, effectively, an expansion in

$\frac{b}{\gamma\beta}$ (or rather: in the ratio of the duration of the interaction to the characteristic orbit times (Pechukas & Light)).

- Secondly, in order to neglect the transformation to the interaction picture we must demand that the time interval that contributes to the time integral in equation (145) is much smaller than the time $\frac{\hbar}{\Delta E}$ that characterises the *electronic process*, and this time interval is of the order of the time it takes the ion to pass over the dimensions of the target atom.

Eichler did not point out the fact that two different assumptions are involved, since this is not necessary in the case of ionisation in the nonrelativistic domain.

This approach was later used by Salop & Eichler for the study of ionisation in ion-atom collisions. The SA has also been used by a number of other authors; Wille, for instance, used it for the process of rotationally induced inner-shell excitation, where he was able to limit his calculations to a finite basis.

In the course of the work on the present thesis, some work has been done along these lines. It has been realized, however, that the approximation of taking the transformed and untransformed interaction potentials to be equal is wholly inapplicable in the relativistic regime. Indeed, if one were to set $V_p = \bar{V_p}$, the SA would become

$$a_{fi} =< f|e^{-i\int_{-\infty}^{\infty} V(\mathbf{r},t)dt}|i >, \tag{154}$$

where the integral in the exponent is

$$\int_{-\infty}^{\infty} dt V(\mathbf{r},t) = -\gamma(1-\beta\alpha_z)\alpha Z_p \int_{-\infty}^{\infty} dt \frac{1}{\sqrt{(x-b)^2+y^2+\gamma^2(z-vt)^2}} \tag{155}$$

This integral is divergent, but it can be shown, that this divergence only contributes a constant (but infinite) phase factor, and thus does not contribute to probabilities. Indeed, if in the Born approximation integral (152) we let $E_{1s}+E_p$ tend towards zero, the argument of the modified Bessel function will tend to zero, and we can introduce the approximation

$$K_0(x) \sim -\ln x \text{ for } x \ll 1 \tag{156}$$

Thus we obtain

$$\int_{-\infty}^{\infty} dt V(\mathbf{r},t) = -2\frac{\alpha Z_p}{\beta}(1-\beta\alpha_Z) K_0\left(\frac{(E_{1s}+E_p)}{\beta}\frac{\sqrt{(x-b)^2+y^2}}{\gamma}\right) \tag{157}$$

$$\sim 2\frac{\alpha Z_p}{\beta}(1-\beta\alpha_Z)\left[\ln\sqrt{(x-b)^2+y^2} + \ln\frac{E_{1s}+E_p}{\gamma\beta}\right]$$

The last term inside the square bracket diverges as $E_{1s}+E_p \to 0$, but since it is does not depend on r, it will only contribute to the matrix element with a

phase factor, which (albeit infinite) will have no influence on probabilities.
As a result, the transition amplitude then becomes

$$a_{fi} =< f|e^{-2i\frac{\alpha Z_p}{\beta}\ln\sqrt{(x-b)^2+y^2}}|i > \tag{158}$$

If this approximation were feasible, it would provide an interesting non-perturbative approximation (that is, it would, in principle, take exact account of both the particle and target potential) in the high-energy limit.

This is unfortunately not so, since it should then reduce to the Born approximation (152) in the limit of low Z_p. But it does not, since it lacks the "translation factor" $e^{i\frac{(E_{1s}+E_p)z}{\beta}}$ which is definitely not negligible in the present case.

If one compares with (152), one finds that a translation factor similar to $e^{i\frac{E_{1s}+E_p}{\beta}z}$ also occurs in the non-relativistic case[16] and it becomes clear that in the limit where the Born approximation becomes valid, this corresponds to the dipole approximation known from the theory of electromagnetic transitions, which again corresponds to the neglecting of retardation effects (as discussed by Pratt *et al*, page 303).

But if we want to attempt the SA and retain the transformation to the interaction picture, we would, indeed recuperate the Born approximation; a complication is that the matrix elements of the operator $e^{-i\int_{-\infty}^{\infty}dte^{iH_0t}V_pe^{-iH_0t}}$ would become difficult to compute. Indeed, by introducing the definition of the exponential function, we obtain

$$< f|e^{-i\int_{-\infty}^{\infty}dte^{iH_0t}V_pe^{-iH_0t}}|i >= \delta_{fi} - i < f|\int_{-\infty}^{\infty}dtV_p(\mathbf{r},t)e^{i(E_f-E_i)t}|i > \tag{159}$$

$$+\frac{i^2}{2!} < f|\int_{-\infty}^{\infty}dt\int_{-\infty}^{\infty}dt'e^{iE_ft}V_p(\mathbf{r},t)e^{-iH_0(t-t')}V_p(\mathbf{r},t')e^{-iE_it'}|i > +\ldots$$

The only simple way to calculate this operator would probably be by diagonalising the interaction potential $\bar{V_p}$, and this could only be done numerically, in a finite basis. Thus, the impossibility of neglecting the transformation of the interaction potential leads to the necessity of introducing a truncated basis set - and the procedure would be no simpler and less reliable than the coupled channels approach.
This should be a sufficient demonstration that the last of Eichler's assumptions will not hold good in the relativistic regime, and that the SA is, if valid, at least impractical in connection with RHIC.

We thus conclude that while the SA may well be feasible in atom-ion collisions in the nonrelativistic regime, it does not appear to be practical in the relativistic case, since it does not appear to be possible to avoid the introduction of a finite basis set.

[16]In the guise of the well-known translation factor $e^{i\mathbf{q}\cdot\mathbf{r}}$, where $\mathbf{q}$ is the momentum transfer: the necessity of this factor is also argued, for instance, in Bransden and McDowell.

Figure 53: Flattening of the electromagnetic field due to a relativistic point charge, and the two corresponding equivalent pulses of photons (from Bertulani & Baur).

13 Weizsäcker-Williams Approximation

13.1 The Virtual Photon Approach

In the virtual photon method, one exploits the fact that the electromagnetic field due to a very fast point charge gets Lorentz contracted, 'flattened', becoming nearly transversal at very high energies. The situation is depicted in figure 53.[17] Indeed, assuming a particle of rest mass M to move in a straight line along the z axis, passing the origin at the distance b on the x axis as described above, with the relativistic parameter γ (corresponding to the energy $E = \gamma Mc^2$), the fields in the laboratory systems are

$$\begin{aligned} E_x(t) &= \frac{Z_p \gamma b}{4\pi} \left[b^2 + \gamma^2 \beta^2 t^2 \right]^{\frac{3}{2}} \\ B_y(t) &= \beta E_z(t) \\ E_z(t) &= \frac{-Z_p \gamma \beta t}{4\pi} \left[b^2 + \gamma^2 \beta^2 t^2 \right]^{\frac{3}{2}} \end{aligned} \tag{160}$$

For $\gamma \gg 1$, the two first fields are completely equivalent to a pulse of photons incident on the particle along the z axis.
The electric field component E_z does not really correspond to any pulse since it has no accompanying magnetic field. One may, nevertheless, add a magnetic field and find that the electric field of the particle becomes equivalent to two incoming pulses, as seen on figure 53.

[17] The theory given in this subsection is an outline of the detailed exposition given by Jackson - a thorough discussion of the method is also given in the article by Williams.

The intensity of the equivalent photon pulses may be expressed in terms of the Fourier transforms of the fields, and read:

$$I_1(\omega) = \frac{1}{4\pi}|E_1(\omega)|^2 = \frac{\alpha Z_p^2}{\pi^2 b^2}\xi^2 K_1^2(\xi) \tag{161}$$

$$I_2(\omega) = \frac{1}{4\pi}|E_1(\omega)|^2 = \frac{\alpha Z_p^2}{\pi^2 b^2}\frac{1}{\gamma^2}\xi^2 K_0^2(\xi),$$

where we have defined $\xi = \frac{\omega b}{\gamma\beta}$, and where the K_0 and K_1 are modified Bessel functions of the second kind.
The probability that a given atomic process occur in the collision may now be expressed in terms of the same process to be caused by the equivalent photons - that is, by integrating the photon intensity spectrum multiplied with the photoelectric cross section for the same process and integrating over the whole spectrum:

$$P(b) = \int (I_1(\omega) + I_2(\omega))\sigma(\omega)\frac{d\omega}{\omega} = \int N(\omega)\sigma(\omega)d\omega \tag{162}$$

where $N(\omega)$ is the *equivalent photon number*, the number of equivalent photons per unit area. The integral over the impact parameter plane may, as discussed by Jackson be done analytically, and the total cross section for the atomic process in question then becomes

$$\sigma = 2\pi\int_{b_{min}}^{\infty} P(b)bdb = \int d\omega\sigma(\omega)\frac{n(\omega)}{\omega}, \tag{163}$$

where

$$n(\omega) = \frac{2\alpha Z_p^2}{\pi\beta^2}\left[xK_0(x)K_1(x) - \tfrac{1}{2}\beta^2 x^2(K_1(x)^2 - K_0(x)^2)\right], \qquad x = \frac{\omega b_{min}}{\gamma\beta}. \tag{164}$$

The integral over b diverges at $b = 0$, so it is necessary to introduce the parameter b_{min}, which is a cutoff parameter which must be chosen differently for different processes.
The contribution for impact parameters below b_{min} must be neglected or accounted for or estimated by some other method. At high energies, the contributions from large impact parameters become increasingly important, and the contribution which is neglected by the introduction of b_{min} is of no consequence. In order for the approximation to be valid, the results so obtained should not depend strongly on the choice of b_{min}. Since the modified Bessel function in (164) decays exponentially for $x \geq 1$, the main contribution to the cross section will come from photons for which

$$\omega \leq \frac{\gamma\beta}{b_{min}}. \tag{165}$$

13.2 The Virtual Photon Approach and Bound-Free Pair Production

The virtual photon approximation may be used, with the exact cross sections for bound-free pair production which we calculated in part II, for obtaining the cross sections for bound-free pair production in RHIC.
The method is perturbative, so it is not expected to give very good results for high projectile charges - on the other hand, it is very easy to implement once the photoproduction cross sections are known, and even for high projectile charges it may provide a valuable estimate of the cross section with exact inclusion of the dependence of the process on the *target* field.
What minimum impact parameter b_{min} must be chosen in this case? As argued by Jackson, it cannot be chosen to be less than the Compton wave length of the lightest particle involved, as also discussed by Hencken *et al.* But we can be more precise than that:
If we compare the arguments to the modified Bessel functions in equations (164) and (153), it becomes clear that one of the approximations involved in the virtual photon approach is to assume that the main contributions to the cross section will come from regions where the transversal distance $\sqrt{(x-b)^2+y^2}$ between the electron and the projectile in equation (153) may be taken to be equal to b, that is, outside the atom (see also the discussion in Baltz *et al*).

The same conclusion is reached by considering the related process of K-shell ionisation (as also argued by Williams) - here, the contributions from impact parameters inside and outside the atom are of a quite different nature, and the equivalent photon model is only applicable in the latter region.

In order to be consistent with this assumption, b_{min} must be chosen equal to or larger than the Bohr radius $\frac{1}{\alpha Z}$ of the target.[18]
The contributions from lower impact parameters must be included or estimated by other means, but at very high energies they will not be important. Since there are certain similarities between the expressions for the Born and WW approximations, as noted above, it would seem consistent to try to estimate the contributions from $b < \frac{1}{\alpha Z}$ by taking the results from the perturbation calculations by Becker *et al.*

Alternatively, one might estimate the result from the more reliable numerical results recently reported by Momberger *et al* (1996) and Baltz *et al* - but this approach involves an assumption that the collision will be well described by perturbation theory for impact parameters higher than $\frac{1}{\alpha Z}$, while nonperturbative calculations must be used in closer collisions - and this assumptions is not *a priori* easy to justify.

[18]This is in contradiction with the practice in much of the literature of recent years, cf. Bertulani & Baur or Aste *et al.* The tendency has been to choose b_{min} equal to one Compton length in analogy with free-free pair production (where the wave functions are not localised in the neighbourhood of the nucleus.)

13.3 Results

Since, as has been mentioned, we have been led to demand that the parameter b_{min} should be chosen approximately equal to (and not smaller than) the Bohr radius of the target, we have only considered our three heavy example elements, that is, Au, Pb and U. Since the exact value of b_{min} should not be important, we will consistently choose $b_{min} = 2$ throughout the calculations.

The calculations have only been performed for capture to the K shell - the result for the L shells may, within the accuracy expected from the virtual photon method, be obtained by multiplying the result for the K shell with the high-energy limits listed in 2.

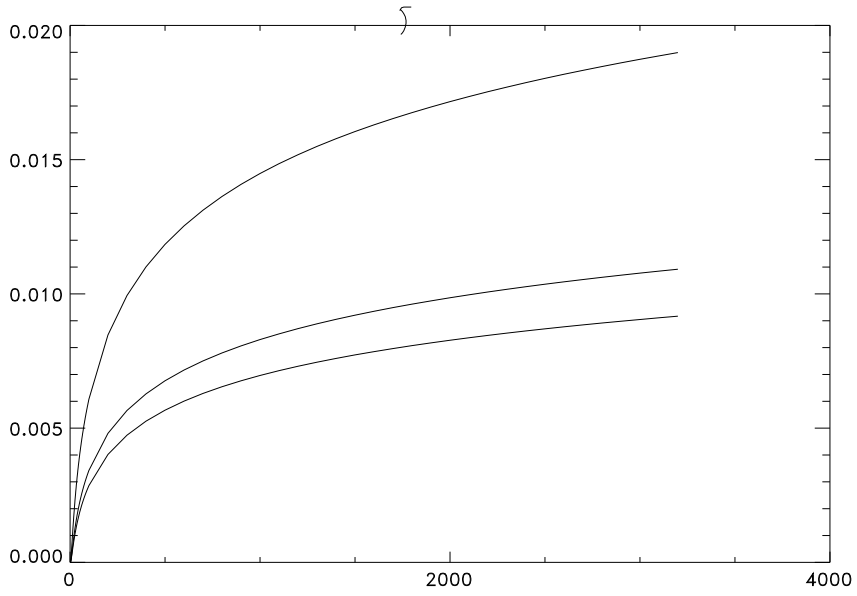

Figure 54: Cross sections for bound free pair production with capture in the collisions $Z_p + Z$ for Z=92, 82 and 79, scaled by Z_p^2, as a function of collision γ ($\gamma = \frac{1}{\sqrt{1-\beta^2}}$).

In figure 54 we display the results of such calculations for γ between 1 and 3400. For $\omega \leq 50$, the integral in (163) was done using the exact cross sections obtained Part II of the present work - for $\omega > 50$, the modified Born approximation (123) was used, where the values for $f(Z)$ were taken from table 1.
In order to compare the results obtained in the present work with those obtained by others, we have also calculated the cross sections choosing $b_{min} = 1$.

In table 3, we display the following data, for collisions with a collision energy of 10,100 and 20.000 Gev/amu (kinetic energy - this corresponds to $\gamma \sim 11.74$, 108.4 and 21.471, respectively) for the collision system Au+U, with U as the

target:

1. Our present results calculated using $b_{min} = 2$, which we believe is the most consistent choice

2. Our present results, obtained using $b_{min} = 1$

3. The results reported by Aste *et al*, using $b_{min} = 1$

4. An estimate of the contribution to the total cross section for bound-free pair production in RHIC from the region $b \leq 2$, estimated from the data of Becker *et al* (for $E = 20.000$ GeV, this contribution was estimated from the data given by Baltz *et al.*).

5. The total cross section σ_{pert}, obtained from perturbation theory, taken from Becker *et al.*

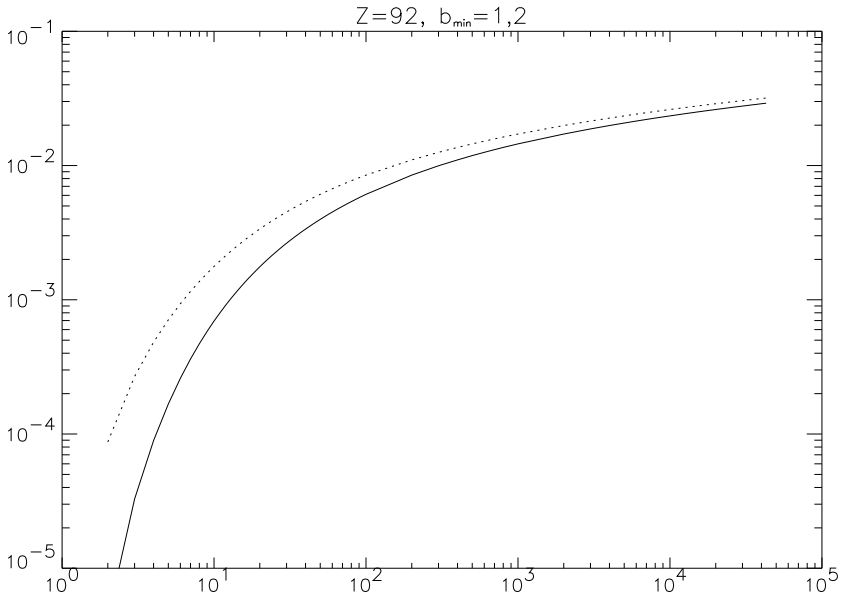

Figure 55: The WW-cross section for bound-free pair production in RHIC for $Z = 92$, scaled by Z_p^2 with $b_{min} = 2$ as a function of collision γ, compared to the corresponding curve for $b_{min} = 1$ (dotted). Wee see that at high energies, the difference between the two curves becomes of no consequence.

First, we observe that the good agreement between our results for $b_{min} = 1$ and those of Aste *et al* serves as a satisfactory check of our calculations.[19]

[19]The small discrepancy may arise from the fact that Aste *et al* actually give an extrapolation formula, and that they have used equation (124) for the high energy limit.

E_{coll}/ (GeV/amu)	$b_{min} = 2$	$b_{min} = 1$	Aste *et al*	$b \leq 2$, pert. theory	σ_{pert}
10	5.58	13.1	-	8	13
100	39.8	54.8	54.4	13	50
20.000	165	182	183	16	295

Table 3: In this table, we compare our virtual photon cross sections (in barns) for $b_{min} = 2$ and $b_{min} = 1$ with those of Aste *et al* and with the Born approximation results obtained by Becker *et al*.

Secondly, we see that the result obtained by setting $b_{min} = 2$ and estimating the contribution from the inner region by perturbation theory yields almost exactly the same result as taking $b_{min} = 1$. It thus seems that even though the choice $b_{min} = 1$ cannot be justified physically, the extra contribution thus obtained is a good approximation to the perturbation result for the contribution for small b.

Thirdly, we see that the results thus obtained actually reproduce the perturbation results of Becker *et al* for $E = 10$ and 100 GeV/amu. For $E = 20.000$, the virtual photon results seem somewhat below the perturbation result - but this result was in fact estimated, not calculated, by Becker *et al*, and if we estimate it from the data given by Baltz *et al*, we obtain σ_{pert}=185 barn.

So it seems that the result of the WW-method using the exact cross sections for photon-impact bound-free pair production is simply that of reproducing the results of perturbation theory - as another example, Baltz *et al* obtained a perturbation cross section of 112 barn for bound free pair production in Pb+Pb collisions at $\gamma = 23.000$ - our calculations yield 114 barn for $b_{min} = 2$, if we use their value for the contribution for $b \leq 2$, and 113 using $b_{min} = 1$.

At sufficiently high energies, it does not really matter whether we use b_{min}=1 or 2. This is illustrated on figure 55, where the two estimates of the cross sections (that is, for $b_min = 1$ or 2) are compared; we see that at very high energies, the relative contribution from the closest collisions becomes negligible, and the difference between the results obtained for the two values of b_{min} becomes of no consequence. The reason for this is that at high energies, the contribution from small impact parameters becomes nearly constant, so that from $\gamma = 1000$, the difference between the two curves is nearly constant (and is equal to 0.0027 barn).

14 Conclusion & Discussion

14.1 Photon Impact

We have performed a thorough theoretical investigation of the process of photon-induced pair production with capture to an atomic shell in a Coulomb potential - after obtaining exact (but not closed) expressions for the total and differential cross sections of this process, we proceeded to present the result of the numerical calculations of these formulae.

Our results for the K and $2s$ shells are in good agreement with the results previously reported by Aste *et al*, Johnson *et al*, Sheth & Swamy and Johnson - our results for the p shells are new, but for $Z = 1$ they agree with the Born approximation. Our results for the high energy limit were in good, but not exact, agreement with the high energy limits previously obtained by Pratt.
As discussed below, we believe that our extrapolation is correct, so that the high energy limit of the four processes mentioned in section 2 has now become better determined. The alternative, that the discrepancy is caused because the present calculations have not been taken to sufficiently high energies, does not seem probable, as was also discussed in section 8.1.

14.2 Relativistic Ion Collisions

Our most important result has been, that the results of the Weizsäcker-Williams approximation using the exact photoelectric cross sections exactly reproduce those of the first Born approximation for collision energies above 10 GeV/amu.
Our comparison of the choices $b_{min} = 1$ and $b_{min} = 2$ shows that even though we think the choice $b_{min} = 1$ cannot be given a physical justification, it is, at least for high target charges, a good approximation to the result obtained by taking $b_{min} \sim$ the Bohr radius of the target ion and estimating the contribution for $b_{min} \leq 2$ by perturbation theory.

The coupled channel results obtained by Baltz *et al* using up to 7936 states in the basis set indicate that the total cross section for Pb+Pb at $\gamma = 23000$ is only about 7 % higher than the result obtained by perturbation theory.

Now, when the Weizsäcker-Williams approximation is capable of reproducing the results obtained by perturbation theory, and if the cross sections obtained by perturbation theory are not expected to be very much lower than the exact results (Baltz *et al*; this is also confirmed by Momberger *et al* (1996), who report that the "nonperturbative enhancement" at low impact parameters is only a factor of 4-5, nowhere near the two orders of magnitude reported by Rumrich *et al*), the virtual photon approximation gives a valuable estimate of these cross sections; moreover, this estimate is very much easier to obtain than the perturbation result, and once the high energy limit is properly determined (as by our modified Born approximation), it can easily be performed for any collision energy above 10

GeV/amu.

14.3 Possible Continuations of the Present Work

What could be done in extension of the present project, and what have we left undone?

Well, obviously we have not performed the calculation of the differential cross sections for the $2p_{\frac{3}{3}}$ subshell - the reason for this is less than flattering, since it was regarded as something that would be quite easy to do, and thus it was postponed until too late. When it turned out to be a little less easy, it was found that we had already enough material for the present thesis, and thus it was left undone.

Another extension would be that of considering bound-free pair production of heavy leptons, especially $\tau^{\pm}$. The cross sections for this process are extremely small - indeed, if we could continue considering the target ion as a point charge, we would be able to reuse the numerical results from part II merely by changing all formulae to units of the Compton wavelengths λ_l of the heavy leptons.

Since the rest mass of the τ leptons is 3491 times that of the electron, this would mean that the threshold energy would be about 3500 MeV instead of about 1 MeV, and at the same time the cross section for the process is reduced by a factor $\left(\frac{\lambda_C}{\lambda_\tau}\right)^{-2} \sim 8 \cdot 10^{-8}$. So pair production of heavy leptons (especially tauons) is a process which is much more difficult to achieve and detect experimentally than the the production of electrons and positrons.

But these considerations may only give a hint, an idea of the order of magnitude of the cross sections for heavy leptons, since the results from the preceding section cannot be 'recycled' in the proposed fashion. The wave functions are modified by a number of additional effects, especially modifications due the the finite nuclear size and quantum electro-dynamical self-energy. The results of these modifications is that the cross sections for bound-free production of $\tau^{\pm}$ is further reduced.

The process is interesting, however, since if the cross sections are not too small, it might be a possible way of forming tauonic atoms, which to the best of my knowledge has never been observed.

It should be possible to obtain a useful estimate of the cross by taking account of the finite nuclear size, which changes the wave functions dramatically (for $Z = 92$, the Bohr radius of the tauonic atom is well within the nucleus) by treating the nucleus as a constant, spherically symmetrical charge density. It has been proposed[20] that it should be possible to obtain a reasonable value for these cross sections by using a nonrelativistic wave function for the ground state and representing the positron as a plane wave.

[20] By Allan H. Sørensen, my supervisor at the present project.

As for the estimates of the cross sections for pair production with capture in relativistic heavy ion collisions, it should be possible to supplement the virtual photon approximation with a high-energy approximation, which in analogy to the modified Born approximation introduced in section 8.1 would make it possible to obtain the correct energy- and projectile charge dependence in the high-energy limit.

We reviewed one such possibility, the sudden collision approximation, and found that it has the same drawback as the coupled channel method, that it probably requires the introduction of a finite basis set. Nevertheless, it may still be easier to apply than the coupled channel method which is very labourious, as all the nonperturbative methods (cf. Momberger *et al*, 1996) which have been attempted. Other high-energy approximations might also be found which do not suffer from this shortcoming.

15 Appendix A: Alternative Calculation of the Integral $K(s, s_b, k, p_0, p, k_0)$

Let us recall that this integral is given by

$$K(s, s_b, k, p_0, p, k_0) = \int_0^\infty dr r^{s+s_b} e^{-(p_0+ip)r} j_k(k_0 r) F(s+1+i\eta, 2s+1; 2ipr) \quad (166)$$

where in our application (for a given charge Z) the parameters s and k are associated with the partial wave quantum numbers, while p and k_0 are associated with the photon energy.

Instead of introducing the finite series expansion (84) for the spherical Bessel function, one may go another way altogether and obtain an alternative analytical expression for the integral.
First, let us recall that the spherical Bessel function may be defined in terms of the ordinary Bessel function,

$$j_k(x) = \sqrt{\frac{\pi}{2x}} J_{n+\frac{1}{2}}(x), \quad (167)$$

Inserting this expression in (166), we obtain

$$K(s, s_b, k, p_0, p, k_0) = \sqrt{\frac{\pi}{2k_0}} \int_0^\infty dr r^{s+s_b-\frac{1}{2}} e^{-(p_0+ip)r} J_{k+\frac{1}{2}}(k_0 r) F(s+1+i\eta, 2s+1; 2ipr). \quad (168)$$

The reason that we are interested in doing an alternative computation of this integral is that the analytical expression which we obtained in section 5 has the drawback of being numerically highly unstable for certain classes of input.

In order to appreciate this, we consider the special choice of parameters

$$K(\tfrac{1}{2}, 0, k, 1, 0, 1) = \sqrt{\frac{\pi}{2}} \int_0^\infty dr e^{-r} J_{k+\frac{1}{2}}(r) \quad (169)$$

This integral may be found in Gradshteyn and Ryzhik, and is given by the simple analytical expression

$$K(\tfrac{1}{2}, 0, k, 1, 0, 1) = \frac{\sqrt{\pi}}{2} (\sqrt{2} - 1)^{k+\frac{1}{2}} \quad (170)$$

It is clear upon inspection, that this expression decreases exponentially as k increases. On the other hand, it is just as clear that if we try to evaluate this expression using the result (93), it will be computed as a sum of an increasing number of terms, the order of magnitude of which *in*creases exponentially with increasing k. This means that the exponential decrease is to arise by the successive cancellation of (for high k) many very large terms.

This is, of course, quite feasible mathematically, but computationally it means that the error of the sum is going to increase at each step. Indeed, it was found that computing (166) using the result (93) and the code given in Appendix B the result was exact up to $k = 10$ - but at $k = 14$, the computation showed an error of more than 4 per cent, and at $k = 20$, the computation of (93) yielded a result that is four orders of magnitude too large!

But this is, of course, a rather special case. Do we have similar problems in the use of (93) in the computation of matrix elements as considered in section 5? The answer is that the parameters used in this case are rather complicated, and that it is in no way clear that we do not.
The purpose of this Appendix is to provide an alternative way of computing (166) which *is* numerically stable using the parameters from (169), and which is totally unrelated to the procedure we already know.

In order to solve the integral (168), we introduce the integral representation (90) of the confluent hypergeometric function, thereby converting our integral into

$$K(s, s_b, k, p_0, p, k_0) = \sqrt{\frac{\pi}{2k_0}} \frac{\Gamma(2s+1)}{\Gamma(s+1+i\eta)\Gamma(s-i\eta)} \times \tag{171}$$

$$\times \int_0^1 du u^{s+i\eta}(1-u)^{s-i\eta-1} \int_0^\infty dr r^{s+s_b-\frac{1}{2}} e^{-(p_0+ip(1-2u))} J_{k+\frac{1}{2}}(k_0 r)$$

$$= \sqrt{\frac{\pi}{2k_0}} \frac{\Gamma(2s+1)}{\Gamma(s+1+i\eta)\Gamma(s-i\eta)} \int_0^1 du u^{s+i\eta}(1-u)^{s-i\eta-1} J(s+s_b+\tfrac{1}{2}, p_0+ip(1-2u), k+\tfrac{1}{2}, k_0)$$

where for convenience we have parametrised the integral

$$J(\mu, \alpha, \nu, \beta) = \int_0^\infty dx x^{\mu-1} e^{-\alpha x} J_\nu(\beta x) \tag{172}$$

This integral may be found in Gradshteyn and Ryzhik (equation 6.621), according to which we may write

$$J(\mu, \alpha, \nu, \beta) = \frac{2^{-\nu}\Gamma(\mu+\nu)}{\beta^\mu \left[1+\frac{\alpha^2}{\beta^2}\right]^{\frac{\nu+\mu}{2}} \Gamma(\nu+1)} F(\frac{\nu+\mu}{2}, \frac{1-\mu-\nu}{2}; \nu+1; \frac{\beta^2}{\alpha^2+\beta^2}) \tag{173}$$

And equation (171) is the main result of the present calculation, since it provides a way of computing the integral (166): if only we can compute the integrand, we may also compute the remaining integral by numerical integration. As opposed to the solution of (166) obtained earlier, that is (93), this result is not "closed", since we express one integral in terms of another, and it is thus less "beautiful".

The purpose, however, of deriving this expression is, as stated, to provide a totally alternative way of computing the integral (166).
The hypergeometric function occurring in (173) could not be calculated using the Gauss series, and the the generalised hypergeometric function was used.

The integral (171) was computed using a a straightforward 5000-step trapeze-integration which gave the correct results for the parameters (169) with an accuracy of about 0.1 per cent.
After that, it was used for computing the cross sections for bound-free pair production for $Z = 82$ and k_0 in the range from 2 to 6, and this gave the same results as the other procedure, again within an accuracy of 0.1 per cent.
So even though it was in no way clear that our recipe for computing (166) was numerically stable, its accuracy for the computation of matrix elements has been confirmed (or at least corroborated).

16 Appendix B: Pair Production Programs

In this section, we will list the code of the program that calculates the total cross sections for the K shell. The implementation of the corresponding differential cross sections is quite straightforward, and the L-shell cross sections are computed after the same principles as for the K shell.
For the actual pair production routines, the whole code will be included, whereas for the supplementary files *functions* and *complex* only the header files will be listed. This Appendix will therefore contain the code taken from the following files:

- The header for the data structure complex, *complex.h*.
- The header for the various necessary help functions, *functions.h*.
- The routines for the calculation of cross sections, radial integrals etc. are specified in the header *pairs. h*, which also defines some useful constants.
- Passing from the specification files to the implementation, we first note that the important integral given by (83) is implemented in a separate file, *K. c*.
- The file *pairs. c* contains routines for computing matrix elements, radial integrals and cross sections for the K shell.
- Finally, the file *K-cross.c* is included as an example of how to use the implementations to produce a data file, *in casu*, producing a listing of the K shell cross section for a given target charge.

compl. h:

```
# include <stdio.h>
# include <math.h>
/*************************************************************************
           Implementation of complex numbers
 *************************************************************************/
#define true 1
#define false 0
typedef char bool;
typedef double  real;
typedef struct comp { real re; real im; } complex;

         /***   Miscellanous standard operations  ***/
void c_write(FILE *f,complex z);
real Re(complex z);
real Im(complex z);
bool is_zero(complex z);
complex one();
```

```
complex i();
complex zero();
real c_mod(complex z);
real c_arg(complex z);
/* gives a value between -pi and pi, and pi on the negative real axis */
complex c_conj(complex z);
complex c_const(real x, real y);

         /***   Arithmetical operations   ***/

complex c_plus(complex z1, complex z2);
complex c_minus(complex z1, complex z2);
complex c_mult(complex z1, complex z2);
complex c_div(complex z1, complex z2);
complex c_re_mult(real a, complex z);

   /***   Logarithms, exponential functions, that kind of thing   ***/

complex c_exp(complex z);
complex c_log(complex z);
/* Branch cut along the negative real line */
complex c_sin(complex z);
complex c_sqrt(complex z);
complex c_pow(complex z,complex a);
complex c_re_pow(complex z, real a);
```

functions.h

```
#define alpha 0.00729927007



# include <stdio.h>
# include "math.h"
# include "compl.h"

#define STP 2.50662827465E0

/* gamma functions, spherical harmonics and other useful functions */

complex c_gammln( complex z);
real gammln(real xx);
int fac(real n);
real plgndr(int l,int m,real x);
complex Y(int l, real m, real theta, real phi);
real sqr(real x);
/* Spherical Bessel functions  and   hypergeometrical functions  */


real j( int l, real x);
```

```
complex hypgeo(complex a, complex b, complex c, complex z);
complex F(complex a, complex b,complex c, complex z);
complex F_deg(complex a, complex c, complex z);
/* Integrationsrutiner */

void trapez(real (* f)(real), real a, real b,real *s,bool clear);

real simpson(real (* f) (real),real a,real b);

real pol_int(real xa[],real ya[],int n,real x, real *y, real *dy);

real romberg(real (* f)(real),real a,real b);


real qromb(real(*func)(real),real a,real b);
```

pairs.h

:

```
# include "functions.h"


/* The units are fixed by the Compton wavelength */

# define lambda_c 38.6159065

/* The crucial  integral */
complex K( real s,real s_b,int k,real p_0,real p,real k_0,real Z);
complex K1( real s,real s_b,int k,real p_0,real p,real k_0,real Z);


/* The integral J from Appendix A  */
complex J(complex mu,complex alph, real nu, real beta);

/* Functions for matrix elements and cross sections for
 *  the K shell
 */
complex m_e(int L,real J, real m, real Z, real k_0);
real matrix_element(int L,real J, real m, real Z, real k_0);
real partial_cross_section(int L, real J, real m, real Z, real k_0);
complex sigma(real m,real Z, real k_0);

/* As well as for the L-shell - a little more this time! */

complex m_e_2p3(int L, real J, real m, real Z, real k_0);
real p3_2_partcs(int L, real J, real m, real Z, real k_0);
complex sigma_2p3(real m,real Z, real k_0);

complex m_e2p1(int L, real J, real m, real Z, real k_0);
```

```
real p2p1_partcs(int L, real J, real m, real Z, real k_0);
complex sigma_2p1(real m,real Z, real k_0);

complex m_e2s(int L, real J, real m, real Z, real k_0);
real p2s_partcs(int L, real J, real m, real Z, real k_0);
complex sigma_2s(real m,real Z, real k_0);

extern FILE *out; /* Used for output in main program */
```

$K.c$

:

```
#include "pairs.h"
#define KMAX 300



complex I_p(real s, real s_b, short iota, real p_0, real p, real k_0, real Z){
  complex fac_log,res;
  real eta,E;
  fac_log = c_minus(c_gammln(c_const(s+s_b-iota,0)),
    c_mult(c_const((s+s_b - iota),0),
   c_log(c_const(p_0,p+k_0))));
  E = sqrt(p*p+1);
   eta = -(alpha*Z*E)/p;
  res =  F(c_const(s+1,eta),c_const(s+s_b-iota,0),c_const(2*s+1,0),
  c_div(c_const(2*p,0),c_const(p+k_0,-p_0))) ;
   res = c_mult(res, c_exp(fac_log));

  return res;
} /* I_p */



complex I_m(real s, real s_b, short iota, real p_0, real p, real k_0, real Z){
 complex fac_log,res;
  real eta,E;
   fac_log = c_minus(c_gammln(c_const(s+s_b-iota,0)),
     c_mult(c_const((s+s_b - iota),0),
    c_log(c_const(p_0,-p-k_0))));
 E = sqrt(p*p+1);
   eta = -(alpha*Z*E)/p;
 res =  F(c_const(s,-eta),c_const(s+s_b-iota,0),c_const(2*s+1,0),
  c_div(c_const(2*p,0),c_const(p+k_0,p_0))) ;
 res = c_mult(res, c_exp(fac_log));

return res;
}/* I_m */



 complex dat_vec[KMAX][KMAX];
 complex dat_vec1[KMAX][KMAX];
```

```
void K_init() {
  int i,j;
  for(i=0;i<KMAX;i++){
    for(j=0;j<KMAX;j++) dat_vec[i][j]=zero();
  }
  for(i=0;i<KMAX;i++){
      for(j=0;j<KMAX;j++) dat_vec1[i][j]=zero();

}
} /* K_init */

complex K( real s,real s_b,int k,real p_0,real p,real k_0,real Z) {
  complex sum;
  register short iota;
  real fac = 1/(2*k_0);
  sum = zero();
  for (iota = 0; iota <= k; iota++)  {
    complex term,term1,term2, ph;
    real ph1;
    ph = c_re_pow(i(), k+1-iota);
    ph1 = ((k+1-iota)%2 == 0) ? 1: -1;
    term1 = I_m(s,s_b,iota,p_0,p,k_0,Z);
    term2 = I_p(s,s_b,iota,p_0,p,k_0,Z);
    term = c_plus(c_re_mult(ph1,term1),term2);
    term = c_re_mult(fac,term);
    term = c_mult(term,ph);
    sum = c_plus(sum,term);
    fac *= ((k+iota+1)*(k-iota ))/((iota+1)*2*k_0);
  }; /* for */
    return sum;
} /*   K   */


complex K1(real s,real s_b,int k,real p_0,real p,real k_0,real Z) {
  int i = floor(s);
  if (k>=0) {
    if (is_zero(dat_vec[k][i])) dat_vec[k][i] = K(s,s_b,k,p_0,p,k_0,Z);
    return dat_vec[k][i];
  }
  else return zero();
} /* K1 */
 complex K2(real s,real s_b,int k,real p_0,real p,real k_0,real Z) {
 int i = floor(s);
  if (k>=0) {
    if (is_zero(dat_vec1[k][i])) dat_vec1[k][i] = K(s,s_b,k,p_0,p,k_0,Z);
    return dat_vec1[k][i];
  }
  else  return zero();
}  /* K2 */
```

pairs.c

```
   :

#include "pairs.h"


FILE *out;
real I_1(int k, int kappa,real Z, real k_0) {
  real s    = sqrt((kappa - alpha*Z)*(kappa + alpha*Z));
  real s_1s = sqrt((1-alpha*Z)*(1+alpha*Z));
  real E =  k_0 - s_1s;
  real p = sqrt((E-1)*(E+1));
  real eta = -(alpha*Z*E)/p;
  complex e_i_delta = c_sqrt(c_div(c_const(-kappa,-eta/E),c_const(s,eta)));
  complex K_int = K1(s,s_1s,k,alpha*Z,p,k_0,Z);
  real Im_fac = Im(c_mult(e_i_delta,c_mult(c_const(s,eta),K_int)));
  real norm_facs;
  if (k<0)  return 0;
  norm_facs = 2*sqrt((p*(E+1)*(1+s_1s))/(2*M_PI*exp(gammln(2*s_1s+1))))
    *exp(.5*M_PI*eta)*pow(2*alpha*Z,s_1s+.5);
  norm_facs = norm_facs*exp(Re(c_gammln(c_const(s,-eta)))
    -gammln(2*s+1)+(s-1)*log(2*p));
  return norm_facs*Im_fac; ;
} /* I_1 */

real I_2(int k, int kappa,real Z, real k_0) {
  real s    = sqrt((kappa - alpha*Z)*(kappa + alpha*Z));
  real s_1s = sqrt((1-alpha*Z)*(1+alpha*Z));
  real E =  k_0 - s_1s;
  real p = sqrt((E-1)*(E+1));
  real eta = -(alpha*Z*E)/p;
  complex e_i_delta = c_sqrt(c_div(c_const(-kappa,-eta/E),c_const(s,eta)));
  complex K_int = K1(s,s_1s,k,alpha*Z,p,k_0,Z);
  real Re_fac = Re(c_mult(e_i_delta,c_mult(c_const(s,eta),K_int)));
  real norm_facs;
  if (k<0)  return 0;
  norm_facs = -2*sqrt((p*(E-1)*(1-s_1s))/(2*M_PI*exp(gammln(2*s_1s+1))))
    *exp(.5*M_PI*eta)*pow(2*alpha*Z,s_1s+.5);
  norm_facs = norm_facs*exp(Re(c_gammln(c_const(s,-eta)))
    -gammln(2*s+1)+(s-1)*log(2*p));
  return norm_facs*Re_fac;
}

complex m_e(int L,real J, real m, real Z, real k_0) {
  int kappa =  (J == L+.5) ? -(L+1) : L;
  if (m==.5) {
    int ph = (J==L+.5)? -1 : 1;
    real plus_fac,minus_fac,elm;
    complex outphase;
    plus_fac = (L+1)/(2.*L+1.);
    minus_fac = L/(2.*L+1.);
    outphase = (J==L+.5) ? c_re_pow(i(),L+2.0) : c_re_pow(i(),L);
    elm = sqrt((2.0*J+1.0))*(I_1(2*J-L,kappa,Z,k_0)+ph*minus_fac*
```

```
          I_2(L-1,kappa,Z,k_0)- ph*plus_fac*I_2(L+1,kappa,Z,k_0));
    return c_re_mult(elm,outphase);
  }else if (m==-.5) {
    real out_fac = (J==L+.5) ? sqrt(2*J+3): sqrt(2*J-1);
    complex outphase = c_re_pow(i(),L);
    real elm;
    out_fac = (out_fac*sqrt(L*(L+1.0)))/(2.0*L+1.0);
    elm = out_fac*(I_2(L+1,kappa,Z,k_0)+I_2(L-1,kappa,Z,k_0));
    return c_re_mult(elm,outphase);
  };
} /* m_e*/


real partial_cross_section(int L, real J, real m, real Z, real k_0)
     /* These are the partial cross sections, to be summed over L,J,M;
      * obviously k_0 is supposed to have a sensible value!
      */
{  real E,p,M;
   E = k_0 - sqrt((1-alpha*Z)*(1+alpha*Z));
   p = sqrt((E-1)*(E+1));
   M = c_mod(m_e(L,J,m,Z,k_0));

   return (4*M_PI*M_PI*lambda_c*lambda_c*alpha*M*M)/k_0;
 }

complex sigma(real m, real Z, real k_0)

{    int L;
   real sum=0, part=0,error=1;
     for(L=0; (L<= 320)&&(error >1E-6); L++)
     {   part = partial_cross_section(L,L+.5,m,Z,k_0);
 if (L!= 0)
           part = part + partial_cross_section(L,L-.5,m,Z,k_0);
 sum = sum+part;
         if (sum ==0){
   if (L<=1) error = 1;
   else error  = 0;
 } else error = part/sum;
       };
   if (L>=320) {fprintf(out,"k=%g, L=320 needed",k_0);fflush(out);}
       return c_const(sum,error);

 } /* sigma */
```

K-cross.c

:

```
#include "pairs.h"
 FILE *out;

main()
{  real k,k_0=3;
   int Z;
  real E_1s;
  real sum=0.0,part;
  complex half = c_const(.5,0);
     char s[8];
   fprintf(stderr,"Beregning af K-skals-tværsnittet \n");
   fprintf(stderr,"Angiv Z: ");
   fscanf(stdin,"%d",&Z);
   fprintf(stderr,"Altså Z=%d \n",Z);
   fprintf(stderr,"Angiv navn på datafil: ");
   fscanf(stdin,"%s",s);
   fprintf(stderr,"Resultaterne skrives til %s.data.\n",s);
   E_1s = sqrt((1+alpha*Z)*(1-alpha*Z));
out = fopen(strcat(s,".data"),"w");


for (k = 1.1; k <5; k+=.1)
       { complex s1,s2;
         K_init();
 s1 = sigma(.5,Z,k+E_1s);
 s2 = sigma(-.5,Z,k+E_1s);
fprintf(out,"%g\t%g\t%g\t%g\n",k,Re(s1),Re(s2),sqrt(sqr(Im(s1))+sqr(Im(s2))));
                  fflush(out);
       }
for (k = 5; k <= 50; k+=1)
       { complex s1,s2;
         K_init();
 s1 = sigma(.5,Z,k+E_1s);
 s2 = sigma(-.5,Z,k+E_1s);
fprintf(out,"%g\t%g\t%g\t%g\n",k,Re(s1),Re(s2),sqrt(sqr(Im(s1))+sqr(Im(s2))));
                  fflush(out);
       }

}
```

Figure 56: Simple kinematic model of Bound-Free Pair Production

17 Appendix C: Kinematical Considerations

As has been mentioned, we consider the target nucleus as an infinitely heavy point charge, which will thus absorb the momentum which must be transferred so that energy and momentum can be conserved in the reaction, but since it is infinitely heavy it will absorb no kinetic energy and remain at rest at all times. This means that we neglect all recoil effects.

Is this approximation valid? And under what conditions? To answer these questions, let us look at the process from a purely kinematical[21] point of view, like in figure 56.

First, it is obvious that pair production could never take place without some external field (or more photons) since the energy-momentum four-vector of the initial state must have zero norm, while that of the *final* state must have a finite, negative norm - so the conservation of energy and momentum requires the presence of an additional mass in the initial state.
Introducing the mass M of the nucleus, the process of bound-free pair production may take place if only k_0 is larger than the threshold energy. This is defined as the energy in which the photon is absorbed and the particles created with zero kinetic energy in the centre-of-mass system of the final state:

$$P_i = (\mathbf{k_0}, ik_0), P_f = (0, i(M^* + m))$$

where M^* is the rest energy of the hydrogen-like system of electron+nucleus, $M^* = M + E_{1s}$. m is the electron mass, of course, which we retain for clarity.

The threshold energy is determined by demanding that the norms of the initial and final states be identical, so that bound-free pair production may occur,

[21] Billiard ball dynamics!

provided that

$$k_0 > (E_{1s} + m)[1 + \frac{E_{1s} + m}{2M}] \tag{174}$$

Neglecting recoil is equivalent to placing the threshold a little lower, and this is justified if the factor in square brackets may be taken equal to unity, that is, if

$$\frac{E_{1s} + m}{2M} \ll 1$$

If the pair production is taking place on a proton , $\frac{E_{1s}+m}{2M} \sim \frac{1}{1836}$, and the threshold is shifted a not quite negligible amount[22] - for heavier elements, however, this shift becomes utterly insignificant.

At photon energies above threshold, the assumption that the nucleus is infinitely heavy is equivalent to neglecting the recoil energy compared to the rest energy of the nucleus. Denoting the momentum transfer of the reaction by $\mathbf{q}$, the condition is that

$$M\sqrt{1 + \frac{q^2}{M^2}} = M \tag{175}$$

or, in other words, that

$$\frac{q^2}{M^2} \ll 1 \tag{176}$$

Looking once again at figure 56, we see from energy and momentum conservation, that

$$\mathbf{q} = \mathbf{k_0} - \mathbf{p}$$

$$k_0 + M = E + M^* \tag{177}$$

Let us assume (for simplicity) that the kinetic energy of the nucleus is indeed negligible. Then $M^* = M + E_{1s}$, and combining the two equations we obtain

$$q^2 = 2k_0(k_0 - E_{1s})[1 - \beta\cos\vartheta] + E_{1s}^2 - 1, \tag{178}$$

where β is the velocity of the emitted positron. When considering the validity of neglecting the recoil, the two final terms may safely be neglected.

If k_0 is of the order of a few electron masses, this condition simply becomes

$$m \ll M$$

If $k_0 \gg 1$, however, (178) reduces to

$$q = 2k_0 \sin\frac{\vartheta}{2} \tag{179}$$

[22] About an electron volt, that is, approximately $\frac{1}{13}$ of the binding energy of hydrogen

which shows that the recoil may (for very large energies) be neglected at low scattering angles, so the condition becomes

$$(k_0\vartheta)^2 \ll \frac{1}{4}M^2 \tag{180}$$

But since the differential cross section at very high energies becomes concentrated in a cone of width $\Delta\vartheta \sim \frac{1}{k_0}$, this relation will practically always be fulfilled.

The approximation of neglecting the recoil is thus valid near threshold for heavy ions, if not to good for protons, and valid for all nuclei at intermediate and high energies.

18 References

A. I. Akhiezer and U. B. Berestetskii, *Quantum Electrodynamics* (Wiley 1965)

W. R. Alling and W. R. Johnson, Phys. Rev. **139**, A1050 (1965)

A. Aste, K. Hencken, D. Trautmann and G. Baur, Phys. Rev. A **50**, 3980 (1994)

A. J. Baltz, M. J. Rhoades-Brown and J. Weneser, Phys. Rev. **50**, 4842 (1994)

U. Becker, N. Grün and W. Scheid, J. Phys B **20**, 2075 (1987)

A. Belkacem, H. Gould, B. Feinberg, R. Bossingham and W. E. Meyerhof, Phys. Rev. Lett. **71**, 1514 (1993)

A. Belkacem, H. Gould, B. Feinberg, R. Bossingham and W. E. Meyerhof, Phys. Rev. Lett. **73**, 2432 (1994)

C. A. Bertulani and G. Baur, Phys Rep **163**, 299 (1988)

H. A. Bethe and L. C. Maximon, Phys. Rev. **93**,768 (1954)

H. A. Bethe and E. E. Salpeter, *Quantum Mechanics of One and Two-Electron Atoms* (Springer-Verlag, Berlin 1957)

B. H. Bransden and M. R. C. McDowell, *Charge Exchange and the Theory of Ion-Atom Collisions*,Oxford University Press (1992)

J. Eichler, Phys. rev. A **15**,1856 (1977)

J. Eichler, Phys. Rep. **193**, 167 (1990)

T. Erber, Ann Phys **8**,435 (1959)

U. Fano, K.W. McVoy and J.R. Albers, Phys. Rev. **116**, 1147 (1959)

R. P. Feynman, *The Theory of Fundamental Processes*, (W. A. Benjamin, Inc, 1962)

M. Gavrila, Phys. Rev. **113**, 514 (1959)

M. Gavrila, Phys. Rev. **124**, 1132 (1961)

M. Gell-Mann, *The Quark and the Jaguar*, (Little, Brown and Co. 1994)

I. S. Gradshteyn and I.M. Ryzhik, *Tables of Integrals, Series and Products* (Academic Press, 1980)

W. Greiner, B. Müller, J. Rafelski, *Quantum Electrodynamics of Strong Fields*, Springer 1985

W. Greiner, *Relativistic Quantum Mechanics -Wave Equations* (Springer, Berlin 1990)

H. Hall, Rev. Mod. Phys. **8** (1936)

W. Heitler, *The Quantum Theory of Radiation*, Oxford University Press (1954)

K. Hencken, D. Trautmann and G. Baur, Phys. Rev. A **49**, 1584 (1994)

H. R. Hulme, J. McDougall, R. A. Buckingham and R. H. Fowler, Proc. Roy. Soc. London **A 149**, 131 (1935)

S. Hultberg, B. Nagel and P. Olsson, Arkiv Fysik **20**, 555 (1962)

D. C. Ionescu, Phys. Rev. A **49**, 3188 (1994)

J. C. Jaeger and H. R.Hulme, Proc. Phil. Soc. Cambridge **32**, 158 (1936) (1936^a)

J. C. Jaeger and H. R.Hulme, Proc. Royal Soc. Lon. **153**, 443 (1936) (1936^b)

J. D. Jackson, *Classical Electrodynamics*, 2nd. ed. (Wiley, New York, 1975)

W. R. Johnson, Phys. Rev. **159**, 61 (1967)

W. R. Johnson, D. J. Buss and C. O. Carroll, Phys. Rev. A **135**, 1232 (1964)

E. Merzbacher, *Quantum Mechanics* (John Wiley & Sons, 1971)

K. Momberger, N. Grün and W. Scheid, Zeitschr. Physik D **18**, 133 (1991)

K. Momberger, A. Belkacem and A.H. Sørensen, accepted for publication i Phys. Rev. A in 1996

A. I. Milstein and V.M. Strakhovenko, Zh Eksp. Teor. Fiz, **103**, 130 (1993)

C. T. Munger, S.J. Brodsky and I. Schmidt, Phys. Rev. D,**49**, 3228 (1994)

P. W. Nielsen, Lecture Notes in QFT 92-93 , IFA 1992

H. Olsen , Springer tracts in modern physics **44**,83 (1968)

J. R. Oppenheimer, Phys. Rev. **35**, 939 (1930)

J. C. Palathingal, P. Asoko-Kumar, K.G. Lynn and X.Y. Wu, Phys. Rev. A **51**, 2122 (1995)

P. Pechukas and J. C. Light, J. Chem. Phys. **44** 3897 (1966)

R. H. Pratt, Phys. Rev. **117**, 1017 (1960^a);

R. H. Pratt, Phys. Rev. **119**, 1619 (1960^b);

R. H. Pratt, A. Ron and H. K. Tseng, Rev Mod Phys **45**, 273 (1973)

W. H. Press, S.A. Teukolsky, W.V. Vetterling and B.P. Flannery, *Numerical Recipes in C*, 2nd. ed. (Cambridge University Press 1992)

M. E. Rose, *Relativistic electron theory* (Wiley, New York, 1961)

K. Rumrich, K. Momberger, G. Soff, W. Greiner, N. Grün and W. Scheid, Phys. Rev. Lett. **66**, 2613 (1991)

A. Salop and J. Eichler, J. Phys. B **12**, 257 (1979)

F. Sauter, Ann der Physik **11**, 454 (1931)

C. V. Sheth and N.V.V.J. Swamy, Phys. Rev. **167**, 319 (1968)

I.I. Sobel'man, *Atomic Spectra and Radiative Transitions*, (2nd. ed., Springer-Verlag Berlin 1992)

K. K. Sud and C. W. Soto Vargas, Phys. Rev. A. **49**, 4624 (1994)

A. H. Sørensen and A. Belkacem, Phys. Rev. A **49**,81 (1994)

U. Wille, Z. Phys. A **308**, 3 (1982)

E. J. Williams, Mat. Fys. Medd. K. Dan. Vidsk. Selsk. XIII no 4 (1935)

I. Øverbø, K.J. Mork and H. Olsen, Phys. Rev. **175**,443 (1968)

I. Øverbø, Arkiv for Det Fys. Seminar Trondheim, **9** (1970)